Dynamic State Estimation in Power Systems

by

© Hamed Tebianian

A Thesis submitted to the

School of Graduate Studies

in partial fulfillment of the requirements for the degree of

Master of Engineering

Faculty of Engineering and Applied Science

Memorial University

May 2014

St. John's   Newfoundland

ABSTRACT

Research in the area of power system transient stability has recently focused on dynamic state estimation using high rate Phasor Measurement Unit (PMU) data. Several mathematical models for synchronous machine are developed and various estimation approaches are proposed for this purpose. In this thesis, the mathematical formulation of nonlinear state space modeling and the principles of Kalman Filter are explained. Extended and Unscented Kalman Filters (EKF and UKF), as two nonlinear estimation methods, are applied for state and parameter estimation in an induction motor. In the next stage, after presenting a thorough explanation about modeling of the synchronous machine, dynamic state estimation is applied on different power system case studies and the results of estimation methods are compared. The simulation results provided in this thesis show the great potential of the proposed estimation approaches for accurately estimating the states of the machine as well as reducing the effect of noise on input signals.

ACKNOWLEDGEMENTS

Table of Contents

List of Tables

List of Figures

List of Symbols, Nomenclature or Abbreviations

BPA   Bonneville Power Administration

EKF   Extended Kalman Filter

DFT   Discrete Fourier Transform

GPS   Global Positioning System

IM   Induction Motor

PDC   Phasor Data Concentrator

pdf   probability density function

PMU   Phasor Measurement Unit

RV   Random Variable

SCADA   Supervisory Control and Data Acquisition

SMIB   Single Machine Infinite Bus

SMT   Synchronized Measurement Technology

UKF   Unscented Kalman Filter

WAMPAC   Wide Area Monitoring, Protection, and Control

WECC   Western Electricity Coordinating Council

CHAPTER 1

1. Introduction

1-1. Introduction

Many researches in the field of dynamic power system estimation have recently focused on Kalman Filter as an efficient recursive estimation approach [1-4]. Before the advent of Phasor Measurement Units (PMUs) [7], online state estimation in power systems using low rate and non-synchronous data provided by Supervisory Control and Data Acquisition (SCADA) measurements was inefficient. But as PMUs are becoming more adopted worldwide, real time state estimation in power systems is becoming more realizable [2]. PMU is a recently developed power system measurement device that samples input three phase voltage and current waveforms, using a common synchronizing

signal received by Global Positioning System (GPS), and calculates the phasors (magnitudes and angles) of the bus by deploying Discrete Fourier Transform [7]. Researchers have used various estimation approaches and case studies to investigate dynamic state estimation in power systems. Kalman and particle filters are among the most referred estimation approaches. Single-Machine-Infinite-Bus (SMIB) and IEEE 3-Generator-9-Bus Test System are also referred as the most popular case studies [1-6]. Also, several models with different orders used in the estimation process can be found in the literature for synchronous machines.

In this thesis, the mathematical background of the state space modeling and optimal estimation using Kalman filters are addressed in detail. Dynamic state and parameter estimation using Kalman filter is applied to induction machine at first stage. After providing some information about synchrophasors and phasor measurement unit (PMU), and deriving and validating the classical and 2-axis fourth order models of the synchronous machine, dynamic state estimation using Kalman Filters is applied to SMIB and IEEE 3-Generator-9-Bus Test System and the results are compared. Finally, some suggestions are proposed for future research in this field.

1-2. Problem Statement

Dynamic state estimation in power system provides accurate and frequent information about internal states of the synchronous machines. This information can be used in state feedback control of the synchronous generator to improve the control performance;

enhance the overall transient stability of the power system; perform real-time analysis of angle, voltage, and frequency of the power system; reduce measurement noise, increase damping property for the inter-area oscillations; and reach to better rush hour power management [8]. Using Kalman Filter, as a powerful recursive estimation method with noise elimination property, helps to design an appropriate estimator for a synchronous machine in a digital platform.

1-3. Focus of the Thesis

The main focus of this thesis is to use Extended Kalman Filter (EKF) and Unscented Kalman Filter (UKF) for dynamic state estimation in different power system case studies, using 2-axis fourth order model of the synchronous machine and one input signal (output power). Also, an attempt is made to present a complete step-by-step package for nonlinear Kalman Filter based estimation methods, synchronous machine state space modeling and validation, and dynamic state estimation in power systems. The optimal estimation approaches are also used for online states and parameter estimation in induction machine and a comprehensive simulation is carried out.

1-4. Thesis Organization

Chapter 2 presents the mathematical background of nonlinear optimal state estimation and step-by-step formulation of Extended and Unscented Kalman Filter.

Chapter 3 discusses state space model of the induction machine, the developed model which includes the main parameters, and applying Kalman Filters for online state and parameter estimation.

Chapter 4 provides a review on synchrophasors, Phasor Measurement Unit (PMU), the application of PMUs in dynamic state estimation in power systems, and some advantages of Wide Area Monitoring, Protection, and Control (WAMPAC).

Chapter 5 describes the mathematical formulation of the synchronous machine classical and 2-axis modeling and the equal area criterion. The developed models are then validated by simulation in MATLAB, using the data provided by PowerWorld Simulator.

Chapter 6 presents the discretized state space model of the synchronous machine, and dynamic state estimation in Single-Machine-Infinite-Bus (SMIB) and IEEE 3-Generator-9-Bus Test System. Comparison between the performance of EKF and UKF as the estimation methods, a suggested application of the dynamic state estimation in power systems, and current challenges of dynamic estimation in large power systems are also presented.

Chapter 7 highlights the contribution of this research and discusses future open areas for research in this field.

CHAPTER 2

2. Nonlinear State Estimation

2-1. Introduction

In this chapter, the principles of linear and nonlinear systems, mean and covariance propagation, linearization and discretization methods, and linear and nonlinear Kalman filtering are explained.

State space model can be used to describe many physical processes. These processes may include different areas such as engineering, economics, physics, chemistry, biology and several others. Mathematical models of processes help us to apply mathematical control tools and also estimate more information about the systems. This is the main reason that state space model is a vital approach in the field of engineering. When the information

about the states of a system in current time are available, and also the present and future inputs are known, then all of the outputs of the system in future are deducible [9].

Generally, state space approach can be categorized into linear and nonlinear models. Although most real systems are nonlinear in their nature, most of the accessible and well-defined mathematical tools of estimation and control are linear. This is the main reason that nonlinear systems are approximated by linear systems most of the time. By this way, the developed estimation and control algorithms for linear systems can be applied to nonlinear systems [9]. In this chapter, an overview about linear and nonlinear systems will be presented. Then two nonlinear estimation methods: Extended Kalman Filter (EKF) and Unscented Kalman Filter (UKF) will be discussed in detail.

2-2. Linear Systems

The state space equations of a deterministic linear system are presented as follows:

$$\dot{x} = Ax + Bu$$
$$y = Cx \tag{2.1}$$

In this equation, x, u, and y are the state, control, and output vectors, respectively. The dimension of matrices A, B, and C is related to the number of states, inputs and outputs of the system. Matrices A, B, and C are often called the system, input, and output matrices. All of these matrices can be time variant or time invariant, while the system is still linear.

Considering A, B, and C as constant matrices, the solution to Equation (2.1) is expressed as [9]

$$x(t) = e^{A(t-t_0)}x(t_0) + \int_{t_0}^{t} e^{A(t-\tau)}Bu(\tau)d\tau$$
$$y(t) = Cx(t) \tag{2.2}$$

t_0 is the initial condition of the system and can be considered as 0 most of the time. e^{At} is called the state-transition matrix of the system, because it describes how the states of the system start changing from their initial values when no external input is applied to the system. If x is an n-element vector, the state transition matrix can be calculated with Euler's formula or Laplace inverse of the exponential function e^{At} as follows [9].

$$e^{At} = \sum_{j=0}^{\infty} \frac{(At)^j}{j!}$$
$$= \mathcal{L}^{-1}[(SI - A)^{-1}] \tag{2.3}$$

For better understanding, an example is provided here.

Example 2.1 [9]

Assume that the angular acceleration of a motor is to be controlled. The derivative of the position is the system's velocity. A simplified model of the motor can be presented as

$$\dot{\theta} = \omega$$
$$\dot{\omega} = u + \omega_1 \tag{2.4}$$

ω_1 is the acceleration noise and can be attributed to the uncertainties in the applied acceleration, motor shaft unusual behaviours, and load fluctuations. The angular position of the motor is considered as the single measurement of the system. As a result, the state space model of the system can be given by

$$\begin{bmatrix} \dot{\theta} \\ \dot{\omega} \end{bmatrix} = \begin{bmatrix} 0 & 1 \\ 0 & 0 \end{bmatrix} \begin{bmatrix} \theta \\ \omega \end{bmatrix} + \begin{bmatrix} 0 \\ 1 \end{bmatrix} u + \begin{bmatrix} 0 \\ \omega_1 \end{bmatrix}$$

$$y = \begin{bmatrix} 1 & 0 \end{bmatrix} x + v \tag{2.5}$$

v is the measurement noise in this equation. Using the first expression for state transition matrix in Equation (2.3) and by ignoring higher order terms in the series, it can be written as

$$e^{At} = \sum_{j=0}^{\infty} \frac{(At)^j}{j!}$$

$$= (At)^0 + (At)^1 + \frac{(At)^2}{2!} + \frac{(At)^3}{3!} + \cdots$$

$$= I + At \tag{2.6}$$

It can be simplified as

$$e^{At} = \begin{bmatrix} 1 & 0 \\ 0 & 1 \end{bmatrix} + \begin{bmatrix} 0 & t \\ 0 & 0 \end{bmatrix}$$

$$= \begin{bmatrix} 1 & t \\ 0 & 1 \end{bmatrix} \tag{2.7}$$

And based on the second definition in Equation (2.3)

$$e^{At} = \mathcal{L}^{-1}[(sI - A)^{-1}]$$

$$= \mathcal{L}^{-1}\left(\begin{bmatrix} s & -1 \\ 0 & s \end{bmatrix}^{-1}\right)$$

$$= \mathcal{L}^{-1}\left(\begin{bmatrix} 1/s & 1/s^2 \\ 0 & 1/s \end{bmatrix}\right)$$

$$= \begin{bmatrix} 1 & t \\ 0 & 1 \end{bmatrix} \tag{2.8}$$

Using the state transition matrix obtained in Equations (2.7) and (2.8), the complete response of the state space model can be obtained, using Equation (2.2).

2-3. Nonlinear Systems

It is not unrealistic to say that all engineering processes are nonlinear. In most cases, we consider nonlinear systems as linear only when their behavior can be approximated to a linear system in a certain operation range. This is the reason that although linear systems do not exist in the real world, the theory of linear systems can be considered as an irreplaceable control and estimation tool for nonlinear systems [9].

A continuous-time nonlinear system can generally be written as the following form.

$$\dot{x} = f(x, u, w)$$

$$y = h(x, y) \tag{2.9}$$

f and h are arbitrary vectors of functions and w and v represent process and measurement noise, respectively. It should be noticed that both f and h can either be time variant or time invariant nonlinear functions. Linear tools are capable of being applied to nonlinear systems after being linearized. A linear system that is roughly equal to the nonlinear system should be found. One way is to use Taylor series expansion of $f(x)$ around a nominal operating point $x = \bar{x}$. By defining $\tilde{x} = x - \bar{x}$, the expansion is as follows:

$$f(x) = f(\bar{x}) + \left.\frac{\partial f}{\partial x}\right|_{\bar{x}} \tilde{x} + \frac{1}{2!}\left.\frac{\partial^2 f}{\partial x^2}\right|_{\bar{x}} \tilde{x}^2 + \frac{1}{3!}\left.\frac{\partial^3 f}{\partial x^3}\right|_{\bar{x}} \tilde{x}^3 + \cdots \qquad (2.10)$$

Considering x as a general $n \times 1$ vector, Equation (2.10) is expanded below.

$$f(x) = f(\bar{x}) + \left(\tilde{x}_1 \frac{\partial}{\partial x_1} + \cdots + \tilde{x}_n \frac{\partial}{\partial x_n}\right) f|_{\bar{x}} +$$

$$\frac{1}{2!}\left(\tilde{x}_1 \frac{\partial}{\partial x_1} + \cdots + \tilde{x}_n \frac{\partial}{\partial x_n}\right)^2 f|_{\bar{x}} +$$

$$\frac{1}{3!}\left(\tilde{x}_1 \frac{\partial}{\partial x_1} + \cdots + \tilde{x}_n \frac{\partial}{\partial x_n}\right)^3 f|_{\bar{x}} + \cdots \qquad (2.11)$$

The higher order derivatives of $f(x)$ in Equation (2.11) can be ignored when the function is smooth around its operating point [9]. These high order derivatives are divided by increasingly larger factorials which in case of small $\tilde{x}$ with growing power, diminishes the magnitude of the higher order terms even more. As a result, the following approximation is reasonable.

$$f(x) \approx f(\bar{x}) + \frac{\partial f}{\partial x}\bigg|_{\bar{x}} \tilde{x}$$

$$\approx f(\bar{x}) + A\tilde{x} \tag{2.12}$$

Nonlinear function presented in Equation (2.9) is able to be expanded around the nominal point $(\bar{x}, \bar{u}, \bar{w})$ as follows:

$$\dot{x} = f(x, u, w)$$

$$\approx f(\bar{x}, \bar{u}, \bar{w}) + \frac{\partial f}{\partial x}\bigg|_{0} (x - \bar{x}) + \frac{\partial f}{\partial u}\bigg|_{0} (u - \bar{u}) + \frac{\partial f}{\partial w}\bigg|_{0} (w - \bar{w})$$

$$= \dot{\bar{x}} + A\tilde{x} + B\tilde{u} + L\tilde{w} \tag{2.13}$$

The subscript 0 is used to emphasize that the function is assessed at its nominal point $(\bar{x}, \bar{u}, \bar{w})$. Matrices $A, B,$ and L can be calculated as described in Equation (2.13). Substituting $\dot{\bar{x}}$ from both sides of Equation (2.13) yields the following:

$$\dot{\tilde{x}} = A\tilde{x} + B\tilde{u} + L\tilde{w} \tag{2.14}$$

w is the process noise and its average $\bar{w}$ can be considered as 0 because we often consider the process noise as white noise with 0 mean and 1 covariance. Replacing $\tilde{w}$ with w in Equation (2.14) gives

$$\dot{\tilde{x}} = A\tilde{x} + B\tilde{u} + Lw \tag{2.15}$$

Equation (2.15) is a linear function of $\tilde{x}, \tilde{u}$ and w. In other words, it is a linear function of the deviations of the states and control inputs from their nominal points. This linearization will precisely characterize the behavior of the system, as long as the deviations from nominal points stay in small region. Also, the nonlinear measurement equation can be linearized around operating point $x = \bar{x}$ and $v = \bar{v} = 0$. The linearization procedure is presented as follows [9]:

$$\tilde{y} = \left.\frac{\partial h}{\partial x}\right|_0 \tilde{x} + \left.\frac{\partial h}{\partial v}\right|_0 \tilde{v}$$

$$= C\tilde{x} + Dv$$

$$(2.16)$$

C and D are defined in Equation (2.16). A complete linearization of a nonlinear system describing the deviations of the states, control signals, and outputs around their nominal operating point is presented in Equation (2.15) and (2.16). In these equations

$$\tilde{x} = x - \bar{x}$$

$$\tilde{u} = u - \bar{u}$$

$$\tilde{y} = y - \bar{y}$$

$$(2.17)$$

As all systems considered for dynamic state estimation in this thesis are nonlinear, using linearizing techniques is inevitable. The following example clarifies the idea of linearizing a nonlinear system.

Example 2.2 [9]

A two-phase permanent magnet synchronous motor can be represented by the following mathematical nonlinear model.

$$\dot{i}_a = -\frac{R}{L}i_a + \frac{\omega\lambda}{L}\sin\theta + \frac{u_a}{L}$$

$$\dot{i}_b = -\frac{R}{L}i_b - \frac{\omega\lambda}{L}\cos\theta + \frac{u_b}{L}$$

$$\dot{\omega} = -\frac{3\lambda}{2J}i_a\sin\theta + \frac{3\lambda}{2J}i_b\cos\theta - \frac{F\omega}{J} - \frac{T_l}{J}$$

$$\dot{\theta} = \omega$$

$$(2.18)$$

i_a and i_b are the two windings currents, R and L are the resistance and inductance of the windings, θ and ω are the angular position and motor speed, λ is the flux constant, u_a and u_b are the voltages applied to the two windings of the motor (inputs), J is the moment of inertia of the rotor and the connected load, F is the viscous friction of the motor, and T_l is the load torque. The model is considered as a time-invariant system. As the system is highly nonlinear, it is not possible to apply linear control and estimation tools to this model. Nevertheless, it is possible to apply linear approaches to this system by linearizing the system around its operating point and assuming small deviations of the states and the control inputs from their nominal values. The state vector of this system can be described as follows.

$$x = [i_a \quad i_b \quad \omega \quad \theta]$$

$$(2.19)$$

With this definition, the state space model of the permanent magnet synchronous machine can be written as

$$\dot{x} = [\dot{x}_1 \quad \dot{x}_2 \quad \dot{x}_3 \quad \dot{x}_4]$$

$$= f(x, u)$$

$$= \begin{bmatrix} -\dfrac{R}{L}x_1 + \dfrac{x_3\lambda}{L}\sin x_4 + \dfrac{u_a}{L} \\ -\dfrac{R}{L}x_2 - \dfrac{x_3\lambda}{L}\cos x_4 + \dfrac{u_b}{L} \\ -\dfrac{3\lambda}{2J}x_1\sin x_4 + \dfrac{3\lambda}{2J}x_2\cos x_4 - \dfrac{Fx_3}{J} - \dfrac{T_l}{J} \\ x_3 \end{bmatrix} \tag{2.20}$$

By taking the partial derivative of $f(x, u)$ with respect to x and u, the linearized model is obtained as follows

$$A = \frac{\partial f}{\partial x}$$

$$= \begin{bmatrix} -\dfrac{R}{L} & 0 & \dfrac{\lambda s_4}{L} & \dfrac{x_3\lambda c_4}{L} \\ 0 & -\dfrac{R}{L} & -\dfrac{\lambda c_4}{L} & \dfrac{x_3\lambda s_4}{L} \\ -\dfrac{3\lambda s_4}{2J} & \dfrac{3\lambda c_4}{2J} & -\dfrac{F}{J} & -\dfrac{3\lambda(x_1 c_4 + x_2 s_4)}{2J} \\ 0 & 0 & 1 & 0 \end{bmatrix}$$

$$B = \frac{\partial f}{\partial u}$$

$$= \begin{bmatrix} 1/L & 0 \\ 0 & 1/L \\ 0 & 0 \\ 0 & 0 \end{bmatrix} \tag{2.21}$$

15

In this equation, $s_4 = \sin x_4$ and $c_4 = \cos x_4$

Using Equation (2.21), the linearized model $\dot{\tilde{x}} = A\tilde{x} + B\tilde{u}$ can approximately portray the small deviation of the state vector x from operating points.

2-4. Discretization Method

Most of the systems are presented in continuous-time models like Equations (2.1) and (2.9) in the real world [9]. However, micro-processors are the platforms that state estimation and control schemes are implemented on. This will lead one to convert continuous-time systems to discrete-time systems using available discretization approaches. The general principles of discretization are explained in this section, and a simple method suitable for this research is then presented.

According to Equation (2.2), the solution of a continuous-time linear system is expressed as follows:

$$x(t) = e^{A(t-t_0)}x(t_0) + \int_{t_0}^{t} e^{A(t-\tau)}Bu(\tau)d\tau \tag{2.22}$$

If $t = t_k$ (a discrete time point) and the initial time $t_0 = t_{k-1}$ (the previous discrete time point) and considering $A(\tau), B(\tau)$, and $u(\tau)$ approximately fixed in the integration interval, Equation (2.2) can be written as

$$x(t_k) = e^{A(t_k-t_{k-1})}x(t_{k-1}) + \int_{t_{k-1}}^{t_k} e^{A(t_k-\tau)}d\tau Bu(t_{k-1}) \tag{2.23}$$

Defining $\Delta t = t_k - t_{k-1}$ and $\alpha = \tau - t_{k-1}$ and substituting for τ in Equation (2.23), it can be written as [9]

$$x(t_k) = e^{A\Delta t} x(t_{k-1}) + \int_0^{\Delta t} e^{A(\Delta t - \alpha)} d\alpha \, Bu(t_{k-1})$$

$$= \underbrace{e^{A\Delta t}}_{F_{k-1}} x(t_{k-1}) + \underbrace{e^{A\Delta t} \int_0^{\Delta t} e^{-A\alpha} d\alpha \, B}_{G_{k-1}} u(t_{k-1})$$

$$x_k = F_{k-1} x_{k-1} + G_{k-1} u_{k-1} \tag{2.24}$$

$x_k, F_k, G_k,$ and u_k are defined in Equation (2.24) which is a linear discrete-time approximation of the continuous-time Equation (2.1). The main challenge in this regard is computing the integral in Equation (2.24) or the G matrix. If A is invertible, the simplified expression for the integral can be given by.

$$\int_0^{\Delta t} e^{-A\tau} d\tau = \int_0^{\Delta t} \sum_{j=0}^{\infty} \frac{(-A\tau)^j}{j!} d\tau$$

$$= \int_0^{\Delta t} \left[I - A\tau + \frac{A^2\tau^2}{2!} - \frac{A^3\tau^3}{3!} + \cdots \right]$$

$$= \left[I\tau - \frac{A\tau^2}{2!} + \frac{A^2\tau^3}{3!} - \cdots \right]_0^{\Delta t}$$

$$= \left[I\Delta t - \frac{A(\Delta t)^2}{2!} + \frac{A^2(\Delta t)^3}{3!} - \cdots \right]$$

$$= \left[A\Delta t - \frac{(A\Delta t)^2}{2!} + \frac{(A\Delta t)^3}{3!} - \cdots \right] A^{-1}$$

$$= \left[I - e^{-A\Delta t} \right] A^{-1} \tag{2.25}$$

Finally, the continuous-time system in Equation (2.1) with matrices A and B converted to a discrete-time system with F and G can be presented as [9]

$$F = e^{A\Delta t}$$
$$G = F \int_0^{\Delta t} e^{-A\tau} d\tau \, B$$
$$= F[I - e^{-A\Delta t}]A^{-1}B \tag{2.26}$$

Where Δt is the time step of discretization.

It is difficult to use Equation (2.26) for discretizing a nonlinear system. Instead, it might be more convenient to use the basic definition of the time derivative of a variable x as follows:

$$\dot{x} = \frac{x_k - x_{k-1}}{\Delta t} \xrightarrow{yields} x_k = \dot{x} \, \Delta t + x_{k-1} \tag{2.27}$$

Equation (2.27) can also be used for numerical integration. Using Equation (2.9), it can be written

$$x_k = f_{k-1}(x_{k-1}, u_{k-1}, w_{k-1})\Delta t + x_{k-1} \tag{2.28}$$

2-5. Optimal State Estimation

Optimal state estimation is key to modern control [9]. The final goal of the state estimation is to provide accurate knowledge about some or all of the states of a system to

be used for control or monitoring purposes. Basically, it is not possible to measure all of the states of a system using sensors because of either high installation and maintenance cost or unfeasibility. For example, it might not be cost effective in a certain project to put an encoder (speed sensor) for an electrical machine. On the other hand, it is definitely impossible to install sensor for measuring flux of the windings. Therefore, the optimal state estimation has the following advantages:

1. Providing information about the immeasurable states of a system

2. Providing more accurate information about measurable states of a system by reducing effect of noise and uncertainty of the installed sensors

Kalman Filter as a powerful and popular state estimation algorithm for both linear and nonlinear systems is chosen for this research. The nature of this mathematical tool is based on minimizing the mean of squared error between real states and estimated ones [10]. The mathematical foundation of Kalman Filter is to know how the mean and covariance of variables propagate through linear and nonlinear systems. To avoid complexity, the linear case is explained below and nonlinear propagation is discussed in Section 2-5-2 and 2-5-3.

Suppose that $X \sim N(\bar{x}, \sigma_x^2)$ and $Y = g(x) = aX + b$, it is known from probability theory that

$$\bar{y} = a\bar{x} + b$$

$$\sigma_Y^2 = a^2 \sigma_X^2 \tag{2.29}$$

Using Equation (2.29), consider the linear system provided in the following equation

$$x_k = F_{k-1}x_{k-1} + G_{k-1}u_{k-1} + w_{k-1}$$

(2.30)

The equations that govern the propagation of the mean of the states through a linear system can be derived as follows:

$$\bar{x}_k = E(x_k)$$

$$= F_{k-1}\bar{x}_{k-1} + G_{k-1}u_{k-1} + w_{k-1}$$

(2.31)

E is the expectation value. The covariance expression can be derived as follows [9]:

$$(x_k - \bar{x}_k)(\ldots)^T = (F_{k-1}x_{k-1} + G_{k-1}u_{k-1} + w_{k-1})(\ldots)^T$$

$$= [F_{k-1}(x_{k-1} - \bar{x}_{k-1}) + w_{k-1}][\ldots]^T$$

$$= F_{k-1}(x_{k-1} - \bar{x}_{k-1})(x_{k-1} - \bar{x}_{k-1})^T F_{k-1}^T + w_{k-1}w_{k-1}^T$$

$$+ F_{k-1}(x_{k-1} - \bar{x}_{k-1})w_{k-1}^T$$

$$+ w_{k-1}(x_{k-1} - \bar{x}_{k-1})^T F_{k-1}^T$$

(2.32)

The covariance of x_k is the expected value of the above expression. Since $(x_{k-1} - \bar{x}_{k-1})$ is uncorrelated with w_{k-1}, it is obtained

$$P_k = E\big((x_k - \bar{x}_k)(\ldots)^T\big)$$

$$= F_{k-1}P_{k-1}F_{k-1}^T + Q_{k-1}$$

(2.33)

P_{k-1} and Q_{k-1} are error covariance and system noise covariance matrices, respectively. In the subsequent sections, using the equations derived so far for mean and covariance of propagated states of linear systems, the fundamental equations for Kalman Filter which is designed for linear systems are derived. In order to extend the idea for nonlinear systems, two major nonlinear approaches of Kalman Filter, namely Extended Kalman Filter (EKF) and Unscented Kalman Filter (UKF) are explained in details.

2-5-1. Kalman Filter

"The Kalman filter in its various forms is clearly established as a fundamental tool for analyzing and solving a broad class of estimation problems" [11]. This estimation method operates by propagating the mean and covariance of the states of a system through time. To derive the equations that govern the discrete-time Kalman Filter, assume a linear discrete-time system given as follows [9]:

$$x_k = F_{k-1}x_{k-1} + G_{k-1}u_{k-1} + w_{k-1}$$

$$y_k = H_k x_k + v_k \tag{2.34}$$

$\{w_k\}$ and $\{v_k\}$ are process and measurement noises of the system which determine covariance matrices. The process and measurement noises are essentially considered as white, zero-mean, and uncorrelated with the covariance matrices Q_k and R_k, respectively.

$$w_k \sim N(0, Q_k)$$

$$v_k \sim N(0, R_k)$$

$$E\left[w_k w_j^T\right] = Q_k \delta_{k-j}$$

$$E\left[v_k v_j^T\right] = R_k \delta_{k-j}$$

$$E\left[v_k w_j^T\right] = 0 \tag{2.35}$$

In Equation (2.35), δ_{k-j} is the Kronecker delta function in which $\delta_{k-j} = 1$ if $k = j$ and $\delta_{k-j} = 0$ if $k \neq j$ [9]. The main target here is to estimate the states of the system x_k, using the available noisy measurements $\{y_k\}$ and knowledge about the dynamic response which is accessible from the differential equations of the system [9]. In this regard, different kinds of estimation can be defined. If all of the measurements up to and including time k are available for the estimate of x_k, then *a posteriori* estimate can be calculated which is normally represented by $\hat{x}_k^+$. The " $+$ " superscript implies that *a posteriori* estimate is formed. The following equation shows the way to portray the *a posteriori* estimate of x_k using the expected value of x_k conditioned on all of the measurements up to and including time k [9]

$$\hat{x}_k^+ = E[x_k | y_1, y_2, y_3, \dots, y_k] = a\ posteriori\ estimate \tag{2.36}$$

A priori estimate denoted by $\hat{x}_k^-$ can be formed if all of the measurements before and not including time k are available for the estimation purpose. The following equation explains how *a priori* estimate is calculated [9]:

$$\hat{x}_k^- = E[x_k | y_1, y_2, y_3, \ldots, y_{k-1}] = a\ priori\ estimate \tag{2.37}$$

Although $\hat{x}_k^-$ and $\hat{x}_k^+$ are both estimates of the same quantity, the difference between *a priori* and *a posteriori* estimate is that $\hat{x}_k^-$ is the estimate of x_k before the measurement y_k is taken into account, and $\hat{x}_k^+$ is the estimate of x_k after the measurement y_k has been considered [9]. The intuitive expectation here is that $\hat{x}_k^+$ would be a better estimation than $\hat{x}_k^-$, because more information is used for its computation. The first measurement is taken at time $k = 1$. Due to the lack of available knowledge from previous measurements at this moment, $\hat{x}_0^+$ is considered as the expected value of the initial state x_0.

$$\hat{x}_0^+ = E(x_0) \tag{2.38}$$

The term P_k is used to denote the covariance of the estimation error [10]. Consequently, P_k^- represents the covariance of the estimation error of $\hat{x}_k^-$, and P_k^+ represents the covariance of the estimation error of $\hat{x}_k^+$. These error covariance matrices are defined as follows:

$$P_k^- = E[(x_k - \hat{x}_k^-)(x_k - \hat{x}_k^-)^T]$$
$$P_k^+ = E[(x_k - \hat{x}_k^+)(x_k - \hat{x}_k^+)^T] \tag{2.39}$$

The following timeline depicts the relationship between *a priori* and *a posteriori* state and error covariance estimation.

$$\cdots\cdots\quad \hat{x}^-_{k-1} \quad \Big|\quad \hat{x}^+_{k-1} \longrightarrow \hat{x}^-_k \ \Big|\ \hat{x}^+_k \cdots\cdots$$

$$\cdots\cdots\quad P^-_{k-1} \quad \Big|\quad P^+_{k-1} \longrightarrow P^-_k \ \Big|\ P^+_k \cdots\cdots$$

$$\xrightarrow{\qquad\qquad\qquad\qquad\qquad\qquad\qquad}$$

$$K-1 \qquad\qquad\qquad K \qquad time$$
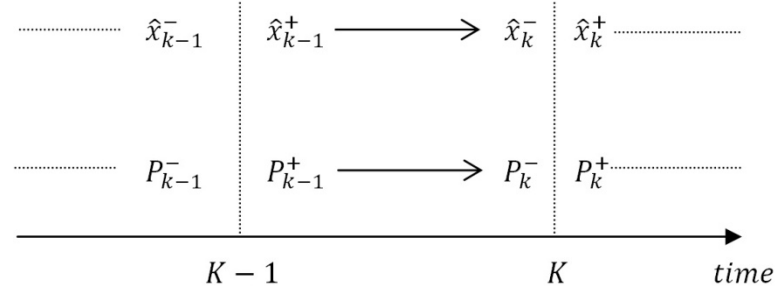
Figure 2-1:Timeline showing *a priori* and *a posteriori* state and error covariance estimation [9]

Now, it is possible to write an update equation for the new estimate (*a posteriori* estimate), by combining the previous estimate (*a priori* estimate) as follows:

$$\hat{x}^+_k = \hat{x}^-_k + K_k[y_k - H_k\hat{x}^-_k] \tag{2.40}$$

The matrix K_k in the above equation is called the Kalman gain and the term $y_k - H_k\hat{x}^-_k$ is known as the *innovation* or *measurement residual* [10]. This matrix is chosen such that the *a posteriori* error covariance (P^+_k) is minimized. The minimization is carried out by substituting Equation (2.40) into the second term of Equation (2.39) which is the definition for P^+_k. Then, the indicated expectation is performed and the derivative of the trace of the result with respect to K is calculated. By setting the result equal to zero and then solving for K, the final expression for the Kalman gain K can be given as [10]

$$K_k = P_k^- H_k^T (H_k P_k^- H_k^T + R_k)^{-1} \tag{2.41}$$

Considering the dynamic system presented in Equations (2.34) and (2.35), the discrete-time Kalman filter is summarized here as a recursive algorithm [9].

1. The filter is initialized as follows:

$$\hat{x}_0^+ = E(x_0)$$
$$P_0^+ = E[(x_0 - \hat{x}_0^+)(x_0 - \hat{x}_0^+)^T] \tag{2.42}$$

2. The prediction step or time update is accomplished as

$$P_k^- = F_{k-1} P_{k-1}^+ F_{k-1}^T + Q_{k-1}$$
$$K_k = P_k^- H_k^T (H_k P_k^- H_k^T + R_k)^{-1}$$
$$\hat{x}_k^- = F_{k-1}\hat{x}_{k-1}^+ + G_{k-1}u_{k-1} = a \; priori \; state \; estimate \tag{2.43}$$

3. The correction step or measurement update is completed by the following equations.

$$\hat{x}_k^+ = \hat{x}_k^- + K_k[y_k - H_k\hat{x}_k^-] = a \; posteriori \; state \; estimate$$
$$P_k^+ = (I - K_k H_k)P_k^- \tag{2.44}$$

The ongoing discrete Kalman filter cycle is presented in the following figure.
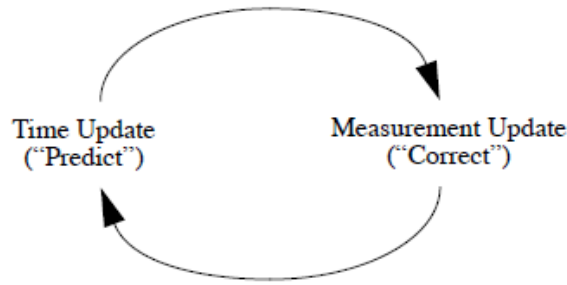
Figure 2-2: The ongoing discrete Kalman filter cycle [10]

2-5-2. Extended Kalman Filter

The discussion hitherto was dedicated to linear systems; however, real systems are eventually nonlinear. Even a simple relationship between current and voltage of a resistor is not linear for all values and Ohm's Law is only an approximation over a certain linear range [9]. This linear function can describe the behavior of a resistor until the voltage does not exceed a certain threshold. Although many systems are close enough to linear such that linear estimation methods provide satisfactory results, in many others this is not true, and some systems are not even linear over a small range of operation. Therefore, the use of nonlinear estimators is inevitable.

Nonlinear estimation is not yet fully developed and there is still a lot of space for research in this field. Extended Kalman Filter (EKF), Unscented Kalman Filter (UKF), and particle filter are among the most popular and widespread nonlinear estimation approaches developed up to this moment. EKF and UKF are selected for this research and explained in detail in the next parts of this chapter.

Extended Kalman filter is a nonlinear extension of Kalman filter [9, 10]. It is also possible to use linearization method explained in Section 2-3 for a nonlinear system and apply linear Kalman filter for state estimation. Nevertheless, the main goal of this section is to develop a nonlinear estimation method based on Kalman filter. In the following section, the equations of discrete-time Extended Kalman filter are derived.

Considering a discretized dynamic system, the system model can be written as [9]

$$
\begin{aligned}
x_k &= f_{k-1}(x_{k-1}, u_{k-1}, w_{k-1}) \\
y_k &= h_k(x_k, v_k) \\
w_k &\sim (0, Q_k) \\
v_k &\sim (0, R_k)
\end{aligned}
\tag{2.45}
$$

In this equation, x_k represents the state vector, u_k is the control input vector, f is the nonlinear function of the states and inputs, y_k is the output vector, w_k and v_k are the process and measurement noise, Q_k and R_k are the process and measurement noise covariance, and k is the time step for the discrete model. By performing a Taylor series expansion of the state equation around $x_{k-1} = \hat{x}_{k-1}^+$ and $w_{k-1} = 0$, Equation (2.45) can be written as [9]

$$
\begin{aligned}
x_k &= f_{k-1}(\hat{x}_{k-1}^+, u_{k-1}, 0) + \left.\frac{\partial f_{k-1}}{\partial x}\right|_{\hat{x}_{k-1}^+} (x_{k-1} - \hat{x}_{k-1}^+) + \left.\frac{\partial f_{k-1}}{\partial w}\right|_{\hat{x}_{k-1}^+} w_{k-1} \\
&= f_{k-1}(\hat{x}_{k-1}^+, u_{k-1}, 0) + F_{k-1}(x_{k-1} - \hat{x}_{k-1}^+) + L_{k-1} w_{k-1} \\
&= F_{k-1} x_{k-1} + [f_{k-1}(\hat{x}_{k-1}^+, u_{k-1}, 0) - F_{k-1}\hat{x}_{k-1}^+] + L_{k-1} w_{k-1} \\
&= F_{k-1} x_{k-1} + \tilde{u}_{k-1} + \tilde{w}_{k-1}
\end{aligned}
\tag{2.46}
$$

The definitions of F_{k-1} and L_{k-1} are presented in Equation (2.46). The known input

signal $\tilde{u}_k$ and the noise signal $\tilde{w}_k$ are also expressed by the following equation.

$$\tilde{u}_k = f_k(\hat{x}_k^+, u_k, 0) - F_k\hat{x}_k^+$$

$$\tilde{w}_k \sim (0, L_k Q_k L_k^T) \qquad (2.47)$$

The measurement equation linearized around $x_k = \hat{x}_k^-$ and $v_k = 0$ is presented below.

$$
\begin{aligned}
y_k &= h_k(\hat{x}_k^-, 0) + \frac{\partial h_k}{\partial x}\bigg|_{\hat{x}_k^-} (x_k - \hat{x}_k^-) + \frac{\partial h_k}{\partial v}\bigg|_{\hat{x}_k^-} v_k \\
&= h_k(\hat{x}_k^-, 0) + H_k(x_k - \hat{x}_k^-) + M_k v_k \\
&= H_k x_k + [h_k(\hat{x}_k^-, 0) - H_k\hat{x}_k^-] + M_k v_k \\
&= H_k x_k + z_{k-1} + \tilde{v}_k \qquad (2.48)
\end{aligned}
$$

H_k and M_k are defined by Equation (2.48) and the known signal z_k and the noise signal

$\tilde{v}_k$ are defined as follows.

$$z_k = h_k(\hat{x}_k^-, 0) - H_k\hat{x}_k^-$$

$$\tilde{v}_k \sim (0, M_k R_k M_k^T) \qquad (2.49)$$

Using the time and measurement update Equations (2.43) and (2.44) for linear Kalman

filter and equations derived for EKF up to this point, the discrete-time EKF for a

nonlinear system presented in Equation (2.45) can be summarized as follows [9, 10]:

1. The filter is initialized as follows:

$$\hat{x}_0^+ = E(x_0)$$

$$P_0^+ = E[(x_0 - \hat{x}_0^+)(x_0 - \hat{x}_0^+)^T] \tag{2.50}$$

2. Partial derivative matrices of the system equation are derived using the following equation.

$$F_{k-1} = \left.\frac{\partial f_{k-1}}{\partial x}\right|_{\hat{x}_{k-1}^+}$$

$$L_{k-1} = \left.\frac{\partial f_{k-1}}{\partial w}\right|_{\hat{x}_{k-1}^+} \tag{2.51}$$

3. Time update equations of EKF are as follows:

$$P_k^- = F_{k-1}P_{k-1}^+F_{k-1}^T + L_{k-1}Q_{k-1}L_{k-1}^T$$

$$\hat{x}_k^- = f_{k-1}(\hat{x}_{k-1}^+, u_{k-1}, 0) \tag{2.52}$$

4. Partial derivative matrices of the output equation are obtained by Equation (2.53).

$$H_k = \left.\frac{\partial h_k}{\partial x}\right|_{\hat{x}_k^-}$$

$$M_k = \left.\frac{\partial h_k}{\partial v}\right|_{\hat{x}_k^-} \tag{2.53}$$

5. The final step is the measurement update for which the related equations are as follows:

$$K_k = P_k^- H_k^T (H_k P_k^- H_k^T + M_k R_k M_k^T)^{-1}$$

$$\hat{x}_k^+ = \hat{x}_k^- + K_k[y_k - h_k(\hat{x}_k^-, 0)]$$

$$P_k^+ = (I - K_k H_k)P_k^- \qquad (2.54)$$

In the above expressions, $\hat{x}_k^-$ is *a priori* state estimate at step k based on the knowledge of the process prior to this step, $\hat{x}_k^+$ is *a posteriori* state estimate at step k based on the measurement y_k, P_k^- and P_k^+ is the *a priori* and *a posteriori* estimate error covariance, F_{k-1} is the Jacobian matrix of f with respect to x, and K_k is the Kalman gain that minimizes the error covariance.

One of the interesting and unique features of EKF is its ability for online parameter estimation. In other words, the state vector of the system can be augmented to the parameters of the system and they become updated in each iteration. This capability has a great value for systems with slow changing parameters during operational conditions. An example for this physical phenomenon is an electrical machine in different operating conditions. The main parameters of the machine like rotor and stator resistances are influenced by the frequency and the temperature of the machine. However, as EKF linearizes the system equations around each state estimation and deploys only the first order term of Taylor series, in systems with high degree of nonlinearity, it might not capture the whole nonlinearity of the system and the mean and covariance of the estimated states are occasionally different from the real states. This problem may lead us to use UKF which approximates mean and covariance of states up to third order.

2-5-3. Unscented Kalman Filter

The basis of the unscented transformation is that "*it is easier to approximate a probability distribution than it is to approximate an arbitrary nonlinear function or transformation*" [12]. It is worth to investigate how mean and covariance propagate in nonlinear equations to understand better the idea of unscented transformation.

Consider the following nonlinear functions [9]

$$y_1 = r \cos \theta$$
$$y_2 = r \sin \theta \qquad (2.55)$$

Which is a standard polar to rectangular transformation. This coordinate transformation can be generally written as follows:

$$y = h(x) \qquad (2.56)$$

In this equation, y is the two-element function of $h(x)$ and the two-element vector x is defined as

$$x = \begin{bmatrix} r \\ \theta \end{bmatrix} \qquad (2.57)$$

Suppose that x_1 and x_2 are random variables defined as

$$x_1 \sim (1, \sigma_r)$$
$$x_1 \sim (\pi/2, \sigma_\theta) \qquad (2.58)$$

Performing a first order linearization of Equation (2.56) and taking the expected value of both sides results in

$$\bar{y} = E[h(x)]$$

$$\approx E\left[h(\bar{x}) + \frac{\partial h}{\partial x}\bigg|_{\bar{x}} (x - \bar{x})\right]$$

$$= h(\bar{x}) + \frac{\partial h}{\partial x}\bigg|_{\bar{x}} E(x - \bar{x})$$

$$= h(\bar{x})$$

$$= \begin{bmatrix} 0 \\ 1 \end{bmatrix} \tag{2.59}$$

For more accurate evaluation of the mean through a nonlinear system, r and θ can be expressed as

$$r = \bar{r} + \tilde{r}$$

$$\theta = \bar{\theta} + \tilde{\theta} \tag{2.60}$$

Which $\tilde{r}$ and $\tilde{\theta}$ are the deviations of r and θ from their means. A thorough analysis of the mean of y_1 can be written as follows [9]:

$$\bar{y}_1 = E(r \cos \theta)$$

$$= E\left[(\bar{r} + \tilde{r}) \cos(\bar{\theta} + \tilde{\theta})\right]$$

$$= E\left[(\bar{r} + \tilde{r})(\cos \bar{\theta} \cos \tilde{\theta} - \sin \bar{\theta} \sin \tilde{\theta})\right] \tag{2.61}$$

By performing the multiplication, keeping in mind that $\tilde{r}$ and $\tilde{\theta}$ are independent with symmetric probability density functions (pdf), the expected value of y_1 is equal to

$$\bar{y}_1 = \bar{r} \cos \bar{\theta}$$

$$= 0 \tag{2.62}$$

The first order approximation of $\bar{y}_1$ is confirmed by Equation (2.62). For $\bar{y}_2$ it can be written as [9]

$$\bar{y}_2 = E(r \sin \theta)$$

$$= E[(\bar{r} + \tilde{r}) \sin(\bar{\theta} + \tilde{\theta})]$$

$$= E[(\bar{r} + \tilde{r})(\sin \bar{\theta} \cos \tilde{\theta} + \cos \bar{\theta} \sin \tilde{\theta})] \tag{2.63}$$

As $E[\tilde{r}] = 0$, Equation (2.63) is simplified as follows:

$$\bar{y}_2 = \bar{r} \sin \bar{\theta} \, E(\cos \tilde{\theta})$$

$$= E(\cos \tilde{\theta}) \tag{2.64}$$

Without assuming the distribution for $\tilde{\theta}$, it is not possible to simplify this expression further. If $\tilde{\theta}$ is uniformly distributed between $\pm \theta_m$, the mean of y_2 is

$$\bar{y}_2 = E(\cos \tilde{\theta})$$

$$= \frac{\sin \theta_m}{\theta_m} \tag{2.65}$$

The mean calculated from Equation (2.65) is less than 1, which is different from the mean calculated in Equation (2.59). This difference can be seen in the following figure which is a plot of 300 randomly generated r and θ values, in which $\tilde{r}$ is uniformly distributed between ± 0.01, and $\tilde{\theta}$ is uniformly distributed between ± 0.35 radians [9].
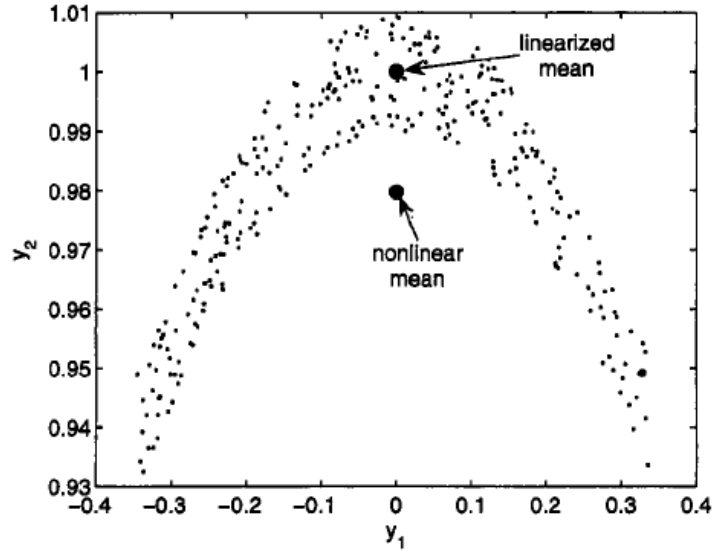
Figure 2-3: Linearized and nonlinear mean of 300 randomly generated points [9]

Based on the complete analysis of the mean propagation in [9], and by defining operator $D_{\tilde{x}}^{k} f$ as

$$D_{\tilde{x}}^{k} f = \left(\sum_{i=1}^{n} \tilde{x}_i \frac{\partial}{\partial x_i} \right)^{k} f(x)\big|_{\bar{x}} \tag{2.66}$$

and Taylor series expansion of $f(x)$ as

$$f(x) = f(\bar{x}) + D_{\tilde{x}} f + \frac{1}{2!} D_{\tilde{x}}^{2} f + \frac{1}{3!} D_{\tilde{x}}^{3} f + \cdots \tag{2.67}$$

$\bar{y}$ vector can be written as

$$\bar{y} = E \left[h(\bar{x}) + D_{\tilde{x}} h + \frac{1}{2!} D_{\tilde{x}}^{2} h + \frac{1}{3!} D_{\tilde{x}}^{3} h + \cdots \right]$$

$$= h(\bar{x}) + E\left[D_{\tilde{x}}h + \frac{1}{2!}D_{\tilde{x}}^2 h + \frac{1}{3!}D_{\tilde{x}}^3 h + \cdots\right] \tag{2.68}$$

It has been shown in [9] that odd orders in Equation (2.68) are equal to zero. Equation (2.68) is therefore simplified as follows:

$$\bar{y} = h(\bar{x}) + E\left[\frac{1}{2!}D_{\tilde{x}}^2 h + \frac{1}{4!}D_{\tilde{x}}^4 h + \cdots\right] \tag{2.69}$$

Now it is more obvious why the mean calculation in Equation (2.59) is not accurate; it is a first order approximation and as the considered system in Equation (2.55) is highly nonlinear, a major discrepancy exists between linearized and nonlinear mean. The same analysis can be done for variance of the nonlinear system to show the difference between linearized and nonlinear covariance. A comparison of the nonlinear and linearized mean and covariance of 300 randomly generated points propagated through the nonlinear system is presented in Figure 2-4.
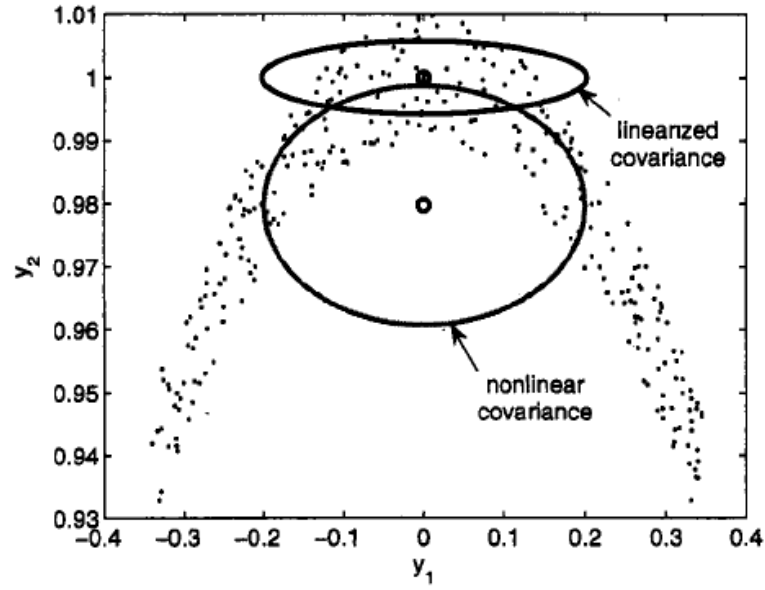
Figure 2-4: linearized and nonlinear mean and covariance of 300 randomly generated points [9]

It has been shown in [9] that the unscented transformation has the ability to propagate mean and covariance of states of a system through nonlinear dynamic model while capturing their nonlinearity up to the third order. The unscented transformation procedure is as follows:

1. An n-element vector x with known mean $\bar{x}$ and covariance P is considered. The aim is to estimate the mean and covariance of $y = h(x)$ denoted as $\bar{y}_u$ and P_u.

2. $2n$ sigma point vectors $x^{(i)}$ is formed as follows:

$$x^{(i)} = \bar{x} + \tilde{x}^{(i)} \qquad\qquad i = 1, \dots, 2n$$

$$\tilde{x}^{(i)} = \left(\sqrt{nP}\right)_i^T \qquad\qquad i = 1, \dots, n$$

$$\tilde{x}^{(n+i)} = -\left(\sqrt{nP}\right)_i^T \qquad i = 1, \ldots, n \tag{2.70}$$

Where $\sqrt{nP}$ is the matrix square root of nP such that $\left(\sqrt{nP}\right)^T \sqrt{nP} = nP$ and $\left(\sqrt{nP_{k-1}^+}\right)_i^T$

is the ith row of the matrix.

3. The sigma points are transformed as follows:

$$y^{(i)} = h\left(x^{(i)}\right) \qquad i = 1, \ldots, 2n \tag{2.71}$$

4. The mean and covariance of y are approximated as follows:

$$\bar{y}_u = \frac{1}{2n} \sum_{i=1}^{2n} y^{(i)}$$

$$P_u = \frac{1}{2n} \sum_{i=1}^{2n} \left(y^{(i)} - \bar{y}_u\right)\left(y^{(i)} - \bar{y}_u\right)^T \tag{2.72}$$

The results of the mean and covariance propagation of the 300 randomly generated points through the nonlinear system presented in Equation (2.55) using unscented, linearized and nonlinear transformation are presented in Figure 2-5. This figure shows clearly the difference between EKF and UKF in terms of mean and covariance propagation through a nonlinear system. The center point is the nonlinear and unscented mean which are the same, while the upper point is the linearized mean which has a considerable discrepancy from the true one. The unscented and exact nonlinear covariances have almost the same shape; in contrast, the linearized covariance has a totally different shape.
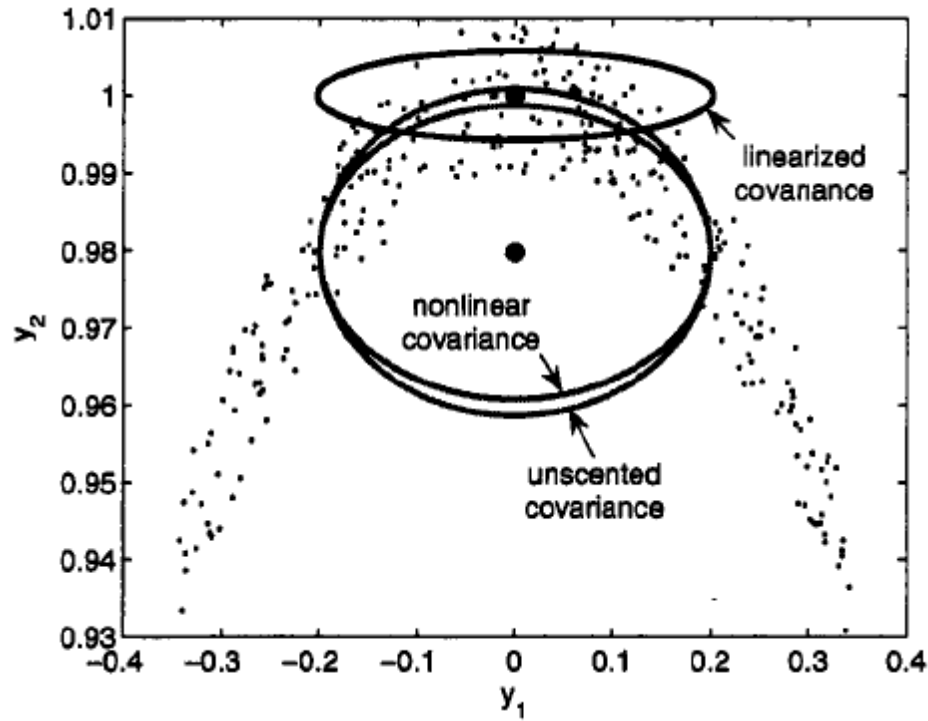
Figure 2-5: The comparison among exact, linearized, and unscented mean and covariance of 300 randomly generated points [9]

Based on the information provided in this section, it can be concluded that since EKF uses the first order linearization of the mean and the covariance of the states of a system, it is not able to find the exact values of the mean and the covariance of the propagated states in a system with high degree of nonlinearity like the system provided in Equation (2.55). In contrast, Figure 2-5 reveals the superiority of the unscented transform (UKF) over linearization approach (EKF). Using the unscented transform hitherto introduced, the Unscented Kalman filter steps can be expressed as follows:

1. The filter is initialized as follows [9]:

$$\hat{x}_0^+ = E(x_0)$$

$$P_0^+ = E[(x_0 - \hat{x}_0^+)(x_0 - \hat{x}_0^+)^T] \tag{2.73}$$

The mean and the covariance of the estimated states at each measurement to the next one is propagated through the following time update steps.

2. As the current best guess for the mean and covariance of x_k are $\hat{x}_{k-1}^+$ and P_{k-1}^+, sigma points $x_{k-1}^{(i)}$ are derived using the following equations and these sigma points are propagated through the nonlinear system from time step $(k-1)$ to (k).

$$\hat{x}_{k-1}^{(i)} = \hat{x}_{k-1}^- + \tilde{x}^{(i)} \qquad i = 1, 2, \dots, 2n$$

$$\tilde{x}^{(i)} = \left(\sqrt{nP_{k-1}^+}\right)_i^T \qquad i = 1, 2, \dots, n$$

$$\tilde{x}^{(n+i)} = -\left(\sqrt{nP_{k-1}^+}\right)_i^T \qquad i = 1, 2, \dots, n \tag{2.74}$$

In this equation, n is the number of system's states, and $\sqrt{nP}$ is the matrix square root of nP such that $\left(\sqrt{nP}\right)^T \sqrt{nP} = nP$ and $\left(\sqrt{nP_{k-1}^+}\right)_i^T$ is the ith row of the matrix.

3. In this step using the known nonlinear system equation f, $2n$ sigma points created in the previous step are propagated through the system and $\hat{x}_k^{(i)}$ which also is a $2n$ vector is obtained as follows:

$$\hat{x}_k^{(i)} = f\left(\hat{x}_{k-1}^{(i)}, u_k, t_k\right) \tag{2.75}$$

4. The *a priori* state estimate is obtained by combining all the vectors of $\hat{x}_k^{(i)}$ by Equation (2.76).

$$\hat{x}_k^- = \frac{1}{2n} \sum_{i=1}^{2n} \hat{x}_k^{(i)} \qquad (2.76)$$

5. The *a priori* estimate for error covariance matrix is derived by Equation (2.77).

$$P_k^- = \frac{1}{2n} \sum_{i=1}^{2n} \left(\hat{x}_k^{(i)} - \hat{x}_k^- \right) \left(\hat{x}_k^{(i)} - \hat{x}_k^- \right)^T + Q_{k-1} \qquad (2.77)$$

6. The measurement update steps are presented here. The new sigma points are selected based on updated $\hat{x}_k^-$ and P_k^-.

$$\hat{x}_k^{(i)} = \hat{x}_k^- + \tilde{x}^{(i)} \qquad i = 1,2, \dots, 2n$$

$$\tilde{x}^{(i)} = \left(\sqrt{nP_k^-} \right)_i^T \qquad i = 1,2, \dots, n$$

$$\tilde{x}^{(n+i)} = -\left(\sqrt{nP_k^-} \right)_i^T \qquad i = 1,2, \dots, n \qquad (2.78)$$

7. In this step, the sigma points $\hat{x}_k^{(i)}$ are transformed into $\hat{y}_k^{(i)}$ using the known nonlinear output equation $h(.)$ as follows:

$$\hat{y}_k^{(i)} = h\left(\hat{x}_k^{(i)}, t_k \right) \qquad (2.79)$$

8. The prediction for measurement at time step k is obtained by Equation (2.80).

$$\hat{y}_k = \frac{1}{2n} \sum_{i=1}^{2n} \hat{y}_k^{(i)} \tag{2.80}$$

9. In this step, the covariance of the predicted measurement is calculated.

$$P_y = \frac{1}{2n} \sum_{i=1}^{2n} \left(\hat{y}_k^{(i)} - \hat{y}_k\right)\left(\hat{y}_k^{(i)} - \hat{y}_k\right)^T + R_k \tag{2.81}$$

10. The cross covariance between $\hat{x}_k^-$ and $\hat{y}_k$ is calculated by Equation (2.82).

$$P_{xy} = \frac{1}{2n} \sum_{i=1}^{2n} \left(\hat{x}_k^{(i)} - \hat{x}_k^-\right)\left(\hat{y}_k^{(i)} - \hat{y}_k\right)^T \tag{2.82}$$

11. The measurement update of the states estimates of the system calculated in the previous steps is performed using Equation (2.83).

$$K_k = P_{xy}P_y^{-1}$$
$$\hat{x}_k^+ = \hat{x}_k^- + K_k(y_k - \hat{y}_k)$$
$$P_k^+ = P_k^- - K_k P_y K_k^T \tag{2.83}$$

For better understanding of the nonlinear estimation methods presented in this chapter, EKF and UKF are applied for state and parameter estimation in Induction Motor (IM),

Single-Machine-Infinite-Bus (SMIB), and IEEE 3-Generator-9-Bus Test System in the subsequent chapters.

2-6. Summary

In this chapter, after a brief explanation about state space modeling of the systems, the mathematical principles of linear and nonlinear systems are presented. Different approaches for linearization of nonlinear systems and discretization are discussed in detail. Kalman filter, as one of the most famous approaches of optimal state estimation for linear systems is then presented. Extended Kalman filter, as a developed state estimator for nonlinear systems, and the related step by step formulation are presented. Finally, the principles of unscented transform and unscented Kalman filter procedure are explained.

CHAPTER 3

3. Dynamic State Estimation in Induction Motor

3-1. Introduction

State estimation in Induction Motors (IMs) has been an interesting area of research. Estimation of the main states of an IM including speed of the machine results in mechanical speed sensors (e.g. tachometer) elimination. EKF and UKF are among the most referred estimation methods for this purpose due to the recursive nature which makes them suitable for implementation on digital platforms. Reduced order EKF has been proposed by some authors to reduce computational efforts [13, 14]. Small range of speed and load torque changes can be estimated by this kind of EKF. In [15, 16], to obtain a more powerful observer, a full order EKF is deployed for estimating speed as a

parameter with small variation. The main drawback of this EKF based estimator is that it is not able to follow the states of the system in transient time. In some research, equation of motion is added to the state space model to make it more appropriate for dynamic state estimation [13, 17]. However, the lack of accurate information about the load torque is still a challenge in this approach which encouraged [18] to propose an extended estimator with the ability of online load torque estimation. As the rotor and stator resistances are highly sensitive to temperature and frequency of the motor, the main goal in [19- 23] is to design an EKF based estimator which is capable of estimating parameters of the motor along with its main states. As explained in the previous chapter, EKF is able to approximate the mean and covariance of the states of a nonlinear transformation only to the first order. Thus, UKF is used in [24] for state estimation in an IM to overcome this drawback and capture better the nonlinearity of the system.

In this chapter, several state estimators based on EKF and UKF are designed and simulated on an IM and the simulation results are compared. The aim of this chapter is to show the strong and weak points of both methods, based on different simulation scenarios.

3-2. Induction Motor State Space Model

The state space model of an IM is composed of four independent state variables, namely rotor flux components (ψ_{qr} , ψ_{dr}), stator-current components (i_{qs} , i_{ds}), which are the q and d axis components obtained by Park transformation. By considering the dynamic

motion equation of an IM, the state vector can also be extended to ω_m, angular velocity. There are also two inputs for this model which are stator-voltage components (v_{qs}, v_{ds}) [21, 22]. Also, the stator current components are considered as output signals of this model. Using the general form of nonlinear systems, Equation (2.9), the state space model of an IM extended to speed as a parameter is as follows [21, 22]:

$$
\underbrace{\begin{bmatrix} i'_{ds} \\ i'_{qs} \\ \psi'_{dr} \\ \psi'_{qr} \\ \omega'_m \end{bmatrix}}_{x'} = \underbrace{\begin{bmatrix} -\left(\dfrac{R_s}{L_\delta}+\dfrac{R'_r L_m^2}{L'^2_r L_\delta}\right) & 0 & \dfrac{R'_r L_m}{L'^2_r L_\delta} & \dfrac{L_m}{L_\delta L'_r}P_p\omega_m & 0 \\ 0 & -\left(\dfrac{R_s}{L_\delta}+\dfrac{R'_r L_m^2}{L'^2_r L_\delta}\right) & -\dfrac{L_m}{L_\delta L'_r}P_p\omega_m & \dfrac{R'_r L_m}{L'^2_r L_\delta} & 0 \\ \dfrac{R'_r}{L'_r}L_m & 0 & -\dfrac{R'_r}{L'_r} & -P_p\omega_m & 0 \\ 0 & \dfrac{R'_r}{L'_r}L_m & P_p\omega_m & -\dfrac{R'_r}{L'_r} & 0 \\ 0 & 0 & 0 & 0 & 0 \end{bmatrix}}_{A} \underbrace{\begin{bmatrix} i_{ds} \\ i_{qs} \\ \psi_{dr} \\ \psi_{qr} \\ \omega_m \end{bmatrix}}_{x} + \underbrace{\begin{bmatrix} \dfrac{1}{L_\delta} & 0 \\ 0 & \dfrac{1}{L_\delta} \\ 0 & 0 \\ 0 & 0 \\ 0 & 0 \end{bmatrix}}_{B} \underbrace{\begin{bmatrix} v_{ds} \\ v_{qs} \end{bmatrix}}_{u} + w_t
$$

$$
\underbrace{\begin{bmatrix} i_{ds} \\ i_{qs} \end{bmatrix}}_{y} = \underbrace{\begin{bmatrix} 1 & 0 & 0 & 0 \\ 0 & 1 & 0 & 0 \end{bmatrix}}_{C} \underbrace{\begin{bmatrix} i_{ds} \\ i_{qs} \\ \psi_{dr} \\ \psi_{qr} \end{bmatrix}}_{x} + v_t
$$

(3.1)

In this model, R_s and R_r are the stator and rotor resistances; P_p is the pole pairs; $L_\delta = \delta L_s$ is the stator transient inductance; $\delta = 1 - (L_m^2/L_s L'_r)$ is the leakage or coupling factor; L_m is the mutual inductance; $L_s = L_{ls} + L_m$ and $L'_r = L'_{lr} + L_m$ are the inductances of the stator and the rotor; and L_{ls} and L'_{lr} are the leakage inductances of the stator and the rotor. For more clarity, the estimation process is presented in Figure 3-1.
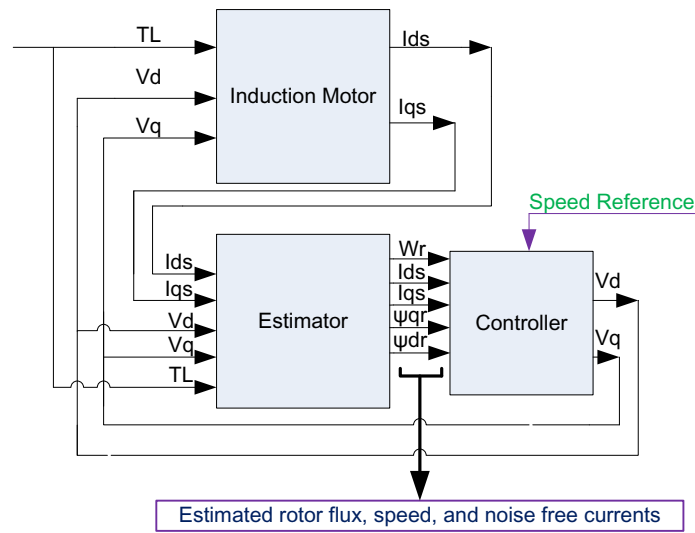
Figure 3-1: General diagram of state estimation in IM

This diagram shows that a general estimator, which is based on a state space model of the motor and an optimal estimation approach such as Kalman filter, is able to estimate all of the states of the system (including measurable and immeasurable ones), and eliminate the effect of noise. The noise free measurements and estimated states are finally used to improve control performance of the system. Another property of this observer is to estimate speed of the rotor with high accuracy which is desirable for sensorless motor drive systems.

3-3. Applying EKF on Induction Motor for State Estimation

In this section, a complete performance evaluation of different Kalman filter based estimators for IM are presented using various practical simulation scenarios. These simulation scenarios are as follows:

1. In scenario one, speed estimation is performed while speed, load torque and IM parameters are considered as constant values.

2. In scenario two, only the load torque varies with small variations.

3. In scenario three, both reference speed and load torque vary with small variations.

4. In scenario four, wide range of changes is considered for reference speed of the IM while load torque and the main parameters vary with small variation.

5. In scenario five speed changes in a wide range but load torque and main parameters are considered with small changes.

6. Finally in scenario six, both reference speed and load torque change in wide ranges while the main parameters of IM have small and slow variations.

In addition, three different state space models are proposed for better evaluation of the estimation methods. The first model (IM-Model 1) uses Equation (3.1) where ω_m is considered as a parameter. The second model (IM-Model 2) contains equation of motion which enriches the dynamic ability of the state space model and also the state vector is augmented by T_L as a parameter. And finally the third state space model (IM-Model 3) is similar to the second model, but its state vector is extended to include both R_r and R_s. These two lateral models (IM-Model 2 and IM-Model 3) are developed in Section 3.3.2 1nd 3.3.3, respectively.

The induction motor parameters and initial value of $x, P, Q,$ and R as well as other consideration of the simulations are listed in Table 3-1.

Table 3-1: Motor parameters and initial simulation values of x, P, Q, R [21]

Parameters	Value
Rated power	2.238 kW
Rated voltage	230 V
Rated frequency	60 Hz
Rated torque	20 N.m
Rated speed	1800 rpm
Stator resistance (R_s)	0.6619 Ω/ph
Rotor resistance (R_r)	0.7322 Ω/ph
Stator inductance (L_s)	0.0375 H/ph
Rotor inductance (L'_r)	0.0376 H/ph
Magnetizing inductance (L_m)	0.0334 H/ph
Pole Pairs	2
Initial value of extended state vector	$x_0 = diag\{0,0,0,0,0,0,0,0\}$
Initial value of estimation error covariance matrix	$P_0 = diag\{10,10,10,10,10,10,10,10\}$
Process noise covariance	Q $= diag\{10^{-8}, 10^{-8}, 4$ $\times 10^{-17}, 4 \times 10^{-17}, 10^{-14}, 10^{-15}, 10^{-16}, 10^{-6}\}$
Measurement noise covariance	$R = diag\{5,5\}$

An IM model is simulated in SIMULINK, MATLAB [25] with Space Vector Modulation (SVM) drive. This model is used to generate data with $T_s = 0.00001\ sec$ sampling time, and it is presented in Figure 3-2. The simulation procedures and results are described in the following sections of this chapter, and for brevity, discretized equations of IM and calculated Jacobian matrix are presented just in Section 3-3-3.
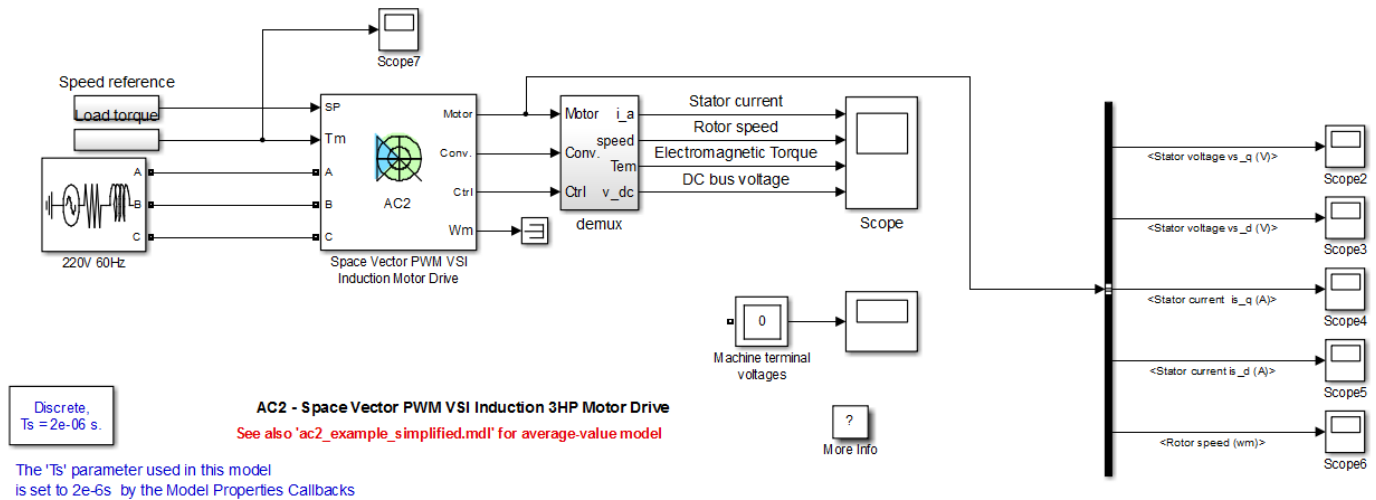
Figure 3-2: Simulink model of IM with SVM controller used for data generation

3-3-1. Speed Estimation with IM-Model 1

The speed of the IM is estimated using Equation (3.1). The equation of motion is not considered in this model and speed is treated as a parameter with slow variations. Figure 3-3 shows a comparison of the real and estimated speed of IM for scenarios one to four.
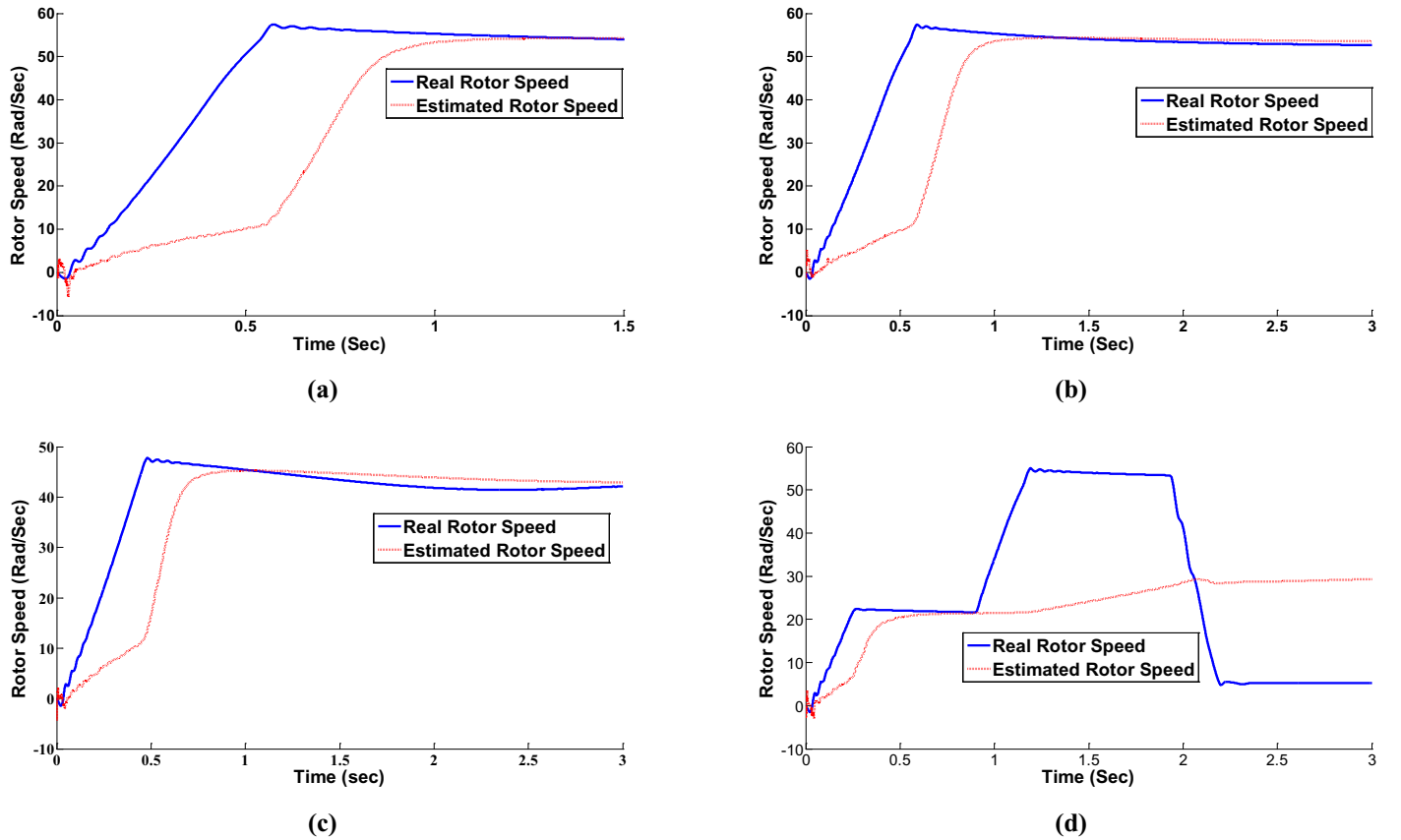
Figure 3-3: Speed estimation with IM-Model 1: (a) Scenario 1 (b) Scenario 2   (c) Scenario 3
(d) Scenario 4

In scenario four, the IM is driven with *200-rpm* reference speed and after a transient time, at $t = 1\ sec$, the speed reference is increased to *500-rpm*. At $t = 2\ sec$, the reference speed is reduced to *50-rpm* to investigate a wide range of speed variation. The load torque

is $20 \pm 1 \, N.m$, and the variation is considered slow through the time. All simulation scenarios are designed in such a way that provides better overview on the tracking ability of the designed observer in practical conditions. Based on simulation results, for applications with almost constant value of speed and small variation of load torque and parameters (Figure 3-3-a, b, and c), this kind of estimator might be acceptable. Otherwise, if the IM is driven with a wide range of speed variation as presented in Figure 3-3-d, the model does not yield accurate results.

3-3-2. Speed Estimation with IM-Model 2

Due to the simulation results of the previous section, for accurate estimation of speed over a wide range of speed variation, the equation of motion in state space model is necessary. Since the load torque is one of the parameters of motion equation, it must also be estimated as an unknown parameter in the estimation process; otherwise, a new input should be added to the model which is not desirable. Thus, the state space model of IM with the above extensions is as follows.

$$
\underbrace{\begin{bmatrix} i'_{ds} \\ i'_{qs} \\ \psi'_{dr} \\ \psi'_{qr} \\ \omega'_m \\ t'_L \end{bmatrix}}_{x'} =
\underbrace{\begin{bmatrix}
-\left(\dfrac{R_s}{L_\delta} + \dfrac{R'_r L_m^2}{L_r'^2 L_\delta} \right) & 0 & \dfrac{R'_r L_m}{L_r'^2 L_\delta} & \dfrac{L_m}{L_\delta L'_r} p_p \omega_m & 0 & 0 \\
0 & -\left(\dfrac{R_s}{L_\delta} + \dfrac{R'_r L_m^2}{L_r'^2 L_\delta} \right) & -\dfrac{L_m}{L_\delta L'_r} p_p \omega_m & \dfrac{R'_r L_m}{L_r'^2 L_\delta} & 0 & 0 \\
\dfrac{R'_r}{L'_r} L_m & 0 & -\dfrac{R'_r}{L'_r} & -p_p \omega_m & 0 & 0 \\
0 & \dfrac{R'_r}{L'_r} L_m & p_p \omega_m & -\dfrac{R'_r}{L'_r} & 0 & 0 \\
-\dfrac{3}{2}\dfrac{P_p}{J_L}\dfrac{L_m}{L'_r}\psi_{qr} & \dfrac{3}{2}\dfrac{P_p}{J_L}\dfrac{L_m}{L'_r}\psi_{dr} & 0 & 0 & 0 & -\dfrac{1}{J_L} \\
0 & 0 & 0 & 0 & 0 & 0
\end{bmatrix}}_{A}
\begin{bmatrix} i_{ds} \\ i_{qs} \\ \psi_{dr} \\ \psi_{qr} \\ \omega_m \\ t_L \end{bmatrix}_x
+
\underbrace{\begin{bmatrix} \dfrac{1}{L_\delta} & 0 \\ 0 & \dfrac{1}{L_\delta} \\ 0 & 0 \\ 0 & 0 \\ 0 & 0 \\ 0 & 0 \end{bmatrix}}_{B}
\begin{bmatrix} v_{ds} \\ v_{qs} \end{bmatrix}_u
+ w_t \quad (3.2)
$$

Note that assuming load torque as a slow changing parameter may be a correct hypothesis for many but not all applications. Therefore, in this part, the IM is simulated under scenarios four and five. The real and estimated speed and the estimated load torque of the IM are illustrated in Figure 3-4.

(a)

(b)

(c)

(d)
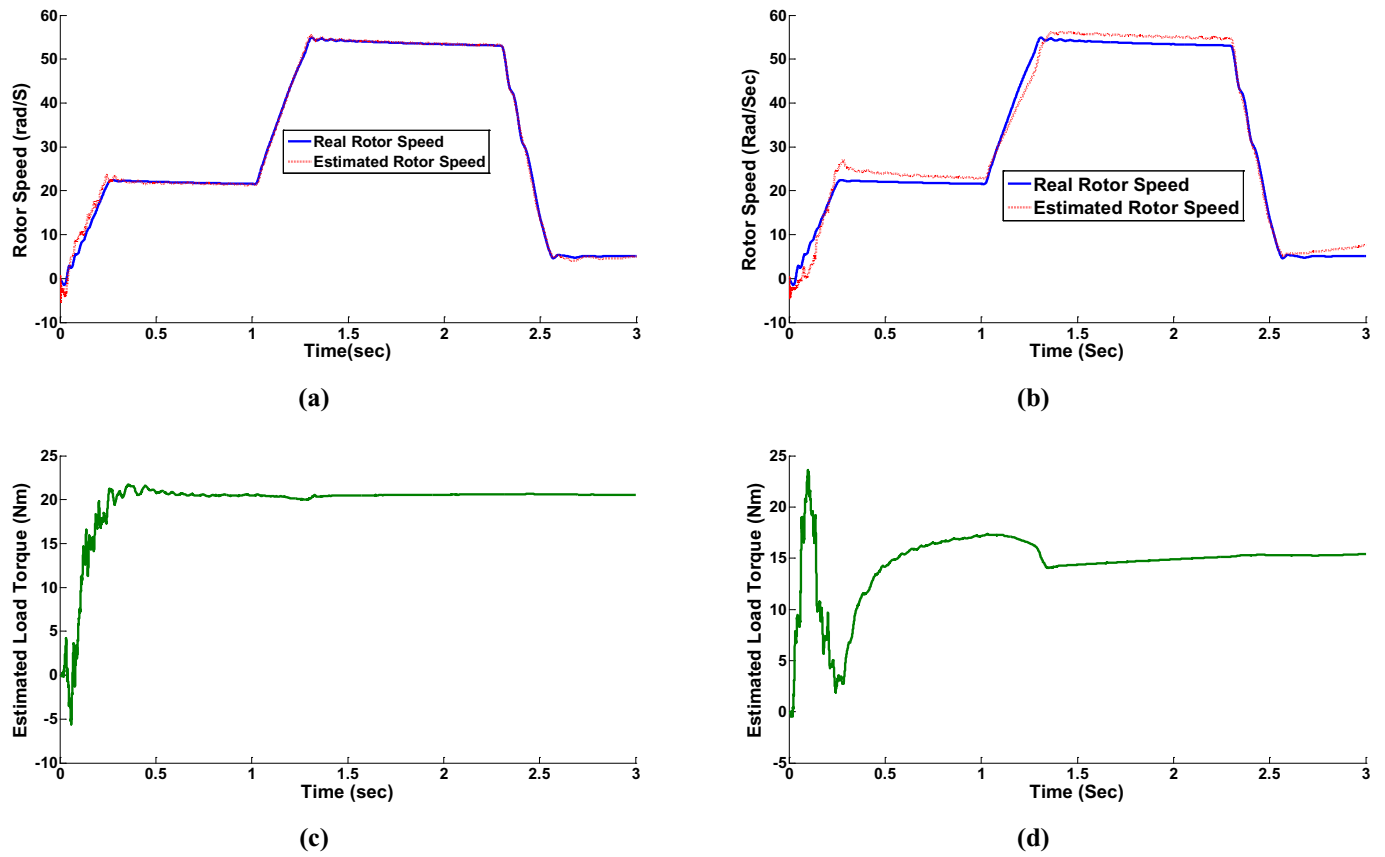
Figure 3-4: State estimation with IM-Model 2: (a) Speed, scenario 4; (b) Speed, scenario 5; (c) Load torque, scenario 4; (d) Load torque, scenario 5

Figure 3-4-b shows that the designed observer based on Equation (3.2) has steady state error in tracking the real speed in scenario five, because assuming the main parameters of

IM (rotor/stator resistances) as constant parameters is not a practical postulate . However, the estimator is able to accurately estimate speed and load torque while the main parameters of the system (rotor and stator resistances) are constant (Figure 3-4 a and b). Therefore, for more reliable estimation, these parameters are added to the state vector and updated during the estimation process, in the next section.

3-3-3. Speed Estimation with IM-Model 3

Based on [21], the rotor and stator resistances are not constant parameters and start changing with variation in motor temperature and speed. In this section, the state vector is extended to these parameters for more precise estimation. The state space model while include R_r and R_s as state variables is given as:

$$
\underbrace{\begin{bmatrix} i'_{ds} \\ i'_{qs} \\ \psi'_{dr} \\ \psi'_{qr} \\ \omega'_m \\ t'_L \\ R'_r \\ R'_s \end{bmatrix}}_{x'} =
\underbrace{\begin{bmatrix}
-\left(\dfrac{R_s}{L_\delta}+\dfrac{R'_r L_m^2}{L_r'^2 L_\delta}\right) & 0 & \dfrac{R'_r L_m}{L_r'^2 L_\delta} & \dfrac{L_m}{L_\delta L_r'}p_p\omega_m & 0 & 0 & 0 & 0 \\
0 & -\left(\dfrac{R_s}{L_\delta}+\dfrac{R'_r L_m^2}{L_r'^2 L_\delta}\right) & -\dfrac{L_m}{L_\delta L_r'}p_p\omega_m & \dfrac{R'_r L_m}{L_r'^2 L_\delta} & 0 & 0 & 0 & 0 \\
\dfrac{R'_r}{L'_r}L_m & 0 & -\dfrac{R'_r}{L'_r} & -p_p\omega_m & 0 & 0 & 0 & 0 \\
0 & \dfrac{R'_r}{L'_r}L_m & p_p\omega_m & -\dfrac{R'_r}{L'_r} & 0 & 0 & 0 & 0 \\
-\dfrac{3}{2}\dfrac{p_p}{J_L}\dfrac{L_m}{L'_r}\psi_{qr} & \dfrac{3}{2}\dfrac{p_p}{J_L}\dfrac{L_m}{L'_r}\psi_{dr} & 0 & 0 & 0 & -\dfrac{1}{J_L} & 0 & 0 \\
0 & 0 & 0 & 0 & 0 & 0 & 0 & 0 \\
0 & 0 & 0 & 0 & 0 & 0 & 0 & 0 \\
0 & 0 & 0 & 0 & 0 & 0 & 0 & 0
\end{bmatrix}}_{A}
\underbrace{\begin{bmatrix} i_{ds} \\ i_{qs} \\ \psi_{dr} \\ \psi_{qr} \\ \omega_m \\ t_L \\ R_r \\ R_s \end{bmatrix}}_{x} +
\underbrace{\begin{bmatrix} \dfrac{1}{L_\delta} & 0 \\ 0 & \dfrac{1}{L_\delta} \\ 0 & 0 \\ 0 & 0 \\ 0 & 0 \\ 0 & 0 \\ 0 & 0 \\ 0 & 0 \end{bmatrix}}_{B}
\underbrace{\begin{bmatrix} v_{ds} \\ v_{qs} \end{bmatrix}}_{u} + w_t
$$

$$
\underbrace{\begin{bmatrix} i_{ds} \\ i_{qs} \end{bmatrix}}_{y} = \underbrace{\begin{bmatrix} 1 & 0 & 0 & 0 & 0 & 0 & 0 & 0 \\ 0 & 1 & 0 & 0 & 0 & 0 & 0 & 0 \end{bmatrix}}_{C} \underbrace{\begin{bmatrix} i_{ds} & i_{qs} & \psi_{ds} & \psi_{qs} & \omega_m & t_L & R_r & R_s \end{bmatrix}^T}_{x} + v_t
$$

(3.3)

The IM state space model presented above, is discretized as Equation (3.4) where T_s is the sampling time.

$$\underbrace{\begin{bmatrix} i_{ds}^{k+1} \\ i_{qs}^{k+1} \\ \psi_{dr}^{k+1} \\ \psi_{qr}^{k+1} \\ \omega_{m}^{k+1} \\ t_{L}^{k+1} \\ R_{r}'^{k+1} \\ R_{s}^{k+1} \end{bmatrix}}_{x_{k+1}} = \underbrace{\begin{bmatrix} 1-Ts\left(\dfrac{R_s^k}{L_\delta}+\dfrac{R_r'^k L_m^2}{L_r'^2 L_\delta}\right) & 0 & Ts\dfrac{R_r'^k L_m}{L_r'^2 L_\delta} & Ts\dfrac{L_m}{L_\delta L_r'}p_p\omega_m^k & 0 & 0 & 0 & 0 \\[6pt] 0 & 1-Ts\left(\dfrac{R_s^k}{L_\delta}+\dfrac{R_r'^k L_m^2}{L_r'^2 L_\delta}\right) & -Ts\dfrac{L_m}{L_\delta L_r'}p_p\omega_m^k & Ts\dfrac{R_r'^k L_m}{L_r'^2 L_\delta} & 0 & 0 & 0 & 0 \\[6pt] Ts\dfrac{R_r'^k}{L_r'}L_m & 0 & 1-Ts\dfrac{R_r'^k}{L_r'} & -Ts\omega_m^k p_p & 0 & 0 & 0 & 0 \\[6pt] 0 & Ts\dfrac{R_r'^k}{L_r'}L_m & Ts\omega_m^k p_p & 1-Ts\dfrac{R_r'^k}{L_r'} & 0 & 0 & 0 & 0 \\[6pt] -\dfrac{3}{2}Ts\dfrac{p_p}{J_L}\dfrac{L_m}{L_r'}\psi_{qr}^k & \dfrac{3}{2}Ts\dfrac{p_p}{J_L}\dfrac{L_m}{L_r'}\psi_{dr}^k & 0 & 0 & 1 & -Ts\dfrac{1}{J_L} & 0 & 0 \\[6pt] 0 & 0 & 0 & 0 & 0 & 1 & 0 & 0 \\ 0 & 0 & 0 & 0 & 0 & 0 & 1 & 0 \\ 0 & 0 & 0 & 0 & 0 & 0 & 0 & 1 \end{bmatrix}}_{A_k} \underbrace{\begin{bmatrix} i_{ds}^{k} \\ i_{qs}^{k} \\ \psi_{dr}^{k} \\ \psi_{qr}^{k} \\ \omega_{m}^{k} \\ t_{L}^{k} \\ R_{r}'^{k} \\ R_{s}^{k} \end{bmatrix}}_{x_k} + \underbrace{\begin{bmatrix} \dfrac{Ts}{L_\delta} & 0 \\[4pt] 0 & \dfrac{Ts}{L_\delta} \\[4pt] 0 & 0 \\ 0 & 0 \\ 0 & 0 \\ 0 & 0 \\ 0 & 0 \\ 0 & 0 \end{bmatrix}}_{B} \underbrace{\begin{bmatrix} v_{ds}^k \\ v_{qs}^k \end{bmatrix}}_{u_k} + w_k$$

$$\underbrace{\begin{bmatrix} i_{ds}^{k+1} \\ i_{qs}^{k+1} \end{bmatrix}}_{y} = \underbrace{\begin{bmatrix} 1 & 0 & 0 & 0 & 0 & 0 & 0 & 0 \\ 0 & 1 & 0 & 0 & 0 & 0 & 0 & 0 \end{bmatrix}}_{C} \underbrace{\begin{bmatrix} i_{ds}^{k+1} & i_{qs}^{k+1} & \psi_{ds}^{k+1} & \psi_{qs}^{k+1} & \omega_{m}^{k+1} & t_{L}^{k+1} & R_{r}^{k+1} & R_{s}^{k+1} \end{bmatrix}^T}_{x} + v_k \qquad (3.4)$$

The Jacobian matrix can be calculated Using Equation (2.51) as follows:

$$F = \begin{bmatrix} 1-Ts\left(\dfrac{R_s^k}{L_\delta}+\dfrac{R_r'^k L_m^2}{L_r'^2 L_\delta}\right) & 0 & Ts\dfrac{R_r'^k L_m}{L_r'^2 L_\delta} & Ts\dfrac{L_m}{L_\delta L_r'}p_p\omega_m^k & Ts\dfrac{L_m}{L_\delta L_r'}p_p\psi_{qr}^k & 0 & -Ts\dfrac{L_m^2}{L_r'^2 L_\delta}i_{ds}^k+Ts\dfrac{L_m}{L_r'^2 L_\delta}\psi_{dr}^k & -Ts\dfrac{i_{ds}^k}{L_\delta} \\[8pt] 0 & 1-Ts\left(\dfrac{R_s^k}{L_\delta}+\dfrac{R_r'^k L_m^2}{L_r'^2 L_\delta}\right) & -Ts\dfrac{L_m}{L_\delta L_r'}p_p\omega_m^k & Ts\dfrac{R_r'^k L_m}{L_r'^2 L_\delta} & -Ts\dfrac{L_m}{L_\delta L_r'}p_p\psi_{dr}^k & 0 & -Ts\dfrac{L_m^2}{L_r'^2 L_\delta}i_{qs}^k+Ts\dfrac{L_m}{L_r'^2 L_\delta}\psi_{qr}^k & -Ts\dfrac{i_{qs}^k}{L_\delta} \\[8pt] Ts\dfrac{R_r'^k}{L_r'}L_m & 0 & 1-Ts\dfrac{R_r'^k}{L_r'} & -Ts\omega_m^k p_p & -Ts\psi_{qr}^k p_p & 0 & Ts\dfrac{L_m}{L_r'}i_{ds}^k-Ts\dfrac{\psi_{dr}^k}{L_r'} & 0 \\[8pt] 0 & Ts\dfrac{R_r'^k}{L_r'}L_m & Ts\omega_m^k p_p & 1-Ts\dfrac{R_r'^k}{L_r'} & Ts\psi_{dr}^k p_p & 0 & Ts\dfrac{L_m}{L_r'}i_{qs}^k-Ts\dfrac{\psi_{qr}^k}{L_r'} & 0 \\[8pt] -\dfrac{3}{2}Ts\dfrac{p_p}{J_L}\dfrac{L_m}{L_r'}\psi_{qr}^k & \dfrac{3}{2}Ts\dfrac{p_p}{J_L}\dfrac{L_m}{L_r'}\psi_{dr}^k & \dfrac{3}{2}Ts\dfrac{p_p}{J_L}\dfrac{L_m}{L_r'}i_{qs}^k & -\dfrac{3}{2}Ts\dfrac{p_p}{J_L}\dfrac{L_m}{L_r'}i_{ds}^k & 1 & -Ts\dfrac{1}{J_L} & 0 & 0 \\[8pt] 0 & 0 & 0 & 0 & 0 & 1 & 0 & 0 \\ 0 & 0 & 0 & 0 & 0 & 0 & 1 & 0 \\ 0 & 0 & 0 & 0 & 0 & 0 & 0 & 1 \end{bmatrix}$$

$$(3.5)$$

Considering the discretized state space model of the IM and Jacobian matrix presented in Equations (3.4) and (3.5), EKF based estimation is carried out under scenario 5 and the results are presented in Figure 3-5.

(a)

(b)

(c)

(d)
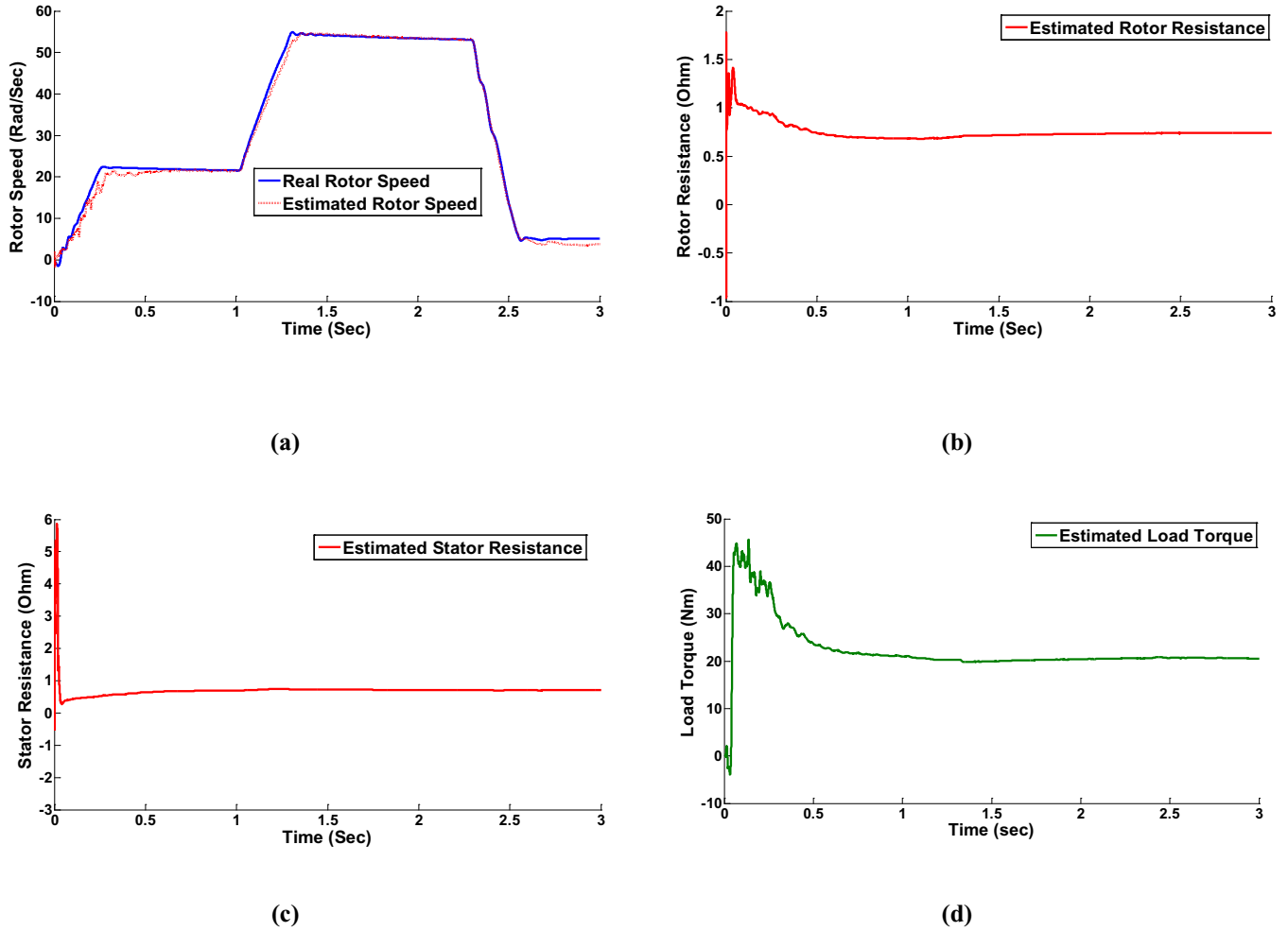
Figure 3-5: State estimation with IM-Model 3 under scenario 5: (a) Speed; (b) Rotor resistance; (c) Stator resistance; (d) Load torque

The results prove that the designed observer in this section has the ability to estimate speed in a wide range without sensitivity to the small variations of the IM's main parameters and the load torque. Comparing Figure 3-5-a and Figure 3-4-b, it can be

concluded that the estimator based on IM-Model 3 has more accurate speed estimation than the previous models. This accuracy is the direct result of estimating load torque and main parameters of the motor along with the primary states of the machine.

Scenario six which is a more complicated operational condition is used to show the ability of EKF for online state and parameter estimation. The time and reference speed vector applied to the motor drive in this simulation scenario is given below.

$$t = \begin{bmatrix} 0 & 1 & 2 & 3 & 4 & 5 \end{bmatrix} \, sec \qquad w_{m,ref} = \begin{bmatrix} 50 & 150 & 450 & 750 & 950 & 80 \end{bmatrix} \, rpm.$$

Also, the time and load torque vector of this simulation scenario is considered as follows:

$$t = \begin{bmatrix} 0 & 1.5 & 2.5 & 3.5 & 4.5 & 5.5 \end{bmatrix} \, sec \qquad T_{l,ref} = \begin{bmatrix} 8 & 20 & 14 & 16 & 20 & 24 \end{bmatrix} \, N.m$$

The simulation results for this scenario are presented in Figure 3-6. Figure 3-6-a shows that except for the transient times, the estimator has accurately followed the real speed of the rotor in a wide range of variation through a short period of time. Figures 3-6-b and 3-6-c reveal the ability of the EKF based estimator designed in this part to reject noise on the measurement signals. Figures 3-6-d and 3-6-e show the variations of the estimated rotor and stator resistances during the motor operation. The EKF based estimator designed in this part using the extended model presented in Equation (3.4) is also able to track load torque with acceptable accuracy based on the results presented in Figure 3-6-f, which results to high accuracy speed estimation in dynamic operation.
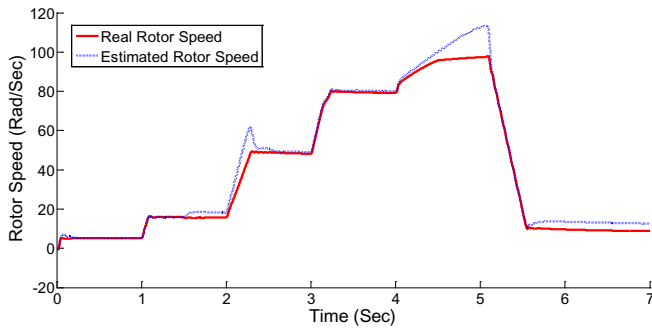
(a)
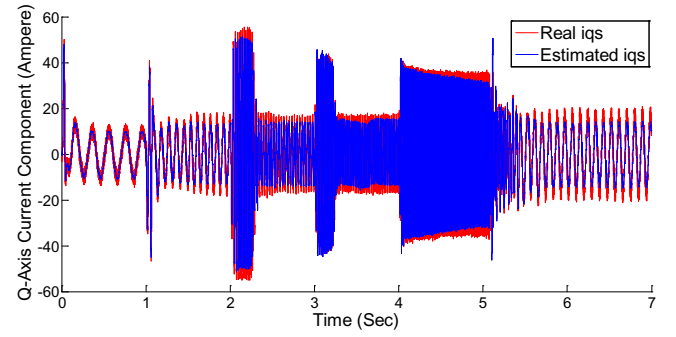
(b)
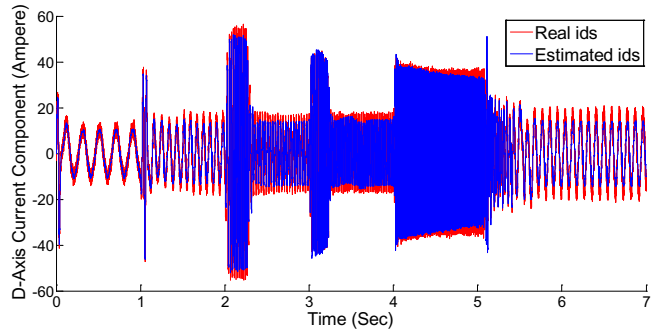
(c)
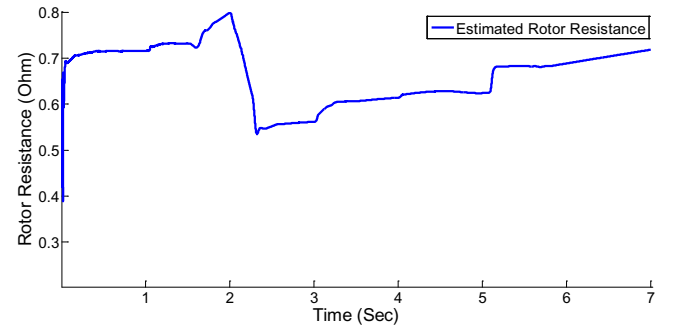
(d)
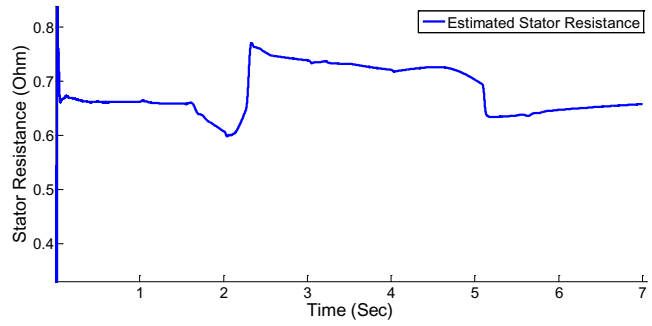
(e)
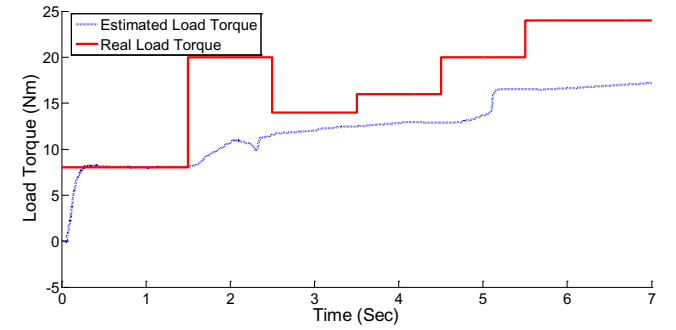
(f)

Figure 3-6: State estimation with IM-Model 3 under scenario 6: (a) Speed; (b) Q-axis current component i_{qs}; (c) D-axis current component i_{ds}; (d) Rotor resistance; (e) Stator resistance; (f) load torque

It is obvious that the value of the main parameters of the IM (R_r, R_s and T_l) are not provided for the estimator and they are estimated in each iteration. The simulation results of this section show that the designed EKF based estimator using IM-Model 3 is able to estimate speed with acceptable error in a wide range of reference speed variations, while load torque has large changes through the time, and the main parameters of IM are not constant.

3-4. Applying UKF on Induction Motor for State Estimation

Although UKF has valuable characteristic of third order estimation of mean and covariance of states of nonlinear models, it has not been completely developed for online parameter estimation and there is lack of literature in this regard. Therefore, the state space model of IM is changed in this part and load torque is considered as an input value. This model is presented below.

$$
\underbrace{\begin{bmatrix} i'_{ds} \\ i'_{qs} \\ \psi'_{dr} \\ \psi'_{qr} \\ \omega'_m \end{bmatrix}}_{x'} = \underbrace{\begin{bmatrix} -\left(\dfrac{R_s}{L_\delta} + \dfrac{R'_r L_m^2}{L'^2_r L_\delta}\right) & 0 & \dfrac{R'_r L_m}{L'^2_r L_\delta} & \dfrac{L_m}{L_\delta L'_r} p_p \omega_m & 0 \\ 0 & -\left(\dfrac{R_s}{L_\delta} + \dfrac{R'_r L_m^2}{L'^2_r L_\delta}\right) & -\dfrac{L_m}{L_\delta L'_r} p_p \omega_m & \dfrac{R'_r L_m}{L'^2_r L_\delta} & 0 \\ \dfrac{R'_r}{L'_r} L_m & 0 & -\dfrac{R'_r}{L'_r} & -p_p \omega_m & 0 \\ 0 & \dfrac{R'_r}{L'_r} L_m & p_p \omega_m & -\dfrac{R'_r}{L'_r} & 0 \\ -\dfrac{3}{2} \dfrac{p_p}{J_L} \dfrac{L_m}{L'_r} \psi_{qr} & \dfrac{3}{2} \dfrac{p_p}{J_L} \dfrac{L_m}{L'_r} \psi_{dr} & 0 & 0 & 0 \end{bmatrix}}_{A} \underbrace{\begin{bmatrix} i_{ds} \\ i_{qs} \\ \psi_{dr} \\ \psi_{qr} \\ \omega_m \end{bmatrix}}_{x} + \underbrace{\begin{bmatrix} \dfrac{1}{L_\delta} & 0 & 0 \\ 0 & \dfrac{1}{L_\delta} & 0 \\ 0 & 0 & 0 \\ 0 & 0 & 0 \\ 0 & 0 & -\dfrac{1}{J_L} \end{bmatrix}}_{B} \underbrace{\begin{bmatrix} v_{ds} \\ v_{qs} \\ T_L \end{bmatrix}}_{u} + w_t
$$

$$
\underbrace{\begin{bmatrix} i_{ds} \\ i_{qs} \end{bmatrix}}_{y} = \begin{bmatrix} 1 & 0 & 0 & 0 & 0 \\ 0 & 1 & 0 & 0 & 0 \end{bmatrix} \begin{bmatrix} i_{ds} \\ i_{qs} \\ \psi_{ds} \\ \psi_{qs} \\ T_L \end{bmatrix} + v_t \tag{3.6}
$$

The simulation scenario 5 is considered in this section to evaluate the performance of UKF based estimator for IM. For better understanding, the estimation results are compared with EKF estimation results. This comparison is presented in Figure 3.7
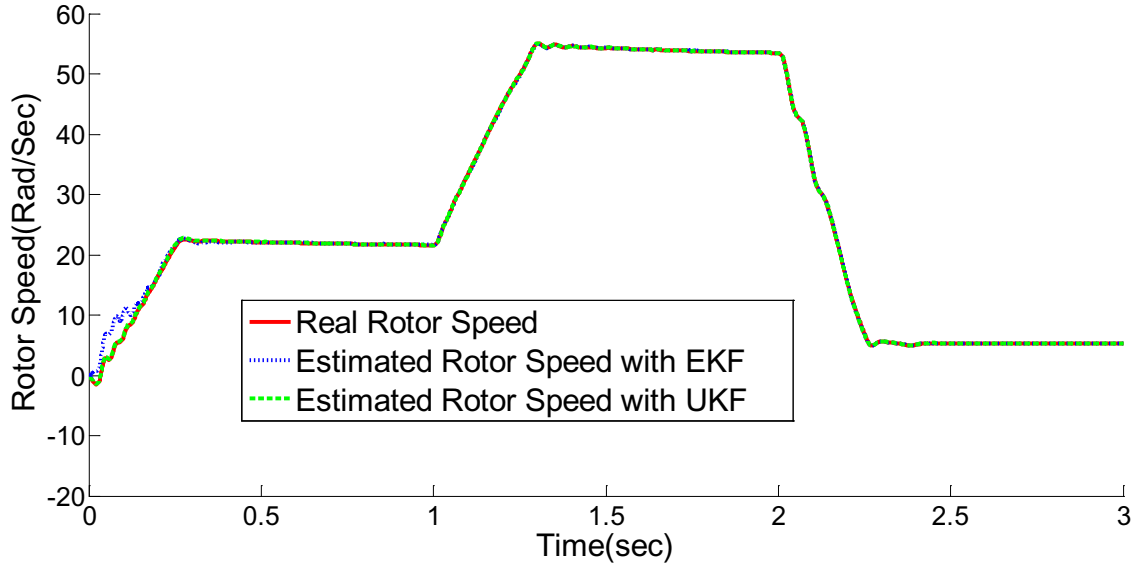
Figure 3-7: Comparison of speed estimation between EKF and UKF, scenario 5

The speed estimation error variances of these approaches are as follows.

EKF Error Variance =   0.4871   UKF Error Variance =   0.0047

Estimation results of i_{ds} by both methods are also presented in Figure 3.8.
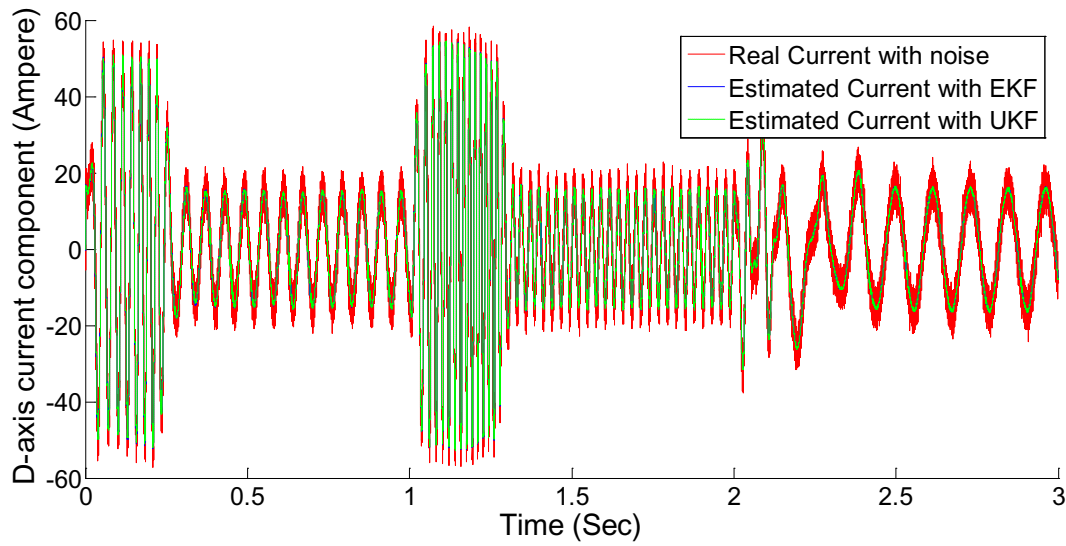
Figure 3-8: Comparison between real and estimated i_{ds} using EKF and UKF

Considering the estimation results presented in Figure 3-8 and the performed error analysis presented in Table 3.2, it can be stated that UKF has better performance. However, the UKF requires that the load torque is injected as an extra input into the model as expressed in the state space model presented in Equation (3.6). This is a considerable drawback, since torque sensor installation is a hard task and imposes more cost on the drive system. As a result, it can be concluded that EKF and its ability to estimate online parameters is a better solution for this case. A comprehensive comparison among all estimators designed in this chapter for state estimation in an IM using EKF and UKF is provided in Table 3-2.

Table 3-2: Performance comparison among the designed estimators

Simulation Scenarios	EKF based Estimators			UKF Estimator
	$[i_{ds} \quad i_{qs} \quad \psi_{dr} \quad \psi_{qr} \quad \omega_m]$	$[i_{ds} \quad i_{qs} \quad \psi_{dr} \quad \psi_{qr} \quad \omega_m \quad T_L]$	$[i_{ds} \quad i_{qs} \quad \psi_{dr} \quad \psi_{qr} \quad \omega_m \quad T_L \quad R_r \quad R_s]$	$[i_{ds} \quad i_{qs} \quad \psi_{dr} \quad \psi_{qr} \quad \omega_m]$
Scenario 1: ✓ Constant reference speed and load torque ✓ Constant main parameters	Speed estimation error variance: **21.03**	Speed estimation error variance: **0.0037**	Speed estimation error variance: **0.0037**	Speed estimation error variance: **0.0006**
Scenario 2: ✓ Constant reference speed ✓ Small variations of load torque ✓ Constant main parameters	Speed estimation error variance: **28.08**	Speed estimation error variance: **0.12**	Speed estimation error variance: **0.024**	Speed estimation error variance: **0.0028**
Scenario 3: ✓ Small variations of reference speed and load torque ✓ Constant main parameters	Speed estimation error variance: **35.05**	Speed estimation error variance: **2.34**	Speed estimation error variance: **0.154**	Speed estimation error variance: **0.021**
Scenario 4: ✓ Large variations of reference speed ✓ Small variations of load torque ✓ Constant main parameters	*Filter diverges*	Speed estimation error variance: **4.43**	Speed estimation error variance: **0.352**	Speed estimation error variance: **0.123**
Scenario 5: ✓ Large variations of reference speed ✓ Small variations of load torque and main parameters	*Filter diverges*	Speed estimation error variance: **8.96**	Speed estimation error variance: **0.4871**	Speed estimation error: **0.0047**
Scenario 6: ✓ Large variations of reference speed and load torque ✓ Small variation of main parameters	*Filter diverges*	Speed estimation error variance: **18.96**	Speed estimation error variance: **2.87**	*Filter diverges*

61

Considering the whole simulation results of this chapter, it can be concluded that EKF based estimator has more acceptable performance for induction motor, based on its ability for concurrent state and parameter estimation. Designing an accurate speed estimator is the first step to reach a sensorless control scheme for an induction motor. Sensorless control improves the control performance, reduces the total wiring of the drive system, and eliminates mechanical speed sensors such as tachogenerator and encoder. As the main parameters of IM such as stator and rotor resistances are not constant during operation, and load torque experiences changes that are slow in terms of time but large in amplitude, an estimator with the ability to estimate the parameters of the IM will be desirable. Nevertheless, it is possible to inject load torque as an extra input to the drive system and use UKF based estimator with higher order of mean and covariance estimation. The main question here can be considered as a trade off: an EKF based estimator with linearized first order approximation and online parameter estimation or a UKF based estimator with third order approximation but one more input and lack of parameter estimation ability.

3-5. Summary

In this chapter, a history of the recent research in state and parameter estimation in induction motor is provided. The mathematical foundations of the state space modeling of induction motor for state and parameter estimation are developed. Following a discussion of the different simulation scenarios, the Extended Kalman Filter is applied for state and

parameter estimation in induction motor. Using an appropriate state space model, the Unscented Kalman Filter is used for state estimation and a comprehensive comparison among all simulation results is finally presented.

CHAPTER 4

4. Synchrophasor Applications in Power Systems

4-1. Introduction

In this chapter, the principles of Synchrophasors and their applications for Wide Area Monitoring, Protection, and Control (WAMPAC) in large power systems are explained. The mathematical formulation of the phasor measurement, the general block diagram of the Phasor Measurement Unit (PMU), and the Phasor Data Concentrator (PDC) are presented. The merits for synchronized data gathering in large interconnected power systems and advantages of the dynamic state estimation in power systems are also addressed in this chapter.

Nowadays our daily lives depend heavily on smart supervision and reliable performance of the important infrastructures, like electric power systems, telecommunication networks, and water distribution systems. Because of the continuous increase in their size, network complexity, inherent uncertainty, random nature of changing loads, and mutual interactions, it has become a demanding task to design, monitor, and control such systems [26]. In terms of power systems, the safe and dependable operation has become a difficult task due to the daily-increasing demand for electric power, the ever-increasing number of the power system interconnections, higher penetration percentage of the various forms of renewable energies, and new regulations of the power market. These are the main motivations for power companies all around the world to invest in a real-time WAMPAC system. Synchronized measurement technology (SMT) can be considered as the central supporting part of this system [26].

Synchrophasors are essentially accurate power grid measurements provided by PMUs installed all over a large scale power system. The measurements are taken at high rate compared to the conventional technologies and are synchronized using a common time reference signal. The synchronized data provided by PMUs helps to better detect stresses on a power grid and improve the accuracy of the corrective decisions to maintain stability of the power system. In 1986, phasor measurements were introduced as a new measurement approach in power systems [27]. The PMU prototype produced by Virginia Tech was used by American Electric Power and Bonneville Power Administration (BPA) in that year. These utilities tested and used the initial versions of the PMUs until the introduction of the first commercial unit in 1991, the Macrodyne 1690 [27]. BPA reconfigured this system into a true real-time, wide area measurement system in 1997,

using commercial PMUs and a customized PDC. Since that time, many newer models of the PMUs have become available with developed ranges of features. Also, several versions of PDC units have been developed with various monitoring, analysis, and control schemes [27].

The major advantages of using synchronized measurement technology in power systems are that measurements from widely spread spots can be synchronized with a signal received by the Global Positioning System (GPS) clock. The direct measurement of the voltage phase angles can be realized and the precision and rapidity of the energy management system applications, e.g. dynamic state estimation, can be increased dramatically [26]. Based on the ability of WAMPAC systems to capture dynamic state information, the state estimators can generate dynamic states of major components of the power system. For example, for the synchronous generator the rotor angle and speed, instead of the static values of the voltage magnitudes and phase angles can be estimated [2, 28].

4-2. Principles of the Phasor Measurement

A phasor is a mathematical representation of a sinusoidal waveform as shown in Figure 4-1.
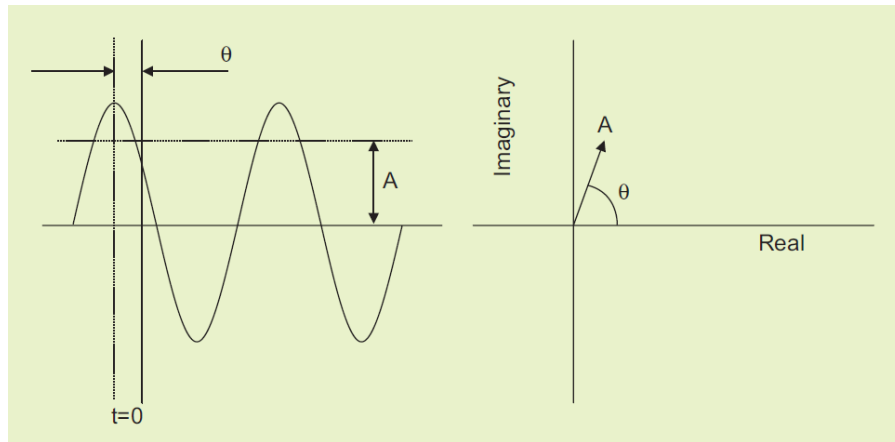
Figure 4-1: Phasor representation of a sinusoidal waveform [27]

The magnitude can be either a peak or RMS value of the signal and the phase angle can be determined by the given sinusoidal frequency and an arbitrary time reference. Synchrophasors are phasor values, representing sinusoidal signals of a power system which are compared to the nominal frequency of the power system and time reference provided by GPS [27]. The introduction of the GPS has made it simply possible to create a universal accurate time reference signal with reasonable cost.

The time domain formula of a waveform can describe the instantaneous phasor value of a sinusoidal signal in each moment. However, it might be a difficult task to find the phasor equivalent of an arbitrary sinusoidal waveform which contains different frequencies. A series of samples captured at certain moments with appropriate time intervals and over a specified period is required to determine the main parameters of a sinusoidal signal [27]. The sampling frequency and phasor estimation method along with the signal content of the waveform are key factors that specify the quality of the estimated phasor. The predominant phasor estimation approach is the Discrete Fourier Transform (DFT) [7]. In this technique, the standard Fourier Transform is applied over one or more cycles at the

nominal system frequency. For better understanding, the details of using DFT for phasor extraction are presented below. Consider, the time representation of a sinusoidal signal as

$$x(t) = X_m \cos(wt + \phi) \tag{4.1}$$

X_m is the peak value of the signal and ϕ is the phase angle in radian. The phasor representation of the signal in Equation (4.1) is as follows:

$$X = (X_m/\sqrt{2})e^{j\phi} \tag{4.2}$$

DFT is accomplished by using discrete steps through a finite window in frequency domain. Suppose the signal shown in Figure 4-1 is sampled at sampling angle $\theta = 2\pi/N$, where N is the number of samples during one finite window. The Fourier representation of the signal $x(t)$ is as follows [7]:

$$x(t) = a_0 + a_k \cos(2\pi k f_0 t) + b_k \sin(2\pi k f_0 t) \tag{4.3}$$

a_k and b_k are the Fourier series coefficients and f_0 is the fundamental frequency. Based on the periodic property of DFT, the coefficients of the Fourier series can be derived from the sampling data as follows:

$$
\begin{aligned}
a_0 &= 2X_0 \\
a_k &= 2Real(X_k) \\
b_k &= 2Imaginary(X_k)
\end{aligned}
\tag{4.4}
$$

68

X_k represents the DFT samples of the signal in complex mode. An example is provided below to clarify the procedure.

Example 4.1

Consider the following Fourier series representation of a signal.

$$x(t) = 9 + 16 \cos(2\pi f_0 t + 40°) + 5 \cos(4\pi f_0 t + 60°) + 3 \cos(6\pi f_0 t + 65°) \qquad (4.5)$$

f_0 is assumed to be $60 Hz$. The signal is shown below in time and frequency domain.
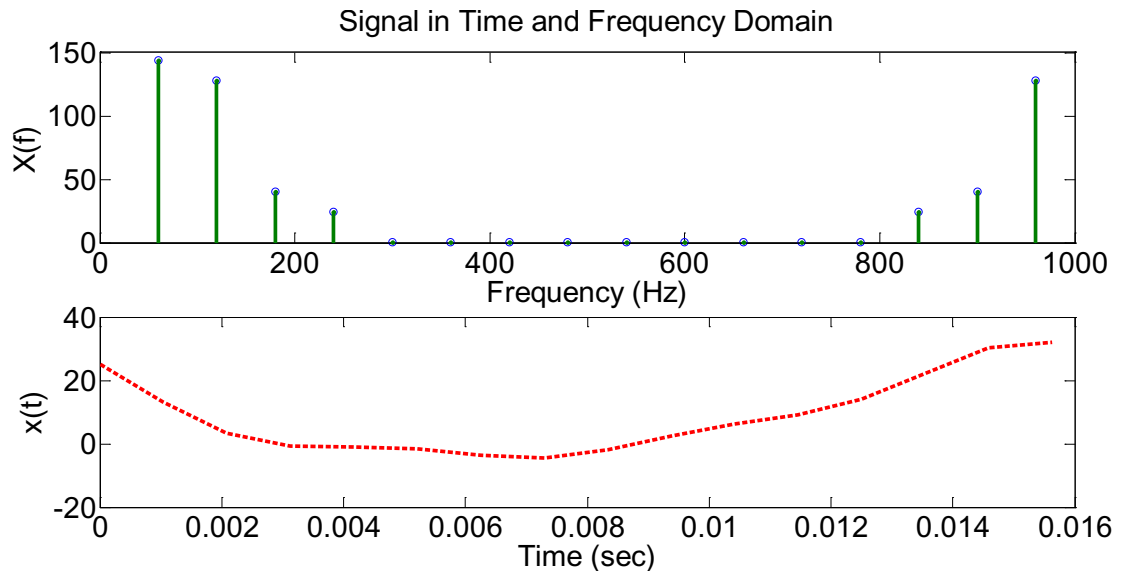

Figure 4-2: Signal in frequency and time domain

The first plot in Figure 4-2 shows amplitude of the signal in frequency range of $0 \sim 1000\ Hz$, and the second plot demonstrates the amplitude in time frame of $0 \sim 0.016\ sec$. Using the Fourier Transform command in Matlab, the DFT coefficients can be obtained for the signal as presented in Table 4.1.

Table 4-1: Sampled data and Fourier transform of the signal

Sample Number(k)	$x(t)$	Frequency	$X_k = DFT/16$
0	25.02	0	9.0047
1	13.06	f_0	6.1276 + 5.1470j
2	3.24	$2f_0$	1.2478 + 2.1659j
3	-0.7727	$3f_0$	0.6314 + 1.3589j
4	-1.0656	$f4_0$	0.0003 - 0.0020j
5	-1.6879	$5f_0$	0.0007 - 0.0011j
6	-3.6376	$6f_0$	8.1406e-04 - 6.1875e-04j
7	-4.4259	$7f_0$	8.6681e-04 - 2.8785e-04j
8	-2.0177	-	8.8192e-04
9	2.3535	$-7f_0$	8.6681e-04 + 2.8785e-04j
10	6.1014	$-6f_0$	8.1406e-04 + 6.1875e-04j
11	9.1211	$-5f_0$	0.0007 + 0.0011j
12	14.0837	$-4f_0$	0.0003 + 0.0020j
13	22.3008	$-3f_0$	0.6314 - 1.3589j
14	30.3135	$-2f_0$	1.2478 - 2.1659j
15	32.077	$-f_0$	6.1276 - 5.1470j

Using Equation (4.4) to calculate the Fourier series coefficients, the recreated signal is as follows:

$$\hat{x}(t) = 9.00479 + 15.987\cos(2\pi f_0 t + 39.2°) + 5.001\cos(4\pi f_0 t + 58.73°) \\ + 3.001\cos(6\pi f_0 t + 64.87°) \tag{4.6}$$

The comparison between the real and estimated signal is presented in Figure 4-3.
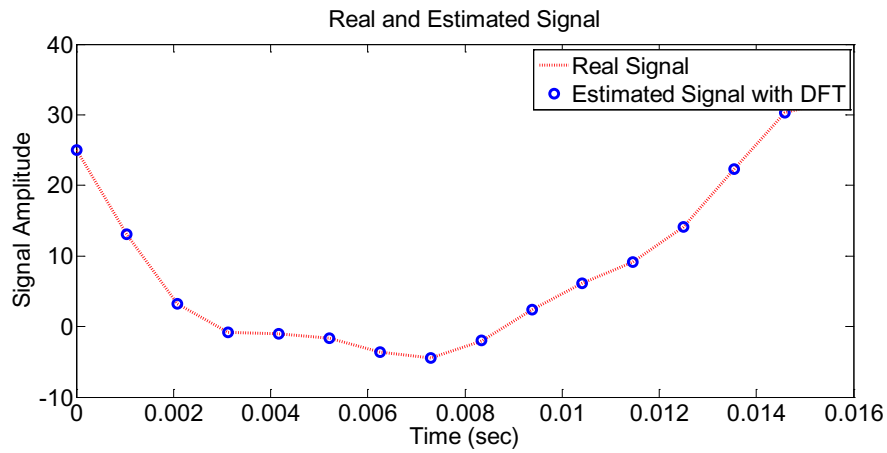

Figure 4-3: Comparison between the real and estimated signal

Figure 4-3 shows that the estimated signal agrees with the real signal. The kth component

of the phasor representation of $x(t)$ can be obtained as follows [7]:

$$X_k = \frac{1}{\sqrt{2}} \frac{2}{N} \sum_{n=0}^{N-1} x(n\Delta T) e^{-\frac{j2\pi kn}{N}} \tag{4.7}$$

n represents the nth sample. The representation of Equation (4.7) in the form of sine and

cosine is given below [7].

$$X_k = \frac{\sqrt{2}}{N} \sum_{n=0}^{N-1} x(n\Delta T)[cos\left(\frac{2\pi kn}{N}\right) - jsin(\frac{2\pi kn}{N})] \tag{4.8}$$

Using the expression $x(n\Delta T) = x_n$, and $\frac{2\pi}{N} = \theta$ (θ is the sampling angle measured based

on the period of the fundamental frequency component), Equation (4.8) cab be written as

$$X_k = \frac{\sqrt{2}}{N} \sum_{n=0}^{N-1} x_n[cos(kn\theta) - jsin(kn\theta)] \tag{4.9}$$

The cosine and sine expressions of Equation (4.9) are defined as

$$X_{kc} = \frac{\sqrt{2}}{N} \sum_{n=0}^{N-1} x_n cos(kn\theta)$$

$$X_{ks} = \frac{\sqrt{2}}{N} \sum_{n=0}^{N-1} x_n sin(kn\theta) \tag{4.10}$$

Therefore, the phasor X_k can be written as

$$X_k = X_{kc} - jX_{ks} \qquad\qquad (4.11)$$

Using this equation, the phasor of a signal can be calculated. Two methods have been developed for this purpose in recent years: non-recursive and recursive updates [7]. The first approach is the easiest one since in this method, each estimation is accomplished for all of the process through N samples. One window could estimate one phasor and the next phasor will use the samples from the next window. This approach is very stable because the new estimation process would not use the previous samples; however, its calculation needs lots of memory space. In recursive method, in contrast, the new phasor is estimated using $N - 1$ samples from the previous window and one new sample. This method is much faster and uses less space for computation [7]. The sample window for non-recursive method is shown in Figure 4-4
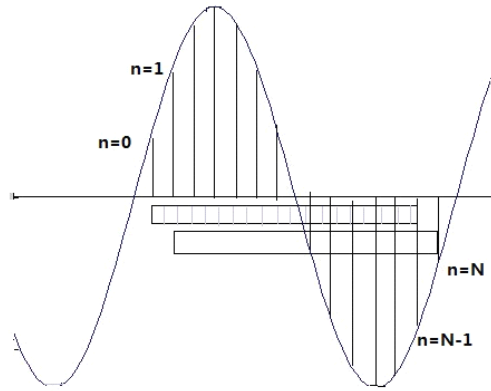

Figure 4-4: Sampling window [7]

The recursive method is currently the most common approach for phasor estimation. For example, the phasor estimation of the $60\ Hz$ signal $x(t) = 100\cos(120\pi t + \pi/4)$

sampled at 12 samples per cycle using both recursive and non-recursive approaches are presented in Table 4-2.

Table 4-2: Phasor estimation of the signal [7]

Sample number	Sample x_n	Non-recursive phasor estimation	Recursive phasor estimation
0	70.71		
1	25.88		
2	-25.88		
3	-70.71		
4	-96.59		
5	-96.59		
6	-70.71		
7	-25.88		
8	25.88		
9	70.71		
10	96.59		
11	96.59		
12	70.71	70.701∠45°	70.701∠45°
13	25.88	70.701∠75°	70.701∠45°
14	-25.88	70.701∠105°	70.701∠45°
15	-70.71	70.701∠135°	70.701∠45°
16	-96.59	70.701∠165°	70.701∠45°
17	-96.59	70.701∠195°	70.701∠45°

The phase shift in the non-recursive method is related to the shift of the sampling window, while there is no phase shift for the recursive method.

4-3. Phasor Measurement Unit

A Phasor Measurement Unit (PMU) is an electronic device that deploys concept of digital signal processing for measuring 50/60 Hz AC voltages or currents typically at a sampling rate of 48 samples per cycle. This phasor technology provides time synchronized data

typically at a rate of 240 samples/second [4]. The general block diagram of a PMU is presented in Figure 4-5.
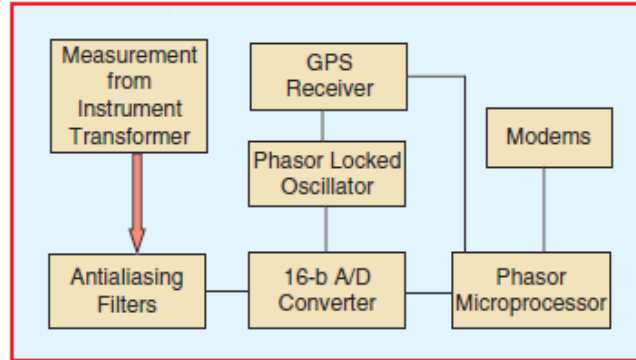
Figure 4-5: Block diagram of a PMU [26]

The analog AC waveforms are sampled by an analog to digital converter. A phase-locked loop oscillator and the GPS clock create a high speed synchronized signal with one microsecond accuracy, while is used for time stamping of all measured data. The detailed function of each block of the PMU can be described as follows:

- The main purpose of the anti-aliasing unit is to avoid samples from measurement aliasing. In other words, if the sampling frequency is not more than two times of the analyzed frequency, there is a possibility of signal overlapping in a specific zone. This phenomenon is called aliasing. The anti-aliasing filter avoids this event by satisfying Nyquist criterion [7].

- The A/D converter is used to convert the signal from the anti-aliasing filter to digital signal which can be used by the phasor micro-processor.

- The GPS receiver is able to collect ceaseless rhythmic time signals sent by the satellite every second.

- The sampling interval is controlled with a phase-locked oscillator which is phase-locked with the GPS clock pulse.

- The phasor micro-processor calculates the phasors of the signals using a specific algorithm.

Typically PMUs are located at various important substations to obtain real-time data of the system and send them to the Phasor Data Concentrator (PDC) normally placed at utility centers, where the data from all PMUs are accumulated. Due to the various distances, available communication technologies, and time delay for data transmission of each device, measurement streams of a certain moment cannot be received by the destination at the same time [27]. Therefore, the early data should be stamped and stored in a mass storage and wait till the other related data is received by the system. However, because of the quite high refresh time of the data, this waiting time cannot be very long. The process of waiting for and sorting measurements is named as "phasor data concentration" which is mainly carried out by a PDC [27]. This aggregated data can be used for monitor and control software which provides frequencies, primary voltages, currents, and output active and reactive powers for system operators. In addition, many PDCs which belong to different utility companies can be a part of a larger PDC or Super PDC to accumulate the information of a large power system and also draw an accurate general picture of the system [8].
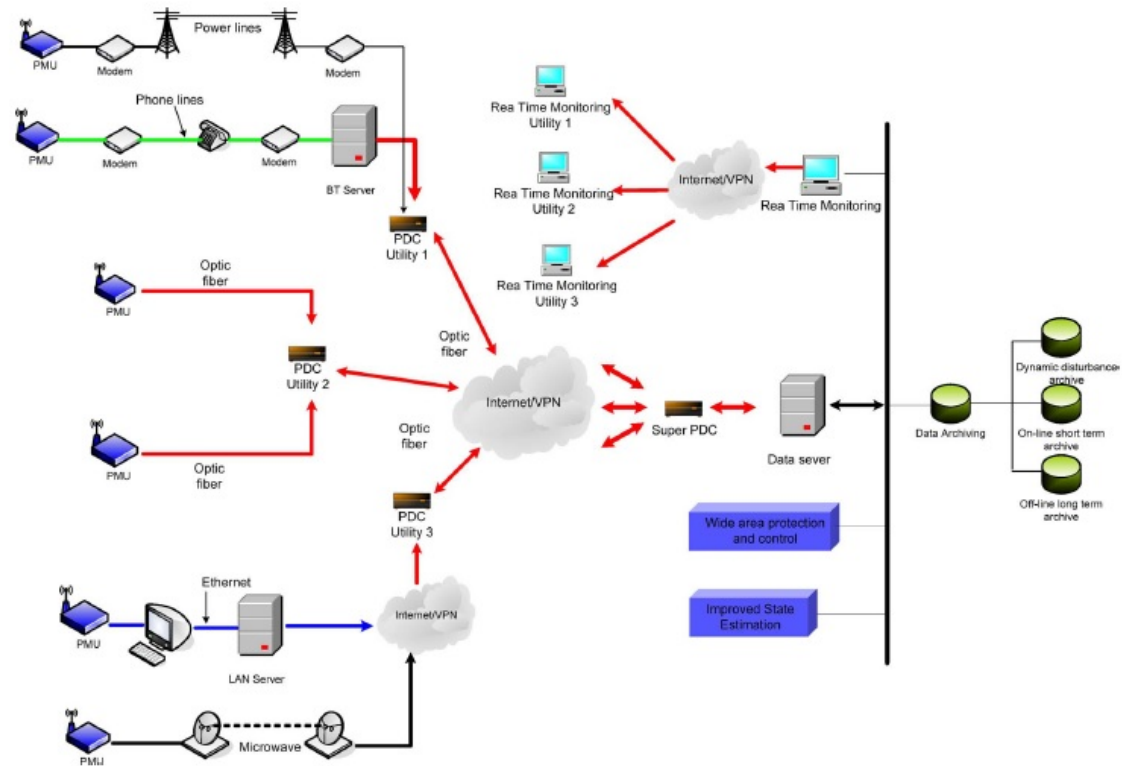
Figure 4-6: Super PDC configuration using different communication infrastructure [8]

Figure 4-6 shows that the data provided by PMUs are transferred to the related utility PDCs through different communication facilities such as power lines, phone lines, fiber optic, Ethernet, and microwave. The accumulated data is then sent to the super PDC by Internet or Virtual Private Network (VPN). The data server placed at the super PDC uses the accumulated data for real time monitoring, wide area protection and control, dynamic state estimation, and data archiving. General applications of WAMPAC system are presented in the Table 4-3, and some of these applications are explained in detail in Section 4-4.

Table 4-3: Applications of WAMPAC [8]

Dynamic state estimation
Real-time rush hour power management
Real time envision of a large power system
Complicated system modeling and validation
Better control of generating units
Design of adaptive models for the system control and protection
Development of a sophisticated early warning centers
Analysis of the reasons for major system blackout
Progress in the damping property of the inter-area oscillations
Real-time angle, voltage, and frequency stability

4-4. Dynamic State Estimation Advantages in Large Power Systems

At the present time, phasor estimation has been essentially performed using steady state measurements. Phasor systems are typically faster than the dynamics of most power systems; therefore, this kind of estimation has been rational and sufficient. Nevertheless, power systems are changing daily and more accurate methods might be needed for difficult operational situations [27]. Data communication systems have also evolved dramatically in recent years. Most of the utilities are equipped with a broadband at 1MB/s and higher for their data communication and the remaining ones at least have plans to do so [27]. LAN and WAN supporting equipments are prevalent and easy to install these days. This progress has been a stimulus to change minimal data sets to more complete

data packages. Based on all these reasons, many institutes all around the world are doing research on dynamic measurement of the power systems. Particularly, an IEEE working group has recently been revising C37.118 to add dynamic performance requirements while paying attention to not invalidating current ones [27]. Recent experiences have proved that synchronized wide area system history of the dynamic events are key in the analysis and understanding of the system performance, behavior, and the types of control decisions made for large scale power system contingencies [8]. It is a time consuming effort to analyze and determine the main reason of major contingencies in a power system without the time-stamped PMU data or the related PDC [8]. For example, the January 23, 2007 recording of the contingency in Western Electricity Coordinating Council (WECC) reveals the value of a wide-area PMU-based monitoring and event recording procedure [8]. The purpose of these systems installed in 1990s has been to capture real-time network state information in the WECC region. The PMU real-time data of the 2007 contingency assists the operators of the system to immediately figure out what happened to the grid and carry out necessary actions to prevent the propagation of the instability [8]. Developing smart centers which can send warnings ahead of a major contingency is one of the greatest applications of WAMPAC.

Dynamic state estimation in a power system provides accurate and synchronized information about the main states of the generating unit which are working in an interconnected large power system. In addition to the noise elimination on measurement signals provided by PMUs, dynamic state estimation provides high rate information of the immeasurable states of the synchronous generators which are advantageous in better control of the power stations; real-time angle, voltage, and frequency transient stability

analysis of the power system; improved damping property for the inter-area oscillations; and better rush hour power management.

In chapter 6 of this thesis, the high rate data provided by PMU is used for dynamic state estimation in different power system case studies. As real power systems equipped with PMUs on high voltage bus were not accessible for this research, PowerWorld Simulator [29] is used for this purpose. Since this software is able to simulate transient stability of the power systems with predetermined faults and desired afterwards resolutions, it is assumed that the outputs of the PMUs installed on the buses of a system are accessible from the PowerWorld simulator. The sampling rate of the present commercialized PMUs are near 240 frames per second. Therefore, different sampling rates are considered in the simulation procedure to evaluate the effect of this factor on the accuracy of the estimation results, and also to examine whether the whole idea of the dynamic state estimation in power systems using existing PMU's technology is realizable. The diagram presented in Figure 4-7 clearly shows the idea being used in this research to generate accurate data for modeling, validation, and dynamic state estimation.
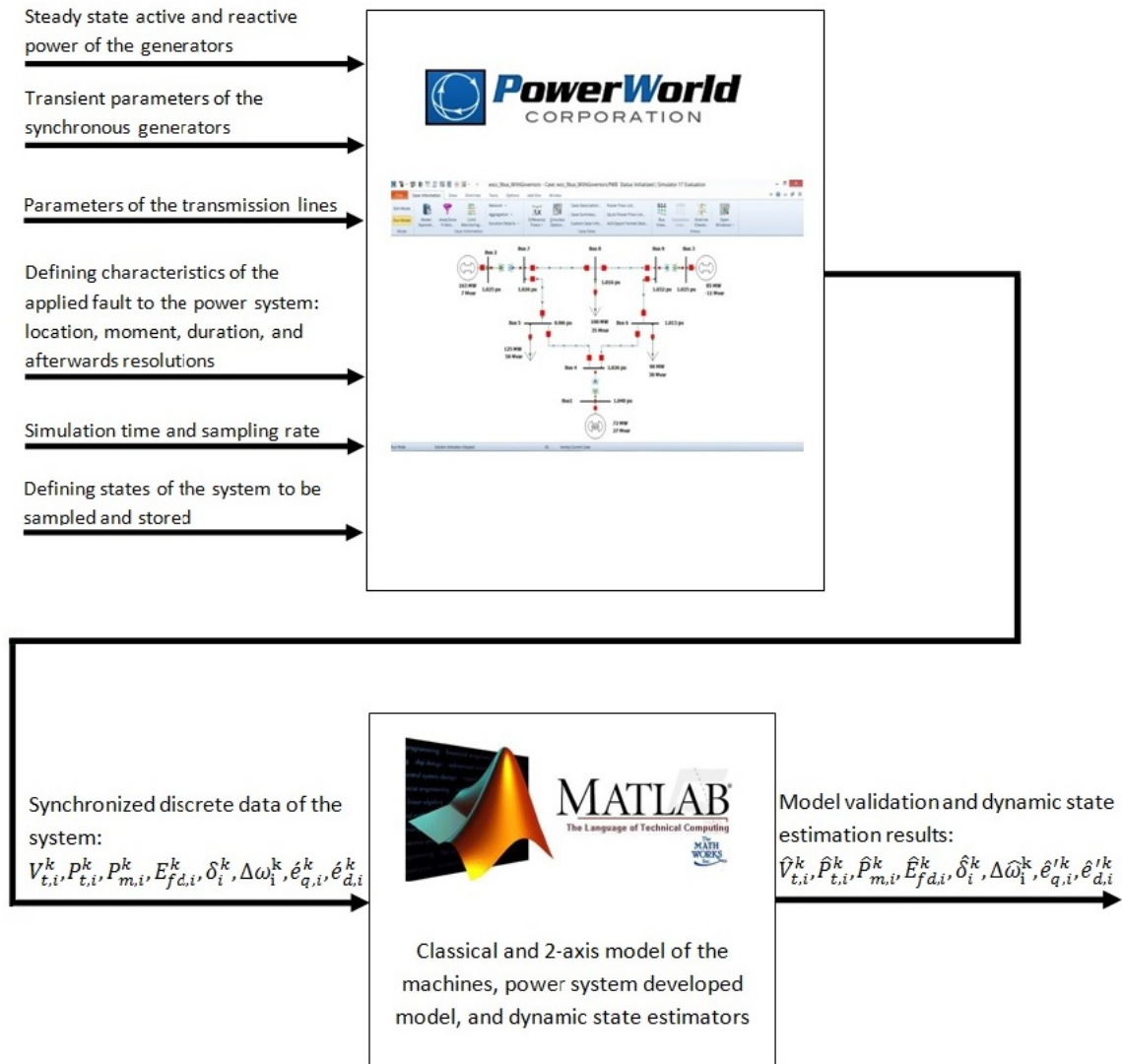
Figure 4-7: Using PowerWorld Simulator instead of real PMU to generate synchronized data for power system case studies

This diagram shows that by designing a desired power system case study in PowerWorld and providing information about steady state active and reactive power of the generators; transient parameters of the generators; parameters and characteristics of the transmission lines; fault location, moment, duration, and afterwards resolutions; simulation time and sampling frequency; and states of the systems to be sampled during the simulation

procedure; synchronized high rate information about the power system can be generated. This data is then used to validate the classical and 2-axis models developed for the synchronous generator. The validated models are then used for dynamic state estimation in different power system case studies. The measurement data provided by PowerWorld are disturbed by a white Gaussian noise to be more similar to the real case.

4-5. Summary

The principals of phasor measurements and the associated benefits for power systems are discussed in this chapter. Brief explanations about Wide Area Monitoring, Protection, and Control (WAMPAC) system are presented. The principles of the phasor measurement and related formulations are explained. Next, the block diagram of the Phasor Measurement Unit (PMU) and function of each part are discussed in detail, and the benefits of the Phasor Data Concentrator (PDC) and the general structure of a Super PDC are explained. Finally, brief explanations about the final aim of the PMU recording data and its application for dynamic state estimation are discussed, and the procedure of data generation for modeling, validation, and state estimation in this research is presented in a complete diagram.

CHAPTER 5

5. Synchronous Generator Mathematical Description and Model Verification

5-1. Introduction

Developing a proper model for the synchronous generator is the first step for any kind of analysis in power systems. In the first section of this chapter, a simple RLC circuit is used to explain the procedure for modeling and validation that will be used for different power system case studies in the subsequent sections. After explaining the mathematical foundations of a synchronous machine, the classical model is derived and formulated. A two-axis fourth order model of the machine is then developed using the mathematical

description of the synchronous generator. The last part of this chapter is dedicated to multi-machine transient stability analysis. Each of these sections discusses the model validation, and the obtained results are compared with the data generated by PowerWorld Simulator for better evaluation of the developed model accuracy. The models obtained in this chapter are used in Chapter 6 for more studies on dynamic state estimation in power systems.

5-2. Series RLC Circuit

In this section, an RLC circuit is used as a simple case study to explain the procedure of the modeling and validation being used in this research for synchronous machine. Consider the following RLC circuit with the specified parameters.
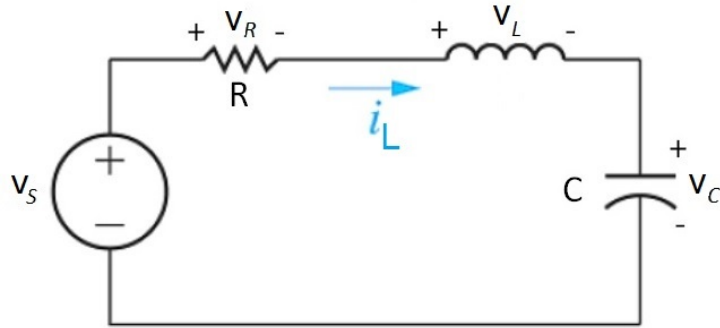

Figure 5-1: Series RLC circuit, $v_s = 10\ cos(2t)$, $R = 4.5\Omega$, $L = 0.5\ H$, and $C = 0.1\ F$

The KVL expression for this circuit is as follows:

$$v_s(t) = v_R(t) + v_L(t) + v_C(t) = Ri_l(t) + L\frac{di_l(t)}{dt} + \frac{1}{C}\int i_l(t)\,dt$$

$$\xrightarrow{yields} 10cos(2t) = 4.5i_l(t) + 0.5\frac{di_l(t)}{dt} + \frac{1}{0.1}\int i_l(t)\,dt \tag{5.1}$$

By differentiating Equation (5.1), the second order differential equation of the circuit can be obtained as:

$$\frac{d^2 i_l(t)}{dt^2} + 9\frac{di_l(t)}{dt} + 20i_l(t) = -40\sin(2t) \tag{5.2}$$

Equation (5.2) is a second order linear nonhomogeneous differential equation, the general and specific results for $i_l(t)$ is as follows:

$$i_l(t) = C_1 e^{-4t} + C_2 e^{-5t} + A\sin(2t) + B\cos(2t) \tag{5.3}$$

The voltage source $v_s(t)$ is applied at $t = 0$. Assume that the initial conditions of the inductor current $i_l(0)$ and capacitor voltage $v_C(0)$ are equal to zero. Another initial condition $(\frac{di_l(0)}{dt})$ is required to solve Equation (5.3), which can be calculated by equating $t = 0$ in Equation (5.1) as follows:

$$10 = 0.5\frac{di_l(0)}{dt} \xrightarrow{yields} \frac{di_l(0)}{dt} = 20 \left(\frac{A}{sec}\right) \tag{5.4}$$

Using the initial conditions, $i_l(0) = 0$ and $\frac{di_l(0)}{dt} = 20$, the coefficients of the above equation can be calculated and the results are as follows:

$$C_1 = 16, \quad C_2 = -17.24, \quad A = -1.1, \quad B = 1.24 \tag{5.5}$$

Therefore, considering the principal equation for capacitor voltage in this circuit, $C\frac{dv_c(t)}{dt} = i_l(t)$, the following equations can be obtained as the analytical solution of the inductor current and the capacitor voltage.

$$i_l(t) = 16e^{-4t} - 17.24e^{-5t} - 1.1\sin(2t) + 1.24\cos(2t)$$

$$v_c(t) = \frac{1}{C}\int_0^t i_l(t)\,dt = -40e^{-4t} + 34.48e^{-5t} + 5.5\cos(2t) + 6.2\sin(2t) \qquad (5.6)$$

Using the second order differential equation of the system, a numerical approach for integration of the differential equation based on the state space model is explained. Equation (5.2) can be separated into two first order differential equations as follows:

$$\frac{di_l(t)}{dt} = -9i_l(t) - 2v_c(t) + 20\cos(2t)$$

$$\frac{dv_c(t)}{dt} = 10i_l(t) \qquad (5.7)$$

By considering the inductor current and the capacitor voltage as two independent states of the systems, x_1 and x_2, the following state space model can be developed for the circuit.

$$\dot{x}_1 = -9x_1 - 2x_2 + 20\cos(2t)$$

$$\dot{x}_2 = 10x_1 \qquad (5.8)$$

Using Equation (2.27) and based on the basic definition of the time derivative of a state variable x, the state space model of the circuit can be discretized as follows:

$$x_1^{k+1} = x_1^k + T_s\left(-9x_1^k - 2x_2^k + 20\cos(2kT_s)\right)$$

$$x_2^{k+1} = x_2^k + 10T_s x_1^k$$

(5.9)

Where T_s is the sampling time for the numerical solution. The comparison between the numerical solution of Equation (5.9), which is the numerical integration of Equation (5.8), and the analytical solution of the circuit (Equation (5.6)) are presented in the following figure.
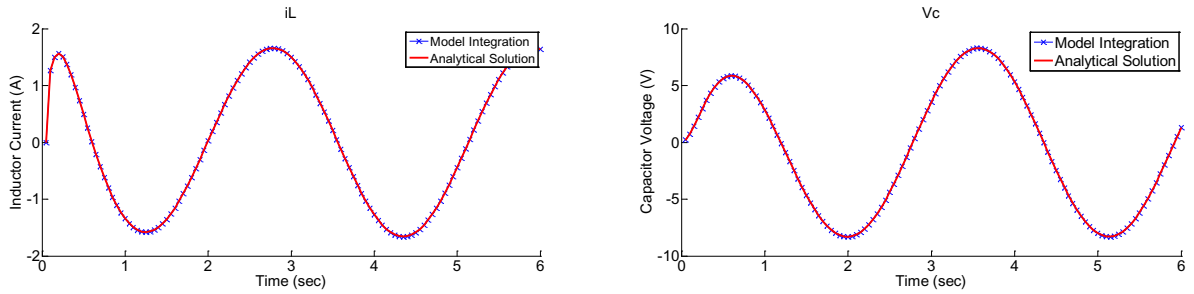

Figure 5-2: Comparison between model integration and analytical solution for the series RLC circuit

Figure 5-2 shows clearly that the results of the numerical solution are the same as the analytical solution for the RLC case study. In the next section, after deriving the model of the synchronous machine, the same approach is used to validate the model and the numerical solution.

5-3. Mathematical Description of the Synchronous Machine and the Classical Model [30]

Based on Newton's second law, the rotor motion of a synchronous generator can be expressed by the following equation

$$J\alpha_m(t) = T_m(t) - T_e(t) \tag{5.10}$$

J is the total moment of inertia of the rotor and the other rotating parts in $Kg{-}m^2$; α_m is the rotor angular acceleration in rad/s^2; T_m is the mechanical torque provided by the prime mover excluding the retarding torque of mechanical losses in $N.m$; and T_e is the electrical torque, which the related per-unit value is equal to the total per-unit three-phase output electrical power of the generator including electrical losses [30]. $\alpha_m(t)$ is also defined as

$$\alpha_m(t) = \frac{d\omega_m(t)}{dt} = \frac{d^2\theta_m(t)}{dt^2} \tag{5.11}$$

$$\omega_m(t) = \frac{d\theta_m(t)}{dt} \tag{5.12}$$

$\omega_m(t)$ is the angular velocity in rad/sec and θ_m is the angular position with respect to a stationary axis (stator) in $radian$. T_m and T_e are normally equal in steady state, resulting in zero rotor acceleration and a constant rotor speed known as synchronous speed. As the generator inductances are functions of θ_m, for more convenient and less complexity of the

equations, the rotor angular position is defined with respect to a synchronously rotating reference frame as follows [30]:

$$\theta_m(t) = \omega_{m0}t + \delta_m(t) \tag{5.13}$$

Where ω_{m0} is the synchronous angular velocity of the rotor in rad/sec, and $\delta_m(t)$ is the angular position of the rotor compared to this new defined reference frame. Equations (5.11) and (5.13) are inserted into (5.10) to obtain

$$J\frac{d^2\theta_m(t)}{dt^2} = J\frac{d^2\delta_m(t)}{dt^2} = T_m(t) - T_e(t) \tag{5.14}$$

Equation (5.14) is multiplied by $\omega_m(t)$ and divided by apparent power S_{rated} which results in

$$\frac{J\omega_m(t)}{S_{rated}}\frac{d^2\delta_m(t)}{dt^2} = \frac{\omega_m(t)T_m(t) - \omega_m(t)T_e(t)}{S_{rated}}$$
$$= \frac{P_m(t) - P_e(t)}{S_{rated}} = P_{mP.U}(t) - P_{eP.U}(t) \tag{5.15}$$

The normalized inertia constant, called the H constant, is defined for more simplicity as follows:

$$H = \frac{\frac{1}{2}J\omega_{m0}^2}{S_{rated}} \qquad \frac{joules}{VA} \, or \, per \, unit - second \tag{5.16}$$

The H constant is normally a value between 1 and 10 $p.u-s$ while J varies widely with different generators physical characteristics [30]. Using Equation (5.16), Equation (5.15) can be written as follows:

$$2H\frac{\omega_m(t)}{\omega_{m0}^2}\frac{d^2\delta_m(t)}{dt^2} = P_{mP.U}(t) - P_{eP.U}(t) \tag{5.17}$$

The per-unit rotor angular velocity is defined as follows:

$$\omega_{P.U}(t) = \frac{\omega_m(t)}{\omega_{m0}} \tag{5.18}$$

Therefore, Equation (5.17) becomes

$$\frac{2H}{\omega_{m0}}\omega_{P.U}(t)\frac{d^2\delta_m(t)}{dt^2} = P_{mP.U}(t) - P_{eP.U}(t) \tag{5.19}$$

The electrical angular acceleration, electrical radian frequency, power angle, and synchronous electrical radian frequency for a synchronous generator with P number of poles are defined as follows [30]:

$$\alpha(t) = \frac{P}{2}\alpha_m(t) \tag{5.20}$$

$$\omega(t) = \frac{P}{2}\omega_m(t) \tag{5.21}$$

$$\delta(t) = \frac{P}{2}\delta_m(t) \tag{5.22}$$

$$\omega_0 = \frac{P}{2}\omega_{m0} \tag{5.23}$$

The per-unit electrical frequency is also expressed as follows:

$$\omega_{P.U}(t) = \frac{\frac{2}{P}\omega(t)}{\frac{2}{P}\omega_0} = \frac{\omega_m(t)}{\omega_{m0}} \tag{5.24}$$

Equation (5.19) is then modified using Equations (5.20) - (5.24), adding the term that represents a damping torque, as follows:

$$\frac{2H}{\omega_0}\omega_{P.U}(t)\frac{d^2\delta(t)}{dt^2} = P_{mP.U}(t) - P_{eP.U}(t) - \frac{D}{\omega_0}\frac{d\delta(t)}{dt} \tag{5.25}$$

Considering Equation (5.25) as two first order equations, the classical model of the synchronous generator is

$$\frac{d\delta(t)}{dt} = \omega(t) - \omega_0 \tag{5.26}$$

$$\frac{2H}{\omega_0}\omega_{P.U}(t)\frac{d\omega(t)}{dt} = P_{mP.U}(t) - P_{eP.U}(t) - \frac{D}{\omega_0}\frac{d\delta(t)}{dt} \tag{5.27}$$

D is the damping factor which is normally a small positive value between 0 and 2 [30]. From now on, for more simplicity, the variable t is eliminated from all functions while

keeping in mind that all variables and functions defined up to the present are functions of time (t). Therefore, the classical model presented in Equations (5.26) and (5.27) can be written as follows:

$$\frac{d\delta}{dt} = \omega - \omega_0 \tag{5.28}$$

$$\frac{2H}{\omega_0} \omega_{P.U} \frac{d\omega}{dt} = P_{mP.U} - P_{eP.U} - \frac{D}{\omega_0} \frac{d\delta}{dt} \tag{5.29}$$

It is more convenient to develop the model based on the speed deviation from synchronous speed in per unit and change the other variables to per unit, as well. It can be written from Equation (5.24) that

$$\omega_{P.U} = \frac{\omega}{\omega_0} \rightarrow \omega = \omega_{P.U}\omega_0$$

$$\xrightarrow{Subtracting\ \omega_0\ from\ both\ sides} \omega - \omega_0 = \omega_{P.U}\omega_0 - \omega_0 = \omega_0(\omega_{P.U} - 1) \tag{5.30}$$

$\Delta\omega$ is then defined as follows:

$$\Delta\omega = \omega_{P.U} - 1 \tag{5.31}$$

Using Equation (5.31), Equation (5.30) can be written as

$$\omega - \omega_0 = \omega_0\Delta\omega \tag{5.32}$$

Therefore, using Equation (5.32), Equation (5.28) can be expressed as follows:

$$\frac{d\delta}{dt} = \omega_0 \Delta\omega \tag{5.33}$$

Using Equation (5.24) and (5.33), Equation (5.29) can be written as

$$\frac{2H}{\omega_0} \frac{\omega}{\omega_0} \frac{d\omega}{dt} = P_{mP.U} - P_{eP.U} - \frac{D}{\omega_0} \omega_0 \Delta\omega \tag{5.34}$$

By differentiating Equation (5.32), following equation can be derived.

$$\frac{d\omega}{dt} = \omega_0 \frac{d\Delta\omega}{dt} \tag{5.35}$$

Using Equation (5.33) and keeping in mind that the term $\frac{\omega}{\omega_0} \cong 1$ is normally negligible, Equation (5.34) is modified as follows:

$$2H \frac{d\Delta\omega}{dt} = P_{mP.U} - P_{eP.U} - D\Delta\omega \tag{5.36}$$

Therefore, the classical dynamic model of the synchronous machine is as follows:

$$\frac{d\delta}{dt} = \omega_0 \Delta\omega$$

$$\frac{d\Delta\omega}{dt} = \frac{1}{2H} (P_m - P_e - D\Delta\omega) \tag{5.37}$$

Since all of the parameters of Equation (5.37) are in per unit; therefore, $p.u$ subscript is also eliminated from the equations of the model for more simplicity.

5-3-1. Classical Model Validation

The best way to validate the model is to integrate it over a period of time with predetermined initial conditions. Figure 5-3 shows a simplified equivalent model of a general power system which is a single generator connected through a transformer and parallel transmission lines to an infinite bus. The so called Single-Machine-Infinite-Bus (SMIB) shown in this figure can be considered as the basis for developing and validating the models in this chapter. This model is simulated in PowerWorld Simulator [29] in order to generate data to validate the model. The data generated by this reliable software is compared with the outputs of the classical model developed in the previous section, (Equation (5.37)) to verify the accuracy of the model. The PowerWorld schematic of SMIB with parallel transmission line is presented in Figure 5-4. The simulation scenario is a symmetrical permanent three-phase-to-ground bolted short circuit which occurs on the middle of the second transmission line at $t = 0.5\ sec$, cleared at $t = 0.6\ sec$ by opening the circuit breakers at the ends of this transmission line.
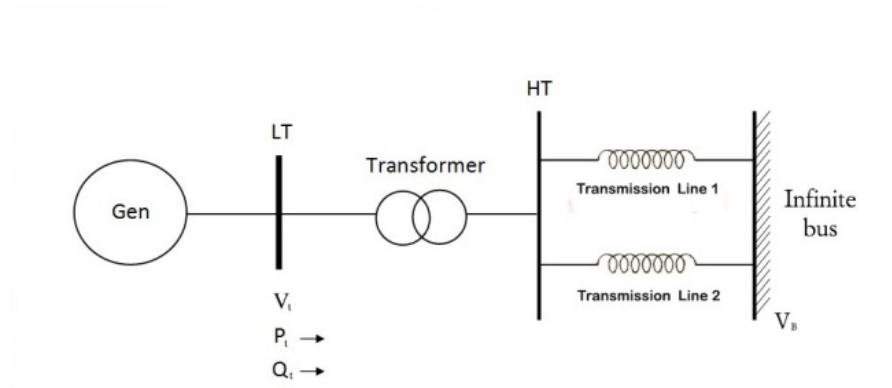
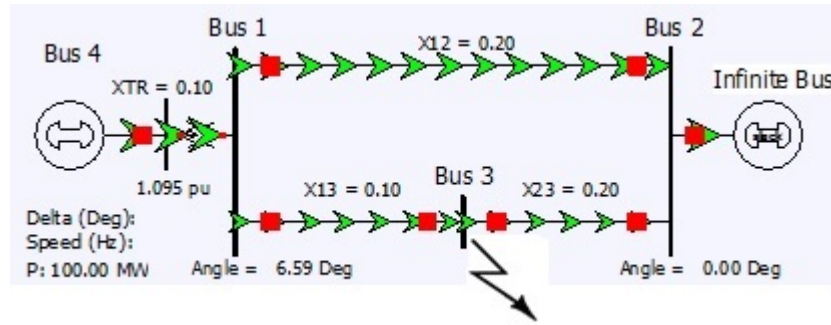**Figure 5-3: Diagram of SMIB connected to the infinite bus through a parallel transmission lines [2]**

Figure 5-4: SMIB model in PowerWorld Simulator

The main parameters of the simulated system are presented in Table 5.1.

Table 5-1: Main parameters of the simulated synchronous generator [2, 30]

D, H	Damping factor and inertia constant, per unit	0.05, 5
$\acute{x}_d$	Direct axis transient reactance, per unit	0.37
T_m	Mechanical input, per unit	1
P_{base}	Generator base power	100 MVA

Before integrating the Equation 5.37, the initial conditions of the system and equations describing the generator power in pre-fault, during-fault, and after-fault periods should be derived. Considering the steady state power delivered by the generator to the infinite bus as $100\ MW$ with 0.95 lagging power factor, the internal voltage of the generator would be as follows:

$$I = \frac{P}{V_{th} \times PF} = 1.05263 \angle - 18.192°\quad per - unit \tag{5.38}$$

$$\begin{aligned} E'\angle\delta &= V_{th} + jX_{th}I = 1.3317\angle 26.29° \\ &= 1\angle 0 + j0.59 \times 1.05263 \angle - 18.192°\quad per - unit \end{aligned}$$

V_{th} and X_{th} are the equivalent Thevenin voltage and reactance as seen from the internal voltage of the generator. The initial states of the system are expressed as follows:

$$\delta_0 = 26.29° \qquad\qquad \Delta\omega_0 = 0 \tag{5.39}$$

The electrical power delivered by the generator to the infinite bus can be expressed as follows:

$$P_e = \frac{E'V_{th}}{X_{th}}\sin(\delta) \tag{5.40}$$

Three equivalent circuits are presented in Figure 5-5 for the SMIB facing a three-phase-to-ground bolted short circuit.
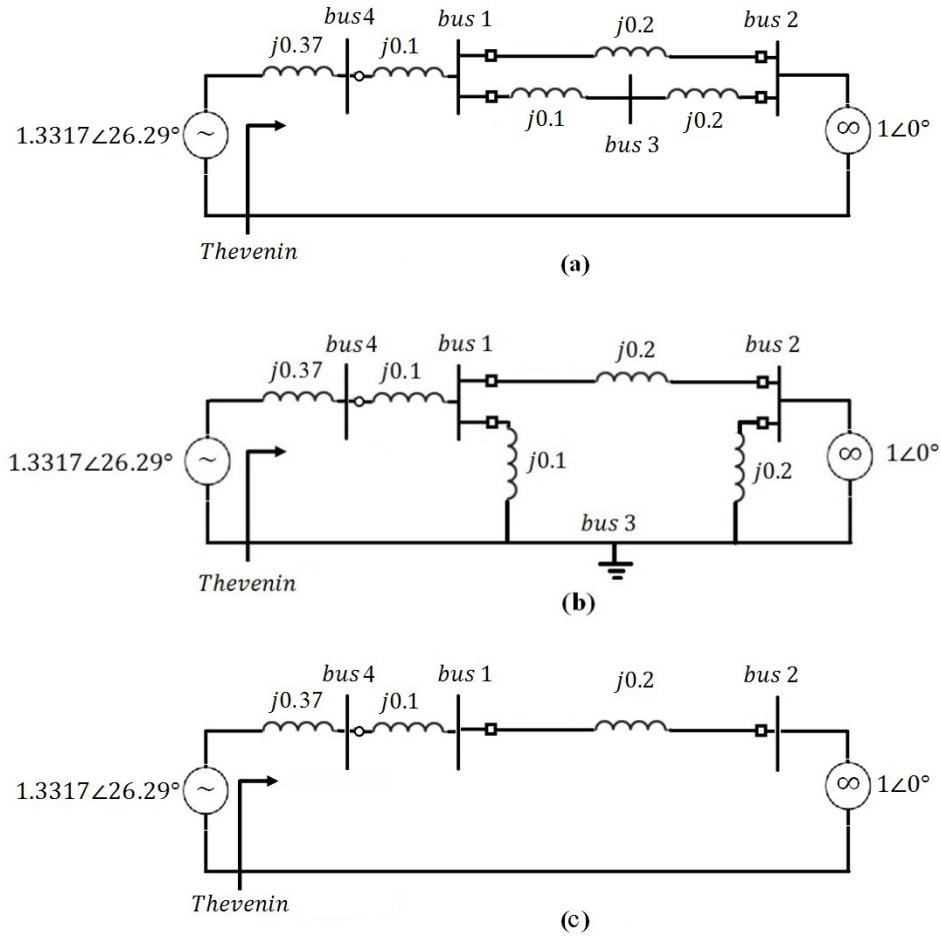
Figure 5-5: Thevenin equivalent of the SMIB facing a short circuit on bus 3, a: before-fault, b: during-fault, c: after-fault

Using Equation (5.40) and by considering the internal voltage of the generator (E') constant during the fault, the following equations can be obtained for the electrical power of the generator.

$$P_{e1} = \frac{1.3317 \times 1.000}{0.59} \sin(\delta) = 2.2571 \sin(\delta)$$

$$P_{e2} = \frac{1.3317 \times 0.333}{0.536} \sin(\delta) = 0.8264 \sin(\delta)$$

$$P_{e3} = \frac{1.3317 \times 1.000}{0.67} \sin(\delta) = 1.9870 \sin(\delta) \tag{5.41}$$

The denominators in Equation (5.41) are the Thevenin reactance (X_{th}) of the three circuits presented in Figure 5-5, as seen from the internal voltage of the generator. P_{e1}, P_{e2}, and P_{e3} are pre-, during-, and post-fault power of the generator, respectively. Performing the integration with the initial conditions, a comparison of the outputs of the model and the data generated by PowerWorld Simulator are provided in the following figures.
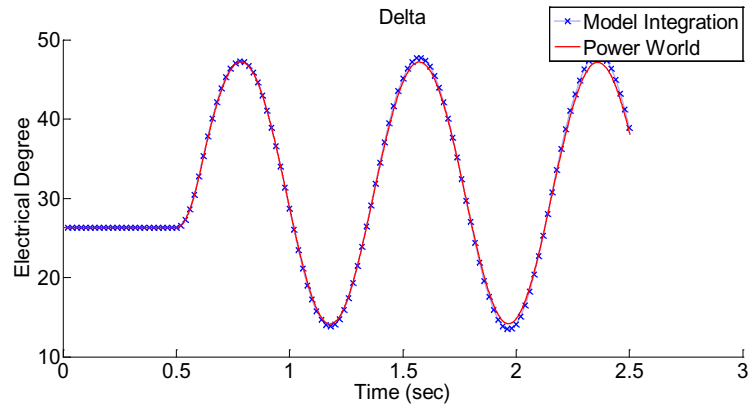

Figure 5-6: Synchronous generator classical model verification of rotor angle. Fault applied at $t = 0.5\ sec$ and cleared at $t = 0.6\ sec$
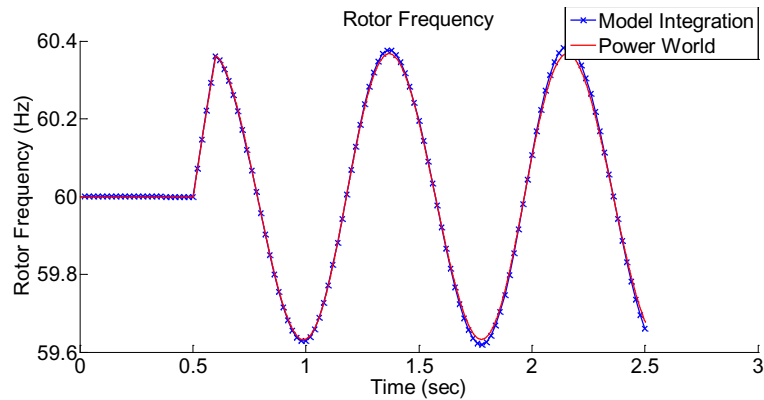

Figure 5-7: Synchronous generator classical model verification of rotor frequency. Fault applied at $t = 0.5\ sec$ and cleared at $t = 0.6\ sec$
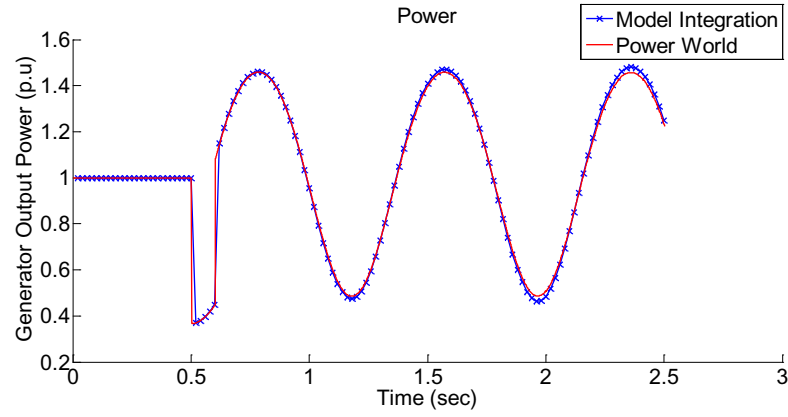
Figure 5-8: Synchronous generator classical model verification of output power. Fault applied at $t = 0.5\ sec$ and cleared at $t = 0.6\ sec$

The validation results show the accuracy of the generator classical model and the numerical integration approach which have been used in this research.

5-3-2. The Equal Area Criterion and Critical Fault Clearing Time

The equal area criterion is a direct method to determine the stability of a power system without solving the nonlinear swing Equation (5.37). This method can be used for SMIB or two machine system [30]. The equal area criterion can be represented by the following equation.

$$\underbrace{\int_{\delta_0}^{\delta_1} (P_m - P_e)\, d\delta}_{A_1} = \underbrace{\int_{\delta_1}^{\delta_2} (P_e - P_m)\, d\delta}_{A_2} \tag{5.42}$$

In the above equation, δ_0 is the initial rotor angle before fault, δ_1 is the rotor angle when the fault is cleared, and δ_2 is the maximum rotor angle which the machine reaches after clearing the fault. The system will remain stable if δ_2 does not exceeds $180 - \delta_0$. Therefore, critical fault clearing time can be obtained by the following equation

$$\int_{\delta_0}^{\delta_{cr}} \left(P_m - P_{e,during\ fault}\right) d\delta = \int_{\delta_{cr}}^{\pi-\delta_0} \left(P_{e,after\ fault} - P_m\right) d\delta \qquad (5.43)$$

The critical fault clearing time for the SMIB case study presented in Section 5-3-1 is calculated here, where $P_{e,during\ fault} = P_{e2}$ and $P_{e,after\ fault} = P_{e3}$ in Equation (5.41)

$$\int_{0.4589}^{\delta_{cr}} \left(1 - 0.8264\ sin(\delta)\right) d\delta = \int_{\delta_{cr}}^{2.6826} \left(1.987\ sin(\delta) - 1\right) d\delta \qquad (5.44)$$

Calculating the above integration, the critical fault clearing angle is obtained as

$$\delta_{cr} = 104.2° \qquad (5.45)$$

Using δ_{cr} and from the solution to Equation (5-37), the critical fault clearing time is obtained as

$$t_{cr} = 0.89\ sec \qquad (5.46)$$

The simulation results of the developed model and PowerWorld simulator for fault clearing time less and greater than $0.89\ sec$ are presented in Figure 5.9.
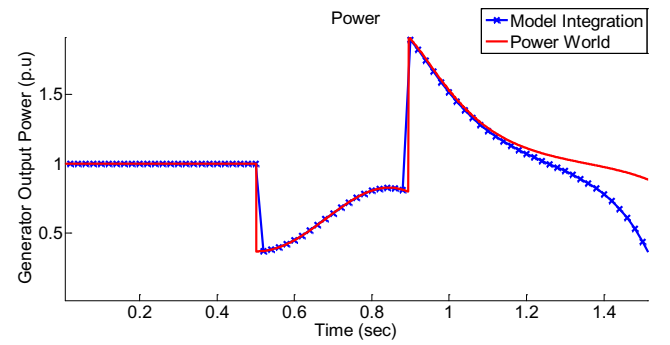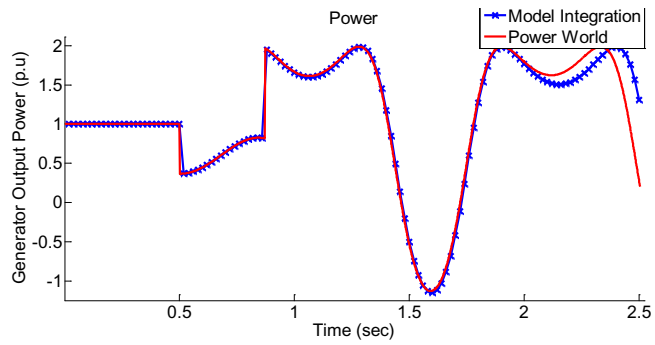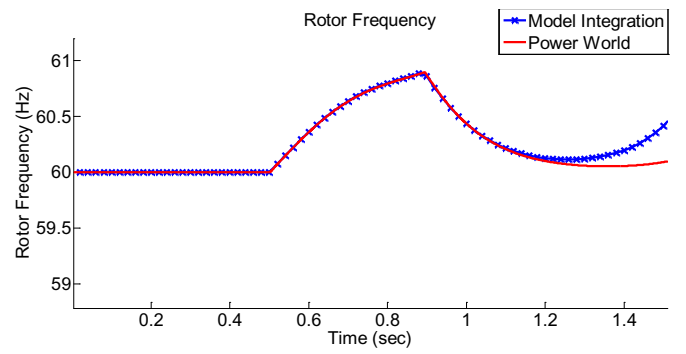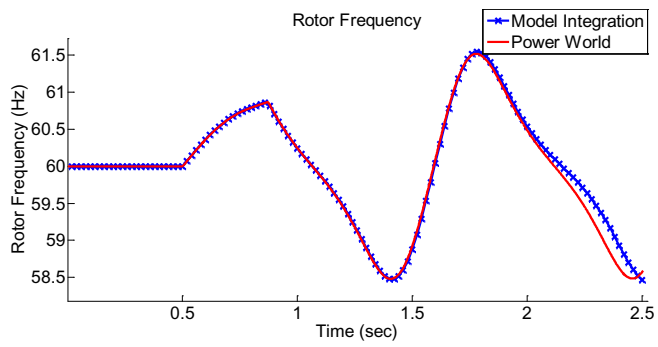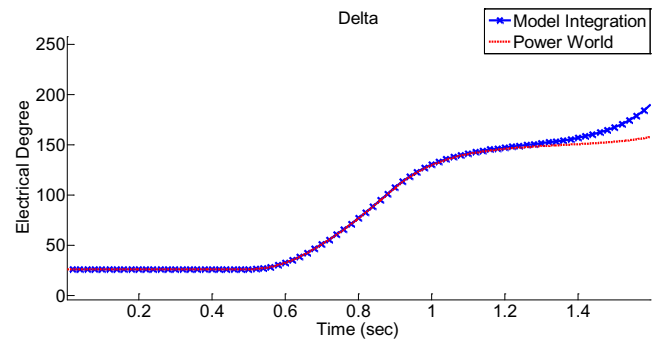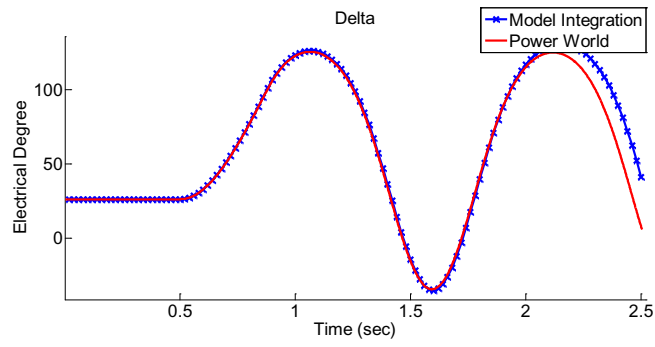
a) $t_{fault-clearing} = 0.87\ sec$

b) $t_{fault-clearing} = 0.892\ sec$

Figure 5-9: Rotor angle, rotor frequency, and output power of the SMIB for fault clearing times: a) less than $t_{cr} = 0.89\ sec$ (stable mode); b) greater than $t_{cr} = 0.89\ sec$ (unstable mode)

Figure 5-9 shows that the fault clearing time should be less than $0.89\ sec$ to ensure stability of the system. This figure also shows the accuracy of the model and numerical integration approach used in this study. For better visual presentation, the $P - \delta$ curves of the simulated system in both stable and unstable modes are presented here.
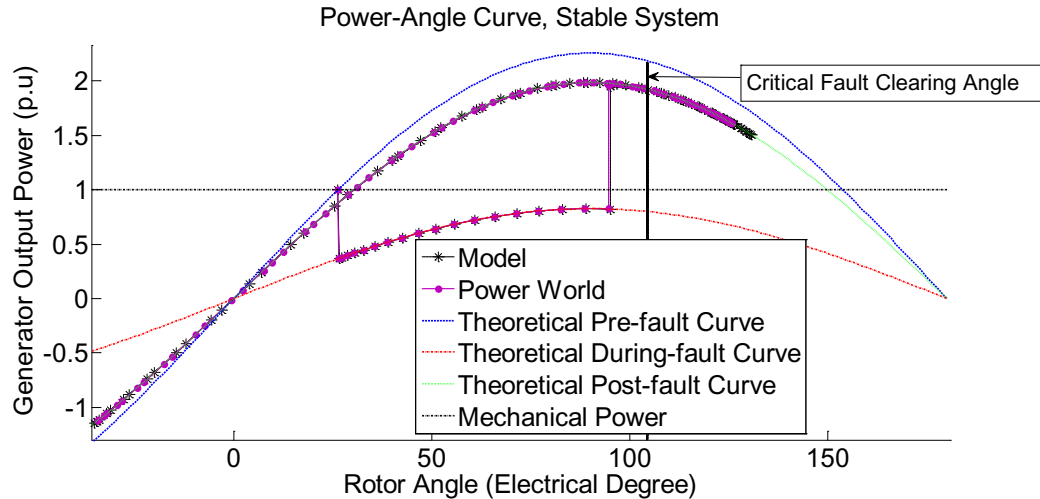
(a)
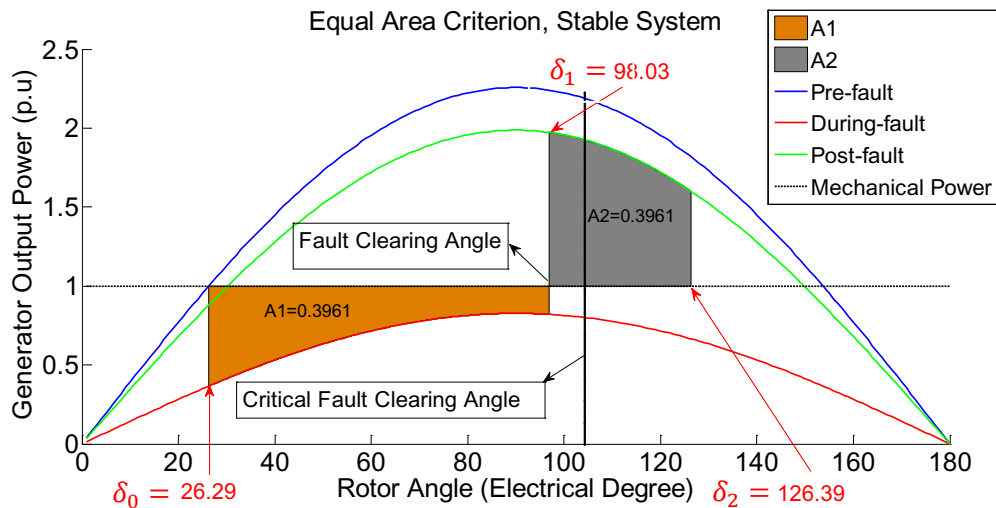
(b)

Figure 5-10: $P - \delta$ curves of the simulated system for the stable mode. a) Power-angle curve, b) equal area criterion: $A_1 = A_2$
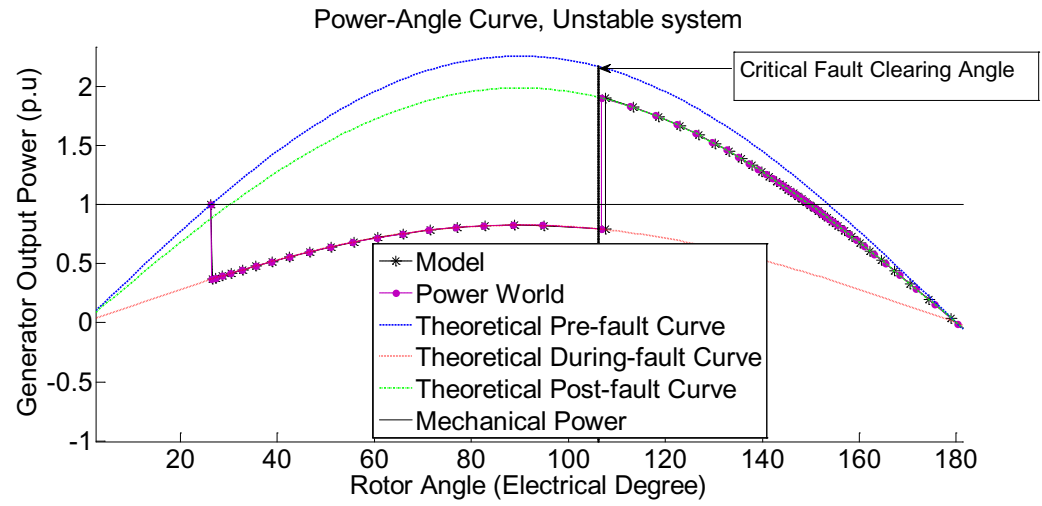
(a)
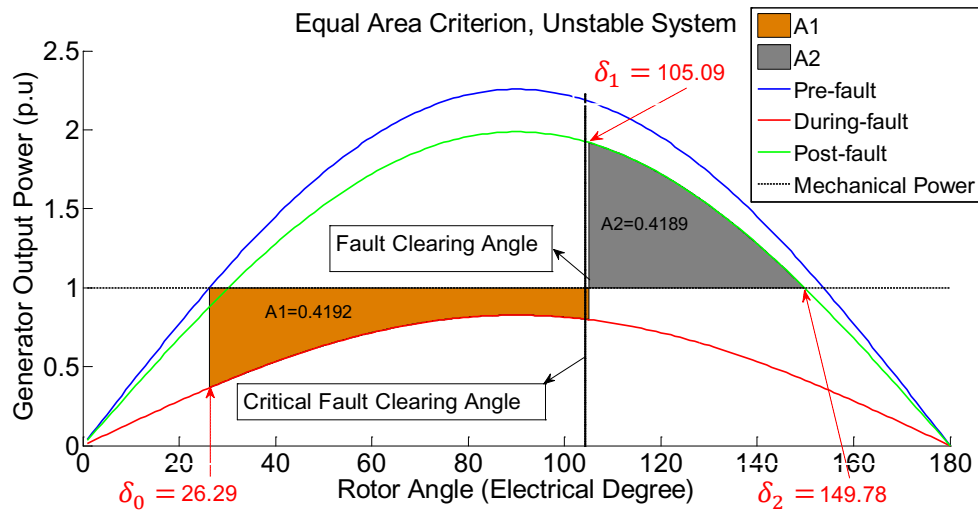
(b)

Figure 5-11: $P - \delta$ **curves of the simulated system for the unstable mode. a) Rotor-angle curve, b) equal area criterion:** $A_1 > A_2$

The during-fault and post-fault areas (A1 and A2), calculated by Equation (5.42), and the values of δ_0, δ_1, and δ_2 are separately specified on each figure.

5-4. 2-Axis Fourth Order Model of the Synchronous Generator

The next step is to develop the fourth order model of the synchronous generator which includes e_q' and e_d', the q and d axis components of the generator internal voltage. Based on the phasor diagram of the synchronous machine presented in Figure 5-12, equations describing the q and d axis components of the generator internal voltage and their first order differential equations are given below [30].

Figure 5-12: Phasor diagram of the synchronous machine [31]

$$e_q' = e_q + R_a i_q + x_d' i_d \tag{5.47}$$

$$e_d' = e_d + R_a i_d - x_q' i_q \tag{5.48}$$

$$\frac{de_q'}{dt} = \frac{1}{\hat{T}_d}\left(E_{fd} - e_q' - (x_d - x_d')i_d\right) \tag{5.49}$$

$$\frac{de_d'}{dt} = \frac{1}{\hat{T}_{qo}}\left(-e_d' + (x_q - x_q')i_q\right) \tag{5.50}$$

x_d and x_q are the direct- and quadrature-axis reactance, and x'_d and x'_q are the direct and

quadrature axis transient reactance, all in per unit. Also, $Ŧ_{do}$ and $Ŧ_{qo}$ are the direct and

quadrature axis transient open circuit time constants in second. δ is defined as the angle

such that e'_q, the q axis component of voltage behind transient reactance x'_d, leads the

terminal bus E_t or V_t. Considering Figure 5-12, the d-axis and q-axis voltages (e_d, e_q)

can be expressed as [2, 31]

$$\begin{cases} e_d = V_t \sin(\delta) \\ e_q = V_t \cos(\delta) \end{cases} \xRightarrow{yielding} E_t = V_t = \sqrt{e_d^2 + e_q^2} \tag{5.51}$$

In addition, the d-axis and q-axis currents (i_d, i_q) are [2, 31]

$$\begin{cases} i_d = I_t \sin(\delta + \phi) \\ i_q = I_t \cos(\delta + \phi) \end{cases} \xRightarrow{yielding} I_t = \sqrt{i_d^2 + i_q^2} \tag{5.52}$$

Using Equations (5.47), (5.48) and (5.51) and by neglecting the stator resistance $(R_a = 0)$, Equation (5.52) can be written as

$$i_d = \frac{e'_q - V_t \cos(\delta)}{x'_d} \tag{5.53}$$

$$i_q = \frac{V_t \sin(\delta) - e'_d}{x'_q} \tag{5.54}$$

The air gap torque T_e of the generator in per unit is equal to the terminal power P_e or P_t (generator terminal electrical power) [2]. Therefore, it is obtained as

$$T_e = P_t + R_a I_t^2 \quad \xrightarrow{R_a=0} \quad T_e \cong P_t = e_d i_d + e_q i_q \tag{5.55}$$

Equations (5.51), (5.53), and (5.54) are inserted into Equation (5.55) to obtain

$$T_e \cong P_t = \frac{V_t}{x_d'} e_q' \sin(\delta) - \frac{V_t}{x_q'} e_d' \cos(\delta) + \frac{V_t^2}{2}\left(\frac{1}{x_q'} - \frac{1}{x_d'}\right) \sin(2\delta) \tag{5.56}$$

Using Equations (5.37), (5.49), (5.50), (5.53), (5.54), and (5.56), the fourth order model of a synchronous generator is derived as follows:

$$\frac{d\delta}{dt} = \omega_0 \Delta\omega$$

$$\frac{d\Delta\omega}{dt} = \frac{1}{2H}\left(P_m - \frac{V_t}{x_d'} e_q' \sin(\delta) + \frac{V_t}{x_q'} e_d' \cos(\delta) - \frac{V_t^2}{2}\left(\frac{1}{x_q'} - \frac{1}{x_d'}\right) \sin(2\delta) - D\Delta\omega\right)$$

$$\frac{de_q'}{dt} = \frac{1}{\acute{T}_{do}}\left(E_{fd} - e_q' - (x_d - x_d')\left(\frac{e_q' - V_t \cos(\delta)}{x_d'}\right)\right)$$

$$\frac{de_d'}{dt} = \frac{1}{\acute{T}_{qo}}\left(-e_d' + (x_q - x_q')\left(\frac{V_t \sin(\delta) - e_d'}{x_q'}\right)\right) \tag{5.57}$$

For numerical integration of Equation (5.57) with initial condition, accurate information about the voltage of the terminal bus is necessary which is not available all the time. Since the voltage phasor of the infinite bus is assumed as $1\angle 0°$ and is constant during simulation, it might be a good practice to express Equation (5.57) by infinite bus voltage

and define δ as the angle such that e'_q leads the infinite bus voltage V_∞. Therefore, this equation is modified as given below.

$$\frac{d\delta}{dt} = \omega_0 \Delta\omega$$

$$\frac{d\Delta\omega}{dt} = \frac{1}{2H}\left(P_m - \frac{V_{th}}{x'_d + x_{th}}e'_q \sin(\delta) + \frac{V_{th}}{x'_q + x_{th}}e'_d \cos(\delta) - \frac{V_{th}^2}{2}\left(\frac{1}{x'_q + x_{th}} - \frac{1}{x'_d + x_{th}}\right)\sin(2\delta)\right.$$
$$\left. - D\Delta\omega\right)$$

$$\frac{de'_q}{dt} = \frac{1}{\acute{T}_{do}}\left(E_{fd} - e'_q - (x_d - x'_d)\left(\frac{e'_q - V_{th}\cos(\delta)}{x'_d + x_{th}}\right)\right)$$

$$\frac{de'_d}{dt} = \frac{1}{\acute{T}_{qo}}\left(-e'_d + (x_q - x'_q)\left(\frac{V_{th}\sin(\delta) - e'_d}{x'_q + x_{th}}\right)\right) \tag{5.58}$$

V_{th} and x_{th} are the Thevenin voltage and reactance as seen from the generator terminal. The Thevenin equivalent circuits of the SMIB case study of this chapter related to the pre-fault, during-fault, and post-fault situations are presented in Figure 5-13.

(a)
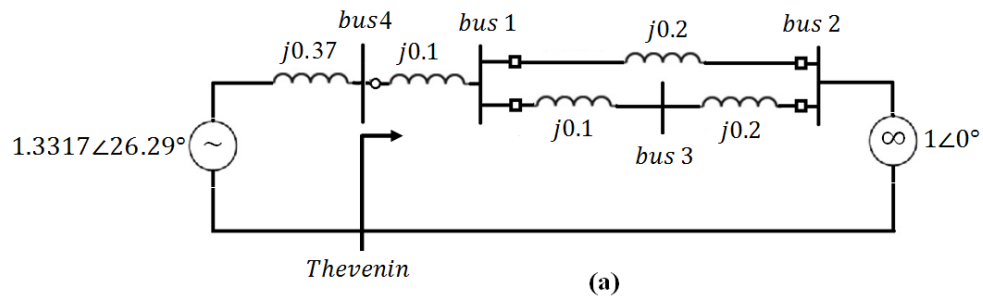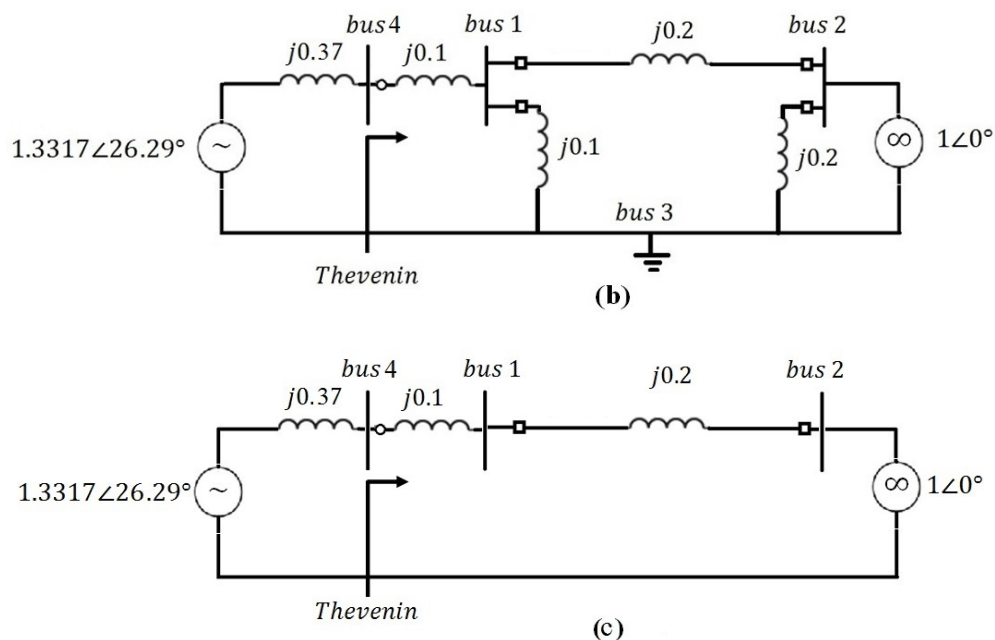
Figure 5-13: Thevenin equivalent of the SMIB case study, a: before-fault, b: during-fault, c: after-fault

The Thevenin voltage and reactances of the circuits are presented in the following table.

Table 5-2: Thevenin equivalent of the SMIB case study for short circuit applied at Bus 3

SMIB case study	V_{th} (p.u)	x_{th}(p.u)
Before fault	1	0.22
During fault	0.333	0.16
After fault	1	0.3

5-4-1. Model Validation

The main parameters of the power system case study used in this part are presented in the following table. The contingency scenario considered for this case is similar to the one used for the validation of the classical model in the previous section.

Table 5-3: Parameters of the simulated synchronous generator

D, H	Damping factor and inertia constant, per unit	0.05, 5
x_d, x_q	Direct and Quadratic axis reactance, per unit	2.06, 1.21
$\acute{x}_d, \acute{x}_q$	Direct and Quadratic axis transient reactance, per unit	0.37, 0.37
$\acute{T}_{do}, \acute{T}_{qo}$	Direct and Quadratic axis open circuit time constant, sec	7, 0.75
T_m	Mechanical input, per unit	1

The only remaining part before performing the integration of the Equation (5.58) is to obtain the initial conditions of the four states of the 2-axis model. Equation (5.38) in complex form is as follows:

$$I = I_r + jI_i = 1.05263 \angle -18.192° = 1 - j0.3287 \ per-unit \tag{5.59}$$

Therefore, the terminal voltage before fault is obtained as

$$V_T = V_\infty + jX_{th}I = 1\angle 0° + (j0.22) \times (1.05263 \angle -18.192°)$$
$$= 1.0723 + j0.22 = V_r + jV_i \ per-unit \tag{5.60}$$

The internal voltage of the generator is obtained as

$$\acute{E} = V_T + jx_q I = E_0 \angle \delta_0 = 2.05 \angle 44.26° \tag{5.61}$$

The equations for transforming the network quantities to $d - q$ reference frame and reverse for voltage and current are given below [30].

$$\begin{bmatrix} V_r \\ V_i \end{bmatrix} = \begin{bmatrix} sin\delta & cos\delta \\ -cos\delta & sin\delta \end{bmatrix} \begin{bmatrix} V_d \\ V_q \end{bmatrix} \qquad \begin{bmatrix} I_r \\ I_i \end{bmatrix} = \begin{bmatrix} sin\delta & cos\delta \\ -cos\delta & sin\delta \end{bmatrix} \begin{bmatrix} I_d \\ I_q \end{bmatrix}$$

$$\begin{bmatrix} V_d \\ V_q \end{bmatrix} = \begin{bmatrix} sin\delta & -cos\delta \\ cos\delta & sin\delta \end{bmatrix} \begin{bmatrix} V_r \\ V_i \end{bmatrix} \qquad \begin{bmatrix} I_d \\ I_q \end{bmatrix} = \begin{bmatrix} sin\delta & -cos\delta \\ cos\delta & sin\delta \end{bmatrix} \begin{bmatrix} I_r \\ I_i \end{bmatrix} \tag{5.62}$$

Using Equation (5.61) in Equation (5.62), the initial values of the voltages and currents are obtained as

$$\begin{bmatrix} V_{d0} \\ V_{q0} \end{bmatrix} = \begin{bmatrix} 0.589 \\ 0.921 \end{bmatrix} \qquad \begin{bmatrix} I_{d0} \\ I_{q0} \end{bmatrix} = \begin{bmatrix} 0.9328 \\ 4875 \end{bmatrix} \tag{5.63}$$

Using Equations (5.47), (5.48), and (5.63), the initial values of the generator internal voltage are obtained as

$$E'_{q0} = 1.266 \; per - unit \qquad\qquad E'_{d0} = 0.4092 \; per - unit \tag{5.64}$$

Now, after calculating all of the initial conditions, the integration can be performed. A comparison among the outputs of the model and the data generated by PowerWorld Simulator are provided in the following figures. Figure 5-14 shows that the 2-axis fourth

order model developed in this part and the linearized numerical integration approach used

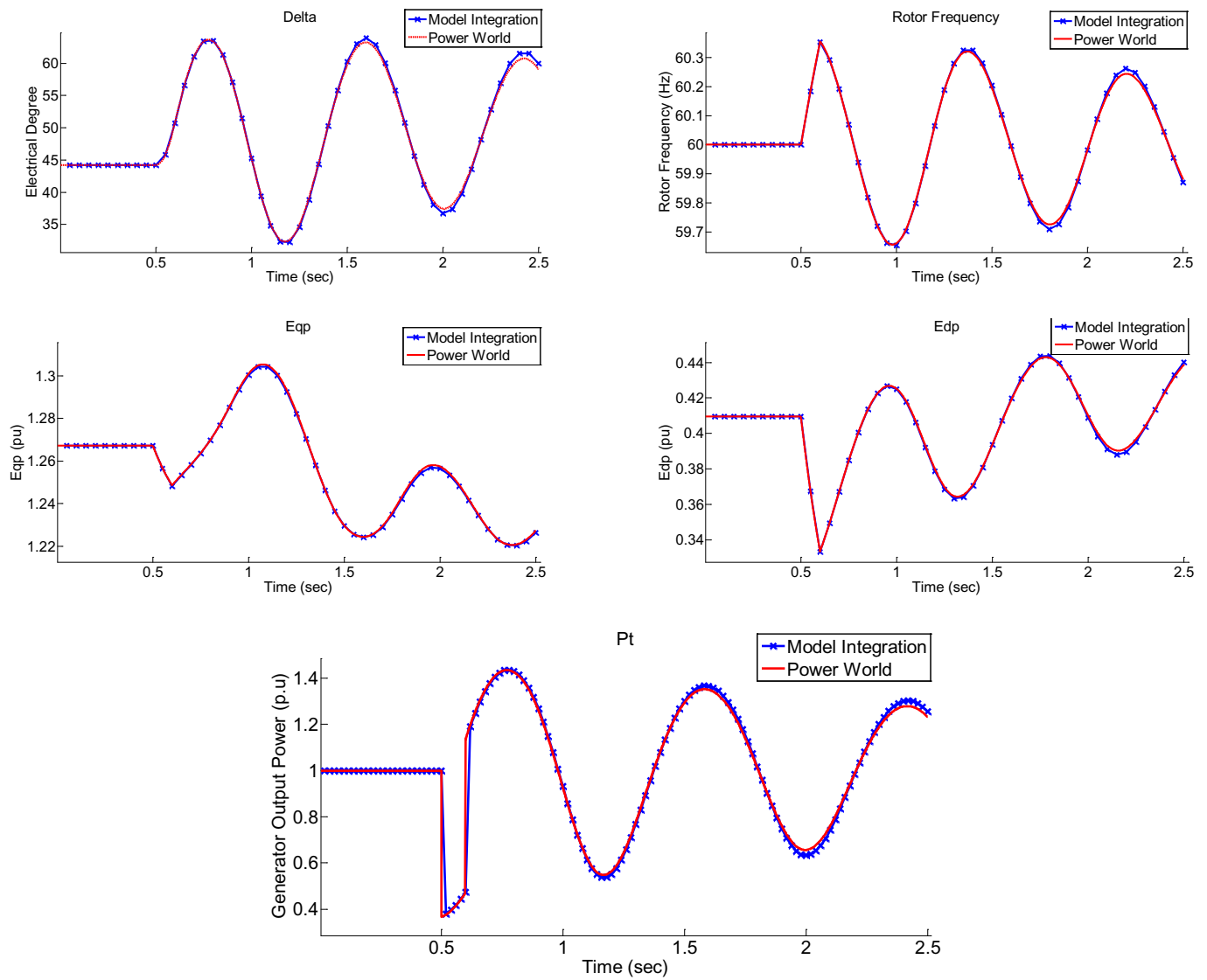in this study have adequate accuracy.

Figure 5-14: Synchronous generator 2-axis model validation

5-5. Multi-Machine Modeling and Stability Analysis

In this section, multi-machine modeling is explained and transient stability analysis is performed. The case study considered for this part is IEEE 3-Generator-9-Bus Test System which is shown in Figure 5-15.
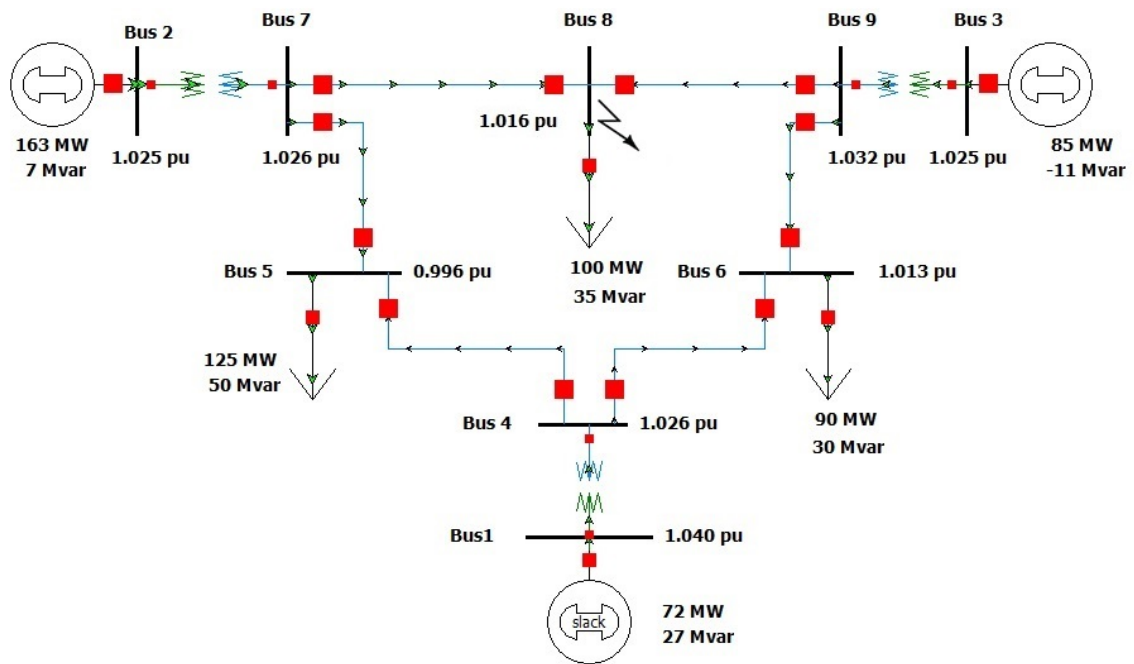
Figure 5-15: IEEE 3-Generator-9-Bus Test System simulated in PowerWorld [29]

All generators are represented by the classical model of the synchronous generator as explained in Section 5-3. The first step for transient stability analysis of a multi-machine system is to find the initial conditions of the generators and buses. The steady state voltages and angles of the buses can be easily obtained by power flow solution. These initial conditions along with the main parameters of the generators are presented in Table 5-4.

Table 5-4: Parameters and initial conditions of the IEEE 3-Generator-9-Bus Test System

D_1, D_2, D_3	Damping factor, per unit	0, 0, 0		
H_1, H_2, H_3	Inertia constant, per unit	23.64, 6.4, 3.01		
$\acute{x}_{d1}, \acute{x}_{d2}, \acute{x}_{d3}$	Direct axis transient reactance, per unit	0.0608, 0.1198, 0.1813		
T_{m1}, T_{m2}, T_{m3}	Mechanical input, per unit	0.7164, 1.63, 0.85		
P_{base}	System base power	100 MVA		
V_1, V_2, V_3, V_4	Bus voltages, per unit	$1\angle0°$ $1.025\angle9.28°$ $1.025\angle4.66°$ $1.0258\angle-2.22°$		
V_5, V_6, V_7, V_8, V_9	Bus voltages, per unit	$0.995\angle-3.99°$ $1.012\angle-3.69°$ $1.025\angle3.72°$ $1.015\angle0.73°$ $1.0323\angle1.97°$		

The initial internal voltages of the generators can be calculated using the following equation [30].

$$E_i' = V_i + jx_d'I_i = E_i'\angle\delta_i \tag{5.65}$$

Where V_i and I_i are the voltages and currents of the generators main bus. Also I_i can be calculated using the following equation [30].

$$I_i = \frac{P_i - jQ_i}{V_i^*} \tag{5.66}$$

Using Equations (5.65) and (5.66), the internal voltages of the generators are as follows:

$$E_1' = |E_1'|\angle\delta_1 = 1.0558 + j0.0421 = 1.0566\angle2.283°$$

$$E_2' = |E_2'|\angle\delta_2 = 0.9887 + j0.3546 = 1.0502\angle19.73°$$

$$E_3' = |E_3'|\angle\delta_3 = 0.9900 + j0.2315 = 1.0169\angle13.16° \tag{5.67}$$

The general equation relating the voltages and currents of a multi-machine system is given below [32].

$$I_{bus} = Y_{bus} V_{bus} \tag{5.68}$$

I_{bus} and V_{bus} are the vector of the injected bus currents and bus voltages. Therefore, separating Y_{bus} to submatrices in a meaningful way leads to

$$\begin{bmatrix} 0 \\ I_i \end{bmatrix} = \begin{bmatrix} Y_{11} & Y_{12} \\ Y_{12}^T & Y_{22} \end{bmatrix} \begin{bmatrix} V_i \\ E_i' \end{bmatrix} \tag{5.69}$$

Y_{11} is similar to the conventional Y_{bus} used for power flow analysis, except that the diagonal elements of Y_{11} include the load admittances and inverted generator transient reactance. The load admittance is calculated by the following equation.

$$Y_{Load,k} = \frac{P_{L,k} - jQ_{L,k}}{V_k{}^2} \tag{5.70}$$

Also, the kth element of Y_{12} is [30]

$$Y_{12km} = \begin{cases} \dfrac{-1}{jx'_{dn}} & if\ k = Gn\ and\ m = n \\ 0 & otherwise \end{cases} \tag{5.71}$$

113

Y_{22} is considered in the general bus matrix of the system (Y_{bus}) in such a way that Equation (5.68) includes internal voltages of the generators. This matrix can be written as follows:

$$Y_{22} = \begin{bmatrix} \dfrac{1}{jx'_{d1}} & 0 & \cdots & 0 \\ 0 & \dfrac{1}{jx'_{d2}} & 0 & \vdots \\ \vdots & 0 & \ddots & 0 \\ 0 & 0 & \cdots & \dfrac{1}{jx'_{dm}} \end{bmatrix} \tag{5.72}$$

m is the number of generators. Equation (5.69) can be written as

$$0 = Y_{11}V_i + Y_{12}E'_i$$
$$I_i = Y_{12}^T V_i + Y_{22}E'_i \tag{5.73}$$

Therefore, calculating V_i from the first expression of the above equation and inserting in the second one, leads to

$$I_i = [Y_{22} - Y_{12}^T Y_{11}^{-1} Y_{12}]E'_i = Y_{bus}^{red} E'_i \tag{5.74}$$

Considering each element of Y_{bus}^{red} as $Y_{ij} = |Y_{ij}|\angle\theta_{ij}$, P_{ei} in each time step can be expressed by the following equation [32].

$$P_{ei} = \sum_{j=1}^{m} |E'_i|\,|E'_j|\,|Y_{ij}|\cos(\theta_{ij} - \delta_i - \delta_j) \tag{5.75}$$

Similar to Equation (5.72), m is the number of generators. The classical model of the

multi-machine system based on Equation (5.37) is represented as follows:

$$\frac{d\delta_1}{dt} = \omega_0 \Delta\omega_1$$

$$\frac{d\Delta\omega_1}{dt} = \frac{1}{2H_1}(P_{m1} - P_{e1} - D\Delta\omega_1)$$

$$\frac{d\delta_2}{dt} = \omega_0 \Delta\omega_2$$

$$\frac{d\Delta\omega_2}{dt} = \frac{1}{2H_2}(P_{m2} - P_{e2} - D\Delta\omega_2)$$

$$\frac{d\delta_3}{dt} = \omega_0 \Delta\omega_3$$

$$\frac{d\Delta\omega_3}{dt} = \frac{1}{2H_3}(P_{m3} - P_{e3} - D\Delta\omega_3) \tag{5.76}$$

In each time step, P_{ei} is calculated using Equation (5.75) and inserted in Equation (5.76)

to find δ_{i+1} and $\Delta\omega_{i+1}$. The absolute values of E_i' and P_{mi} are considered constant during

numerical integration and δ_i is updated during each time step simulation.

The fault scenario considered for this case is a balanced three-phase to ground fault on

Bus 7 at $t = 0.5sec$ which is cleared at $t = 0.6sec$ for the first simulation and

$t = 0.7\ sec$ for the second one to include both stable and unstable analysis. The Y_{bus} of

the system before and after fault are the same. During-fault period, the 7th row and

column of Y_{11} are eliminated, and the Y_{bus} is calculated using Equation (5.74). The

simulation results of this part are presented in Figure 5.16 and Figure 5.17. These results

show clearly that the procedure being used in this section for multi-machine modeling

and fault analysis are valid and have acceptable accuracy.

(a)
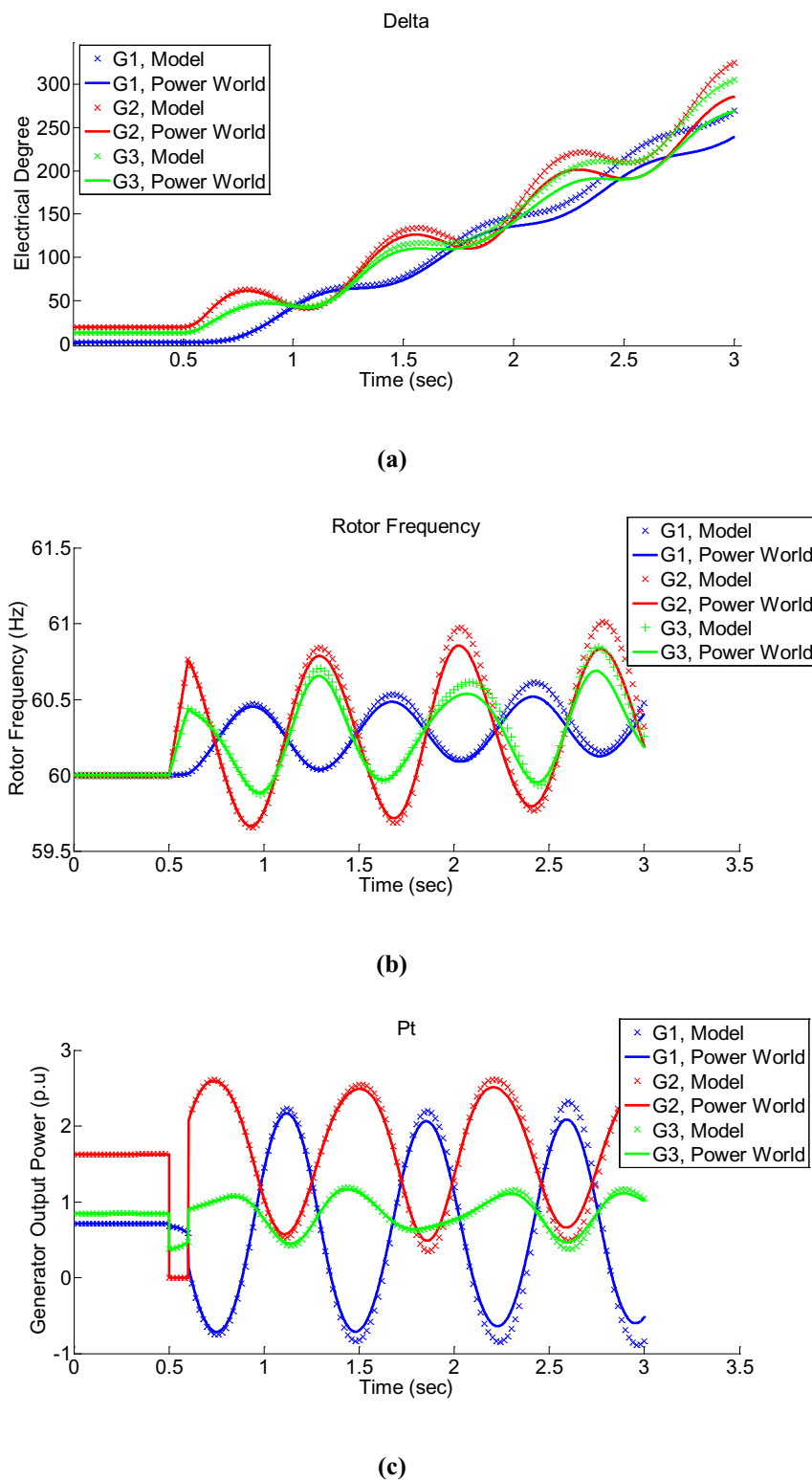

(b)

(c)

Figure 5-16: IEEE 3-Generator-9-Bus Test System transient stability analysis in stable operation; fault applied at $t = 0.5\ sec$ and cleared at= 0.6 sec: a) Rotor angle b) Rotor frequency c) Generator output power

(a)

(b)

(c)

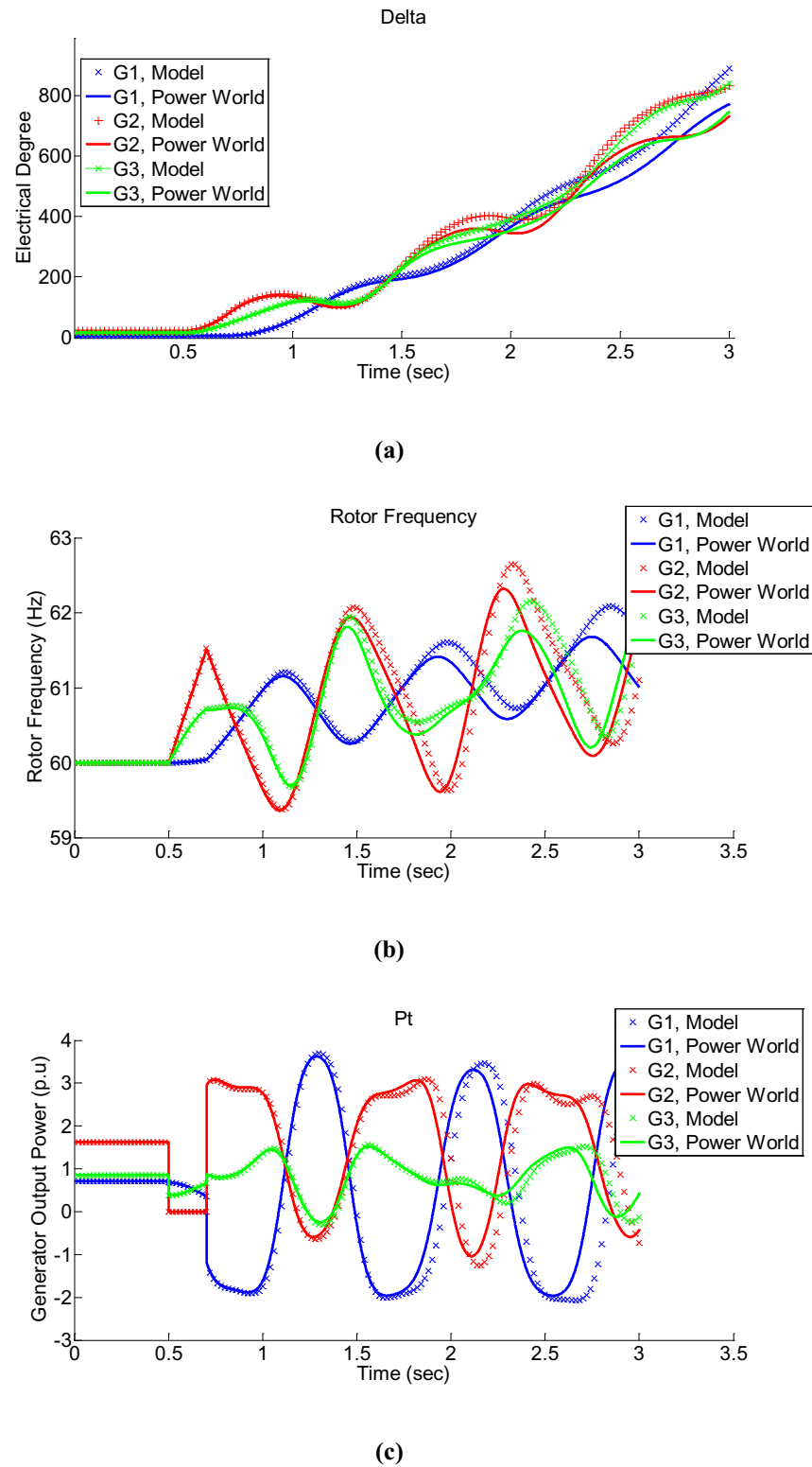**Figure 5-17: IEEE 3-Generator-9-Bus Test System transient stability analysis in unstable operation; fault applied at $t = 0.5\ sec$ and cleared at= 0.7 sec: a) Rotor angle b) Rotor frequency c) Generator output power**

Figure 5.16 shows the simulation results for multi-machine system in stable mode and Figure 5.17 corresponds to the simulation results for unstable multi-machine power system. In both figures, results of the model integration are compared with the data provided by PowerWorld simulator. The multi-machine model presented in Equation (5.76) cannot be used for dynamic state estimation in the IEEE 3-Generator-9-Bus System, because the optimal estimation approaches used in this study are developed based on the fourth order model of the machine. However, as it is assumed that online information of the main buses of the system are provided by PMU data, the fourth order model which is validated for SMIB, is applicable for online state estimation in multi-machine system, without the need for further validation for such a large system.

5-6. Summary

In this chapter, a simple RLC example is presented to clarify the idea of state space modeling and numerical integration. The mathematical description of a synchronous generator is then presented and used for the classical model of the machine. After validating the classical model, the equal area criterion along with two examples and related figures are explained in detail. The 2-axis fourth order model of a synchronous generator is then derived and validated. The multi-machine modeling and transient stability analysis are developed and used for fault analysis of the IEEE 3-Generator-9-Bus Test System. In all the simulations, results of the developed models are compared with the results obtained by PowerWorld Simulator to validate the models.

CHAPTER 6

6. Dynamic State Estimation in Power Systems

6-1. Introduction

In this chapter the nonlinear estimation methods proposed in Chapter 2, EKF and UKF, are applied for dynamic state estimation in the power system case studies discussed in Chapter 5. The first case study is a Single-Machine-Infinite-Bus (SMIB) which can be considered as the smallest part of an interconnected large power system, and the second one is the IEEE 3-Generator-9-Bus Test System. Dynamic state estimation of power systems is necessary for wide area control purposes. Precise, accurate, and well-timed information about rotor angle and speed deviation, among the states of the synchronous machine, have precious value to enhance power system reliability and stability [2, 28].

Therefore, the aim of this chapter is to design suitable estimators using Kalman Filter to estimate the main states of a synchronous machine in the two power system case studies.

In recent years, many researches in the field of dynamic power system estimation have focused on Kalman Filter as an efficient recursive estimation approach [1- 4]. Before the advent of Phasor Measurement Units (PMUs) [7], online state estimation in power systems using low rate and non-synchronous data provided by Supervisory Control and Data Acquisition (SCADA) measurements was inefficient. As PMUs are becoming more adopted worldwide, real time state estimation in power systems is becoming more realizable [2]. As mentioned in Chapter 4, PMU is a recently developed power system measurement device that samples input three phase voltage V_{abc} and current I_{abc} waveforms, using a common synchronizing signal received by Global Positioning System (GPS), and calculates the phasors (magnitudes and angles) of the bus by deploying Discrete Fourier Transform [7].

Researchers have used various estimation approaches and case studies to investigate dynamic state estimation in power systems. In [1], feasibility studies of applying Extended Kalman Filter (EKF) to IEEE 3-Generator-9-Bus Test System using second order model of the synchronous generator are investigated. SMIB is the case study for evaluating an EKF based estimator in [2], considering lack of field voltage. Also, UKF is the main approach in [28] to design an observer for SMIB using PMU installed on the main bus of the generator. Both of these articles have used 2-axis fourth order state space model of the synchronous machine. References [3, 4] have applied UKF to different power system case studies using second order synchronous generator model while considering speed and electrical output power of the machine as available measurements.

In [5], a divide-by-difference-filter based algorithm is proposed for dynamic estimation of the generator rotor angle in a large power system. The results of state estimation in a SMIB using extended particle filter are also presented in [6].

In this chapter, EKF and UKF based estimators are used for dynamic state estimation in SMIB and IEEE 3-Generator-9-Bus Test System case studies. The two-axis fourth order model of the synchronous machine is used in the estimation process, and the obtained simulation results are compared.

6-2. SMIB State Space Model

In this section, the fourth order state space model of a synchronous generator is described, and discretized equations suitable for recursive methods are developed. Four states of a synchronous machine, namely rotor angle δ, rotor speed deviation $\Delta\omega$, and internal voltages $\acute{e}_q$ and $\acute{e}_d$ are estimated simultaneously in the estimation process. In order to reach a noise free output power signal, P_t as the only measurement of the system is also estimated along with the other states. The general block diagram of the dynamic state estimator for SMIB is presented in Figure 6-1.
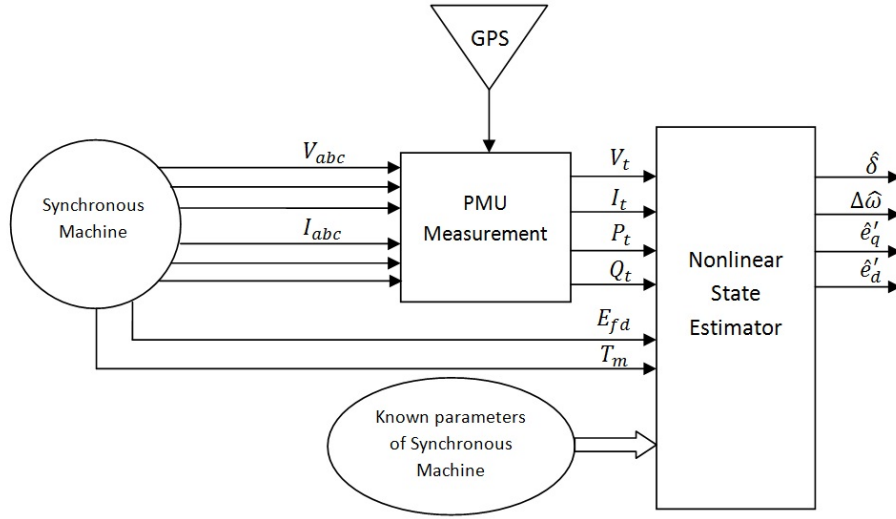
Figure 6-1: General diagram of the online state estimator for SMIB using PMU signal [28]

It is assumed that a PMU is installed on the main bus of the generator; therefore, the 2-axis model presented in Equation (5.57) is used in this part for the dynamic state estimation. V_t is considered as the reference phasor, and the synchronous generator can be represented in the dqo reference frame by the following fourth order nonlinear state space model [2]

$$X = [\delta \quad \Delta\omega \quad \acute{e}_q \quad \acute{e}_d]^T = [x_1 \quad x_2 \quad x_3 \quad x_4]^T$$

$$U = [P_m \quad E_{fd}]^T = [u_1 \quad u_2]^T$$

$$\begin{cases} \dot{x}_1 = \omega_0 x_2 \\ \dot{x}_2 = \dfrac{1}{2H}(u_1 - P_e - Dx_2) \\ \dot{x}_3 = \dfrac{1}{\acute{T}_{do}}(u_2 - x_3 - (x_d - x_d')i_d) \\ \dot{x}_4 = \dfrac{1}{\acute{T}_{qo}}(-x_4 + (x_q - x_q')i_q) \end{cases} \tag{6.1}$$

In Equation (6.1) $\omega_0 = 2\pi f_0$ is the rated synchronous frequency ($elec.\,rad/sec$), P_m the mechanical input power from the prime mover (pu), P_e the air gap electrical output power (pu), E_{fd} the exciter or field voltage as seen from the armature (pu), and δ the rotor angle in ($electrical\ radian$) [2]. Using the fourth order model presented in Equations (5.57) and (6.1) and by including V_t in input vector U, the state space model of the synchronous generator can be expressed as follows:

$$X = [\delta \quad \Delta\omega \quad \acute{e}_q \quad \acute{e}_d]^T = [x_1 \quad x_2 \quad x_3 \quad x_4]^T$$

$$U = [T_m \quad E_{fd} \quad V_t]^T = [u_1 \quad u_2 \quad u_3]^T$$

$$
\begin{bmatrix} \dot{x}_1 \\ \dot{x}_2 \\ \dot{x}_3 \\ \dot{x}_4 \end{bmatrix} =
\begin{bmatrix}
\omega_0 x_2 \\[2mm]
\frac{1}{2H}\left(P_m - \left(\frac{V_t}{x_d'}x_3 \sin(x_1) - \frac{V_t}{x_q'}x_4 \cos(x_1) + \frac{V_t^2}{2}\left(\frac{1}{x_q'} - \frac{1}{x_d'}\right)\sin(2x_1)\right) - Dx_2\right) \\[2mm]
\frac{1}{\acute{T}_{do}}\left(E_{fd} - x_3 - (x_d - x_d')\left(\frac{x_3 - V_t \cos(x_1)}{x_d'}\right)\right) \\[2mm]
\frac{1}{\acute{T}_{qo}}\left(-x_4 + (x_q - x_q')\left(\frac{V_t \sin(x_1) - x_4}{x_q'}\right)\right)
\end{bmatrix}
$$

$$[y_1] = [P_t] = \left[\frac{V_t}{x_d'}x_3 \sin(x_1) - \frac{V_t}{x_q'}x_4 \cos(x_1) + \frac{V_t^2}{2}\left(\frac{1}{x_q'} - \frac{1}{x_d'}\right)\sin(2x_1)\right] \tag{6.2}$$

This model is suitable for discrete-time nonlinear state estimation with the electrical output power as the single measurement signal. However, according to Figure 6-1, $V_t, P_t,$ and Q_t are also accessible signals from the PMU installed on the generator terminal bus

which are not used for this study. The discretized state space model of the system using the first order approximation of Taylor Series is given by

$$X^k = \begin{bmatrix} \delta^k & \Delta\omega^k & \acute{e}_q{}^k & \acute{e}_d{}^k \end{bmatrix}^T = \begin{bmatrix} x_1^k & x_2^k & x_3^k & x_4^k \end{bmatrix}^T$$

$$\begin{bmatrix} x_1^{k+1} \\ x_2^{k+1} \\ x_3^{k+1} \\ x_4^{k+1} \end{bmatrix}$$

$$= \begin{bmatrix} x_1^k + T_s\omega_0 x_2^k \\ \dfrac{T_s}{2H}\left(P_m^k - \dfrac{V_t^k}{x_d'}x_3^k \sin(x_1^k) + \dfrac{V_t^k}{x_q'}x_4^k\cos(x_1^k) - \dfrac{(V_t^k)^2}{2}\left(\dfrac{1}{x_q'}-\dfrac{1}{x_d'}\right)\sin(2x_1^k)\right) + \left(1-\dfrac{DT_s}{J}\right)x_2^k \\ \dfrac{T_s}{\acute{T}_{do}}\left(E_{fd}^k - (x_d - x_d')\left(\dfrac{x_3^k - V_t^k\cos(x_1^k)}{x_d'}\right)\right) + \left(1-\dfrac{T_s}{\acute{T}_{do}}\right)x_3^k \\ \dfrac{T_s}{\acute{T}_{qo}}\left((x_q - x_q')\left(\dfrac{V_t^k\sin(x_1^k) - x_4^k}{x_q'}\right)\right) + \left(1-\dfrac{T_s}{\acute{T}_{qo}}\right)x_4^k \end{bmatrix}$$

$$y_1^k = \dfrac{V_t^k}{x_d'}x_3^k\sin(x_1^k) - \dfrac{V_t^k}{x_q'}x_4^k\cos(x_1^k) + \dfrac{(V_t^k)^2}{2}\left(\dfrac{1}{x_q'}-\dfrac{1}{x_d'}\right)\sin(2x_1^k) \tag{6.3}$$

In the above equation, T_s is the sampling time. Using this model and deploying the high rate data provided by the PMU, designing an online state estimator for SMIB is realizable. In the next section, the Jacobian matrices of the system model and the output equation are calculated.

6-3. SMIB Dynamic State Estimation Using EKF and UKF

The partial derivative matrices of the system and the output equations, necessary for the recursive EKF algorithm, are calculated in this section. These derivatives are performed as follows [2]:

$$F_k = \frac{\partial f_k}{\partial X} = \frac{\partial X_{k+1}}{\partial X} \tag{6.4}$$

$$= \left[\frac{\partial x_1^{k+1}}{\partial X^k} \quad \frac{\partial x_2^{k+1}}{\partial X^k} \quad \frac{\partial x_3^{k+1}}{\partial X^k} \quad \frac{\partial x_4^{k+1}}{\partial X^k} \right]^T$$

$$\frac{\partial x_1^{k+1}}{\partial X^k} = \left[\frac{\partial x_1^{k+1}}{\partial x_1^k} \quad \frac{\partial x_1^{k+1}}{\partial x_2^k} \quad \frac{\partial x_1^{k+1}}{\partial x_3^k} \quad \frac{\partial x_1^{k+1}}{\partial x_4^k} \right] \qquad \frac{\partial x_2^{k+1}}{\partial X^k} = \left[\frac{\partial x_2^{k+1}}{\partial x_1^k} \quad \frac{\partial x_2^{k+1}}{\partial x_2^k} \quad \frac{\partial x_2^{k+1}}{\partial x_3^k} \quad \frac{\partial x_2^{k+1}}{\partial x_4^k} \right]$$

$$= [F_{11} \quad F_{12} \quad F_{13} \quad F_{14}] \qquad\qquad = [F_{21} \quad F_{22} \quad F_{23} \quad F_{24}]$$

$$\frac{\partial x_3^{k+1}}{\partial X^k} = \left[\frac{\partial x_3^{k+1}}{\partial x_1^k} \quad \frac{\partial x_3^{k+1}}{\partial x_2^k} \quad \frac{\partial x_3^{k+1}}{\partial x_3^k} \quad \frac{\partial x_3^{k+1}}{\partial x_4^k} \right] \qquad \frac{\partial x_4^{k+1}}{\partial X^k} = \left[\frac{\partial x_4^{k+1}}{\partial x_1^k} \quad \frac{\partial x_4^{k+1}}{\partial x_2^k} \quad \frac{\partial x_4^{k+1}}{\partial x_3^k} \quad \frac{\partial x_4^{k+1}}{\partial x_4^k} \right]$$

$$= [F_{31} \quad F_{32} \quad F_{33} \quad F_{34}] \qquad\qquad = [F_{41} \quad F_{42} \quad F_{43} \quad F_{44}]$$

Therefore, using Equations (6.3) and (6.4), the elements of the Jacobian matrix can be calculated as follows:

$$F_{11} = 1 \qquad\qquad F_{12} = T_s \omega_0 \qquad\qquad F_{13} = F_{14} = 0$$

$$F_{21} = -\frac{T_s}{2H}\left(\frac{V_t^k}{x_d'}x_3^k\cos(x_1^k) + \frac{V_t^k}{x_q'}x_4^k\sin(x_1^k) + (V_t^k)^2\left(\frac{1}{x_q'} - \frac{1}{x_d'}\right)\cos(2x_1^k)\right)$$

$$F_{22} = \left(1 - \frac{DT_s}{2H}\right) \qquad F_{23} = -\frac{T_s}{2H}\frac{V_t^k}{x_d'}\sin(x_1^k) \qquad F_{24} = \frac{V_t^k}{x_q'}\cos(x_1^k)$$

$$F_{31} = -\frac{T_s}{\acute{T}_{do}}(x_d - x_d')\frac{V_t^k\sin(x_1^k)}{x_d'} \qquad\qquad\qquad F_{32} = 0$$

$$F_{33} = 1 - \frac{T_s}{\acute{T}_{do}}\left(1 + \frac{x_d - x_d'}{x_d'}\right) \qquad\qquad\qquad F_{34} = 0$$

$$F_{41} = \frac{T_s}{\acute{T}_{qo}}(x_q - x_q')\left(\frac{V_t^k\cos(x_1^k)}{x_q'}\right) \qquad\qquad\qquad F_{42} = F_{43} = 0$$

$$F_{44} = 1 - \frac{T_s}{\acute{T}_{qo}}\left(1 + \left(\frac{x_q - x_q'}{x_q'}\right)\right) \qquad\qquad\qquad (6.5)$$

The partial derivative of the output equation is calculated using Equation (2.53) and is presented here.

$$H_k = \frac{\partial h_k}{\partial X} = \left[\frac{\partial h_1^k}{\partial X}\right] = \left[\frac{\partial h_1^k}{\partial x_1^k} \quad \frac{\partial h_1^k}{\partial x_2^k} \quad \frac{\partial h_1^k}{\partial x_3^k} \quad \frac{\partial h_1^k}{\partial x_4^k}\right]^T = [H_{11} \quad H_{12} \quad H_{13} \quad H_{14}]$$

$$H_{11} = \frac{V_t^k}{x_d'}x_3^k\cos(x_1^k) + \frac{V_t^k}{x_q'}x_4^k\sin(x_1^k) + (V_t^k)^2\left(\frac{1}{x_q'} - \frac{1}{x_d'}\right)\cos(2x_1^k)$$

$$H_{12} = 0 \qquad\qquad H_{13} = \frac{V_t^k}{x_d'}\sin(x_1^k) \qquad H_{14} - \frac{V_t^k}{x_q'}\cos(x_1^k) \qquad\qquad (6.6)$$

6-3-1. Simulation Results

In this part EKF and UKF are employed for dynamic state estimation in SMIB using discrete state space model presented in Equation (6.3). Original data obtained from the contingency analysis of the system in PowerWorld Simulator [29] is injected into the designed estimators in MATLAB [25] to have a reliable simulation results. The first simulation scenario is a symmetrical permanent three-phase-to-ground bolted short circuit which occurs on the middle of the second transmission line at $t = 0.5\ sec$. The fault is cleared after $0.1\ sec$ by opening the circuit breakers at the ends of this transmission line, and the system retains its stability after clearing the fault. The parameters of the SMIB are the same as the ones presented in Table 5-3. As shown in Figure 6-1, P_t and V_t (phasor) are accessible from the PMU which is installed on Bus-4. E_{fd} and T_m are also measurable signals from the synchronous generator terminal [2]. Measurement and process noise covariance are considered as $R_k = 0.0002 \times I$ and $Q = 0.07^2 \times I$, respectively [2]. The simulation results for the main states and the single output of the system are presented in Figure 6-3 to Figure 6-6. These figures provide the estimated states of the system plus the measurement estimation with EKF and UKF under different sampling rates. In each figure, the real data obtained from PowerWorld Simulator is also shown to provide better evaluation for the accuracy of the estimation.
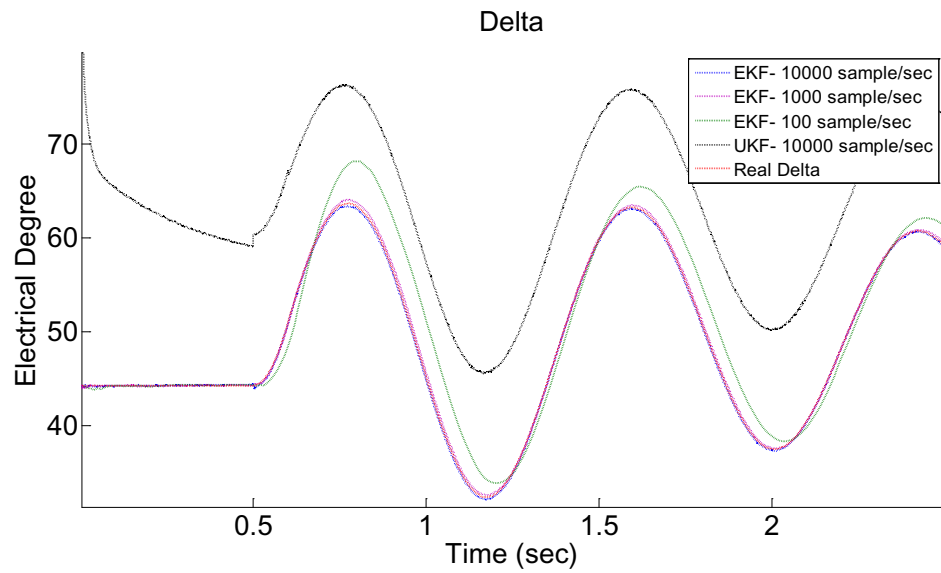
Figure 6-2: Rotor angle estimation using EKF and UKF with different PMU sampling rate (Electrical Degree)
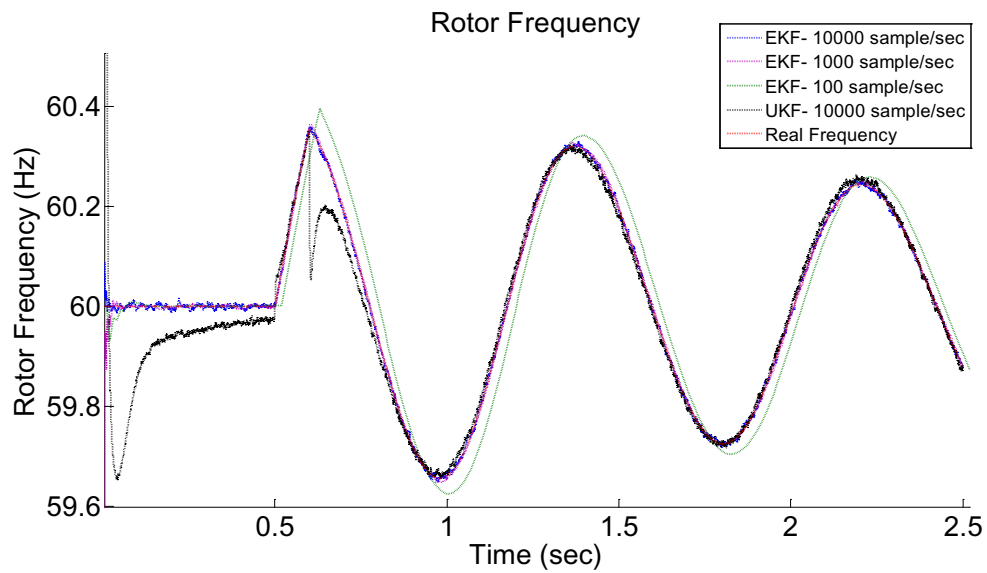

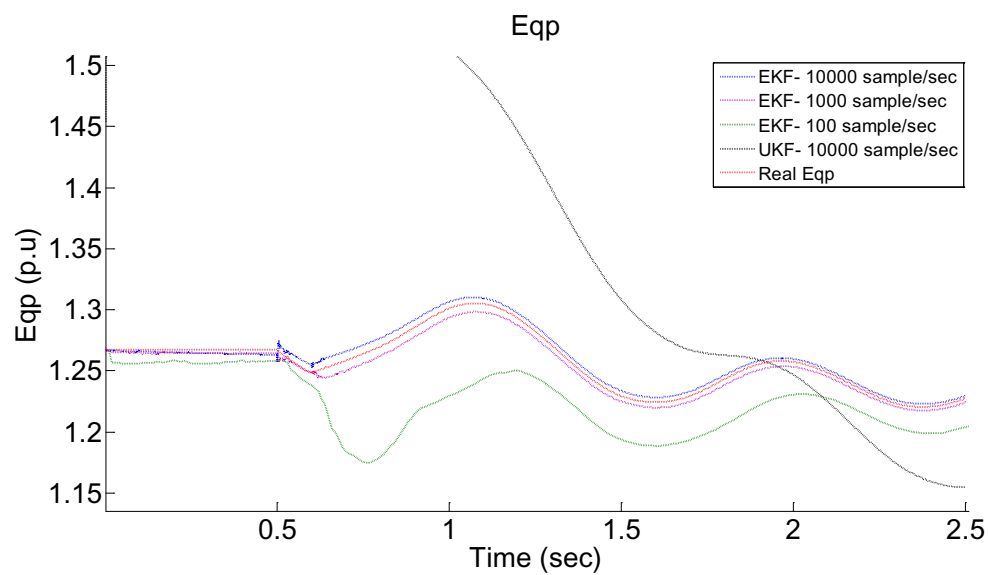**Figure 6-3: Rotor speed estimation using EKF and UKF with different PMU sampling rate (Hz)**

Figure 6-4: Q-axis internal voltage estimation using EKF and UKF with different PMU sampling rate (per unit)
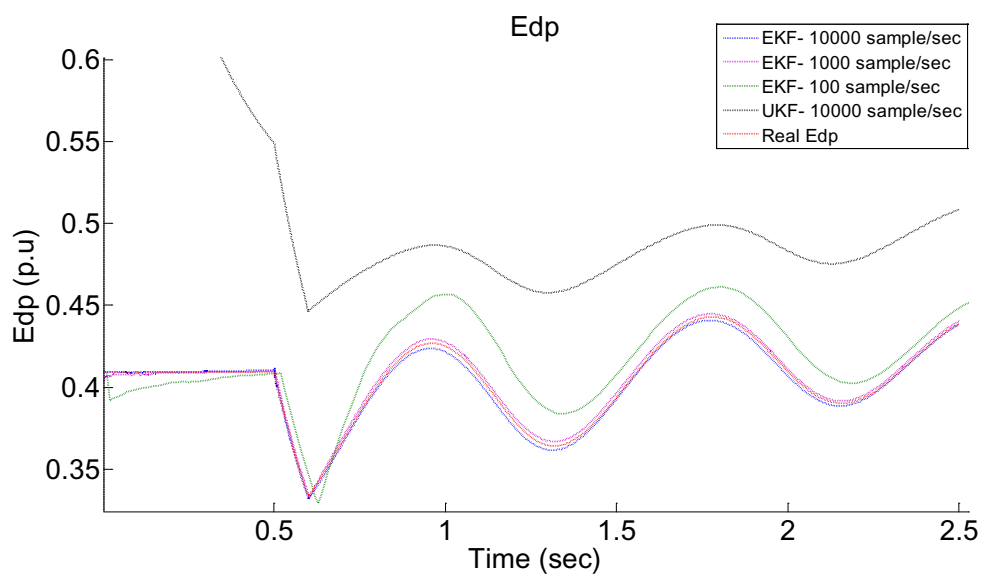

Figure 6-5: D-axis internal voltage estimation using EKF and UKF with different PMU sampling rate (per unit)
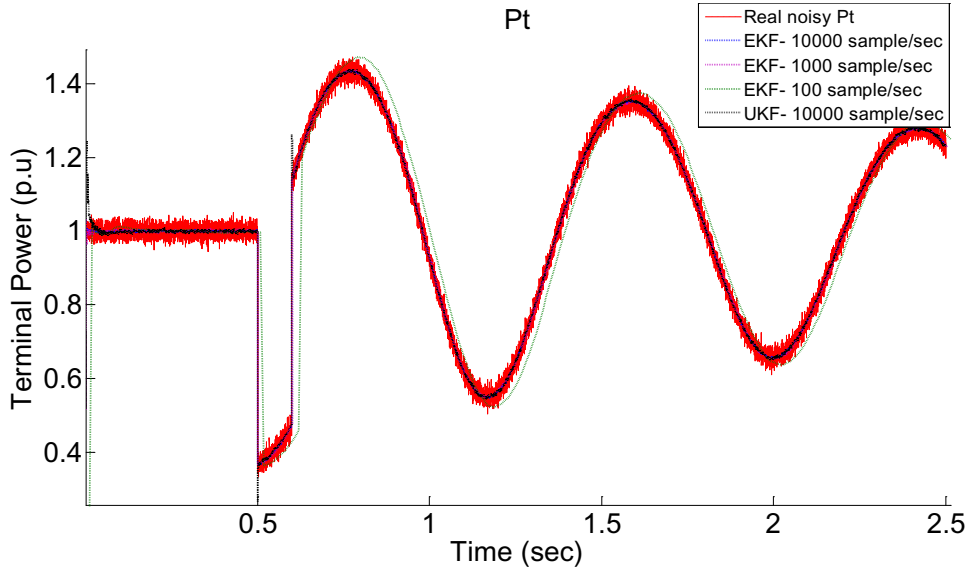
Figure 6-6: Terminal power estimation using EKF and UKF with different PMU sampling rate (per unit)

Simulation results provided in Figure 6-2 to Figure 6-6 show that both methods are capable of capturing the transient and steady state responses of the states and the only output of the SMIB which is facing a major contingency, using data provided by the PMU. UKF diverges with low data sampling rate (1000 and 100 samples/sec) and cannot accurately estimate the states in the transient time. In addition, the simulation time of EKF is much less than that of UKF which might be a major factor for online implementations.

In the next simulation scenario, the output power of the synchronous generator is increased to $200\ MW$. Similar to the previous simulation, symmetrical permanent three-phase-to-ground bolted short circuit is applied on the middle of the second transmission line at $t = 0.5\ sec$ and the fault is cleared after $0.1\ sec$ by opening the circuit breakers at the ends of this transmission line. The system will be unstable after clearing the fault

because of the higher output power. The results of the output power estimation using EKF

and UKF for this operational condition are also presented in Figure 6-7 to Figure 6-11.
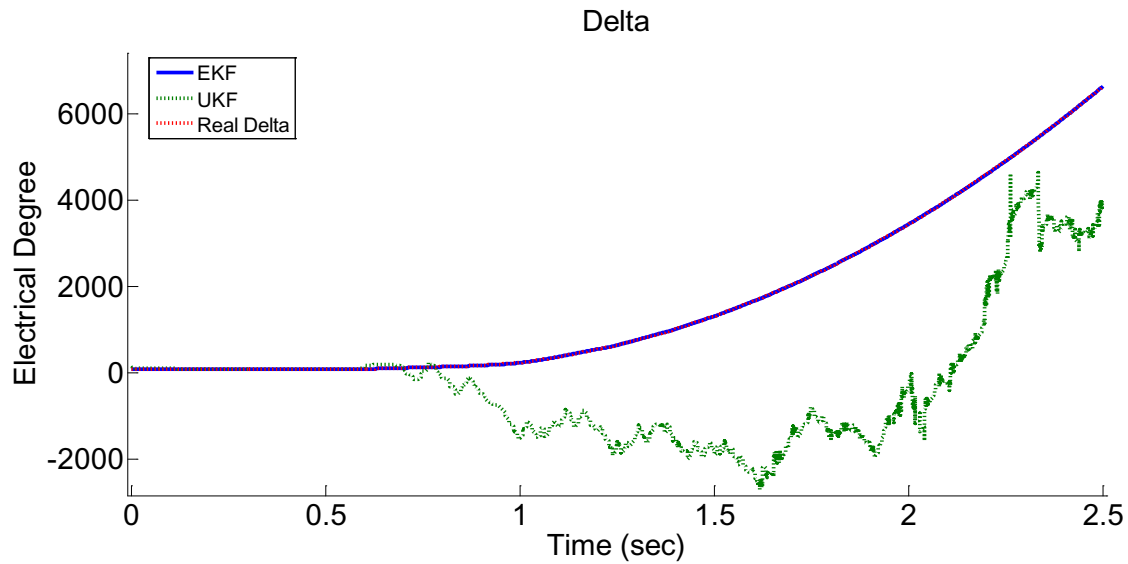

Figure 6-7: Rotor angle estimation using EKF and UKF in unstable mode (Electrical Degree)
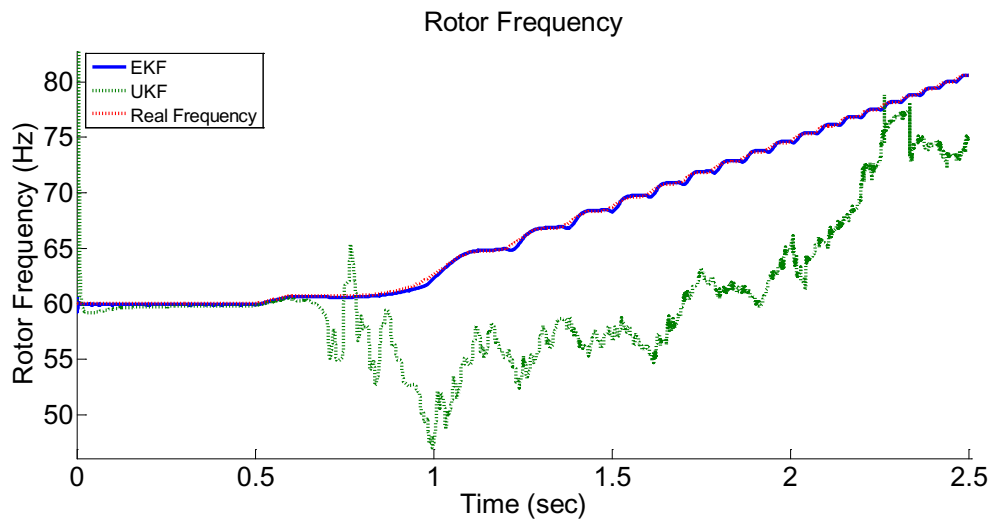

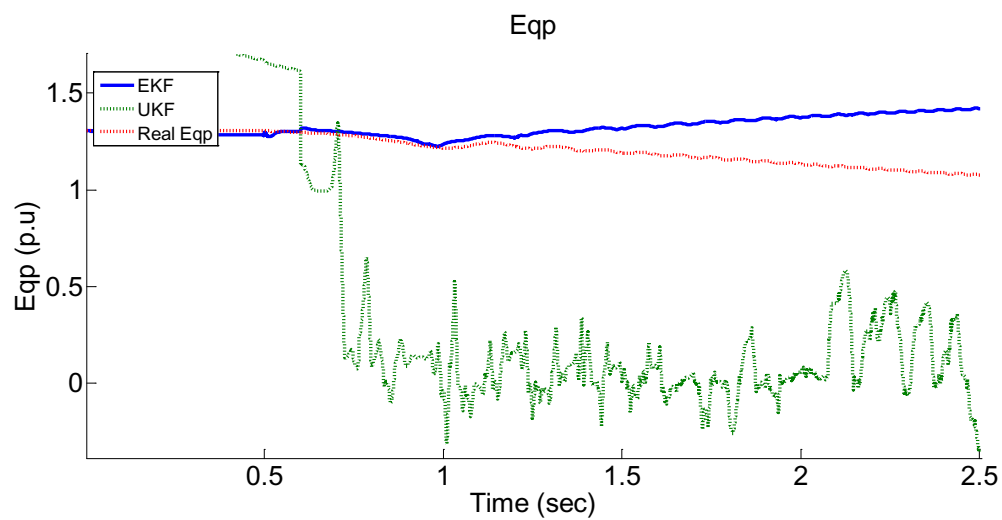**Figure 6-8: Rotor speed estimation using EKF and UKF in unstable mode (Hz)**

Figure 6-9: Q-axis internal voltage estimation using EKF and UKF in unstable mode (per unit)
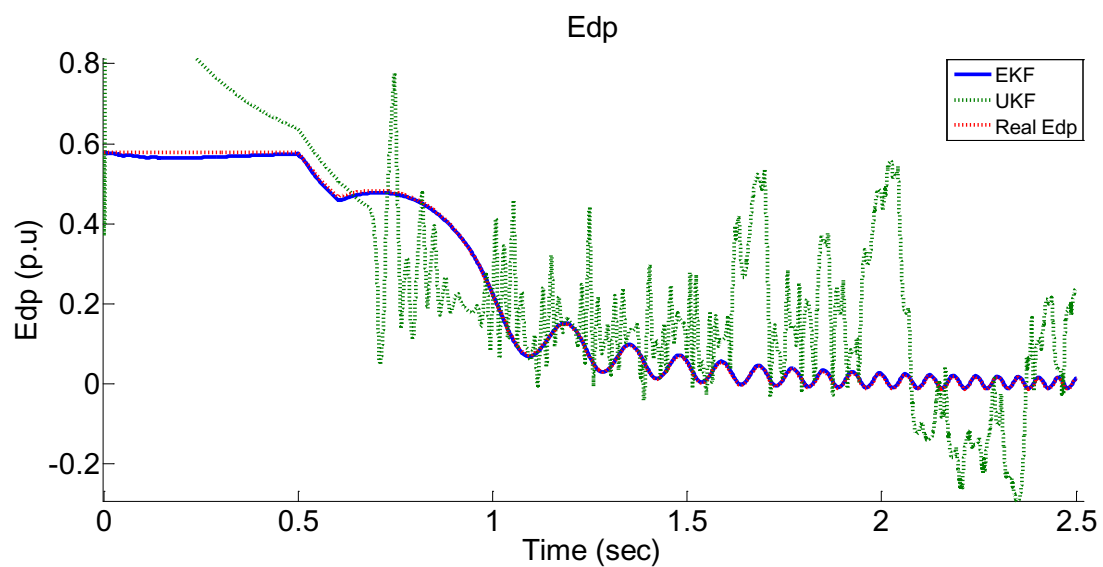

Figure 6-10: D-axis internal voltage estimation using EKF and UKF in unstable mode (per unit)
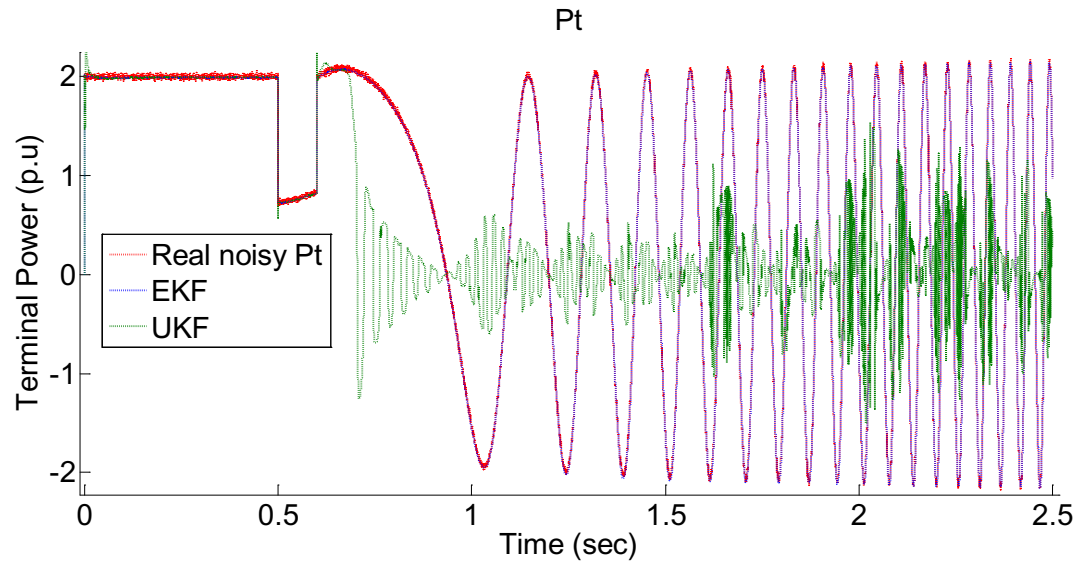
Figure 6-11: Terminal power estimation using EKF and UKF in unstable mode (per unit)

These figures show the estimated states and single output of the machine in comparison with the real data provided by PowerWorld Simulator in unstable mode. Based on the simulation results, it can be concluded that in the unstable mode, EKF is capable of capturing the transient response of the states and rejecting the noise effect on the power signal from the PMU. In contrast, the results of UKF for this mode of operation are not satisfactory.

6-4. Dynamic State Estimation in IEEE 3-Generator-9-Bus Test System Using EKF and UKF

In this section, IEEE 3-Generator-9-Bus Test System model is considered as a simulation case study to evaluate the ability of the designed EKF and UKF based estimators for state estimation in a larger power system, facing a major contingency. The PowerWorld diagram of the system is presented in Figure 6-12.
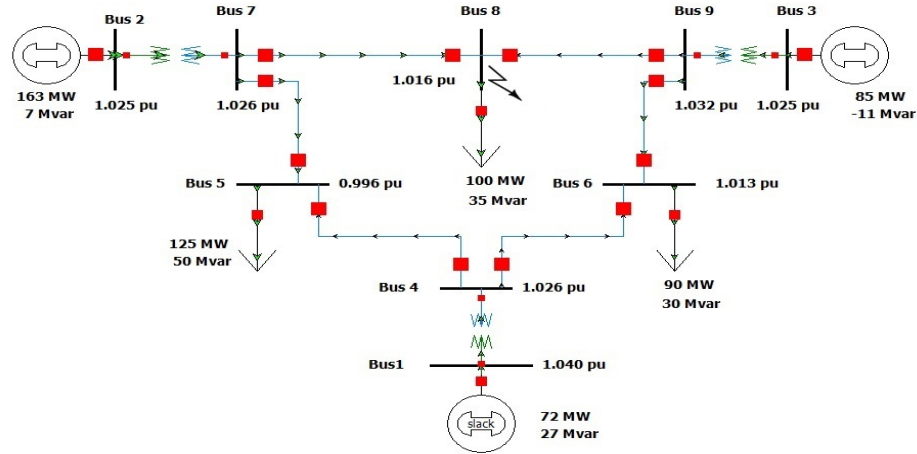
Figure 6-12: IEEE 3-Generator-9-Bus Test System PowerWorld model

It is assumed that three PMUs are installed on bus 1, bus 2, and bus 3, and the data provided by PMUs is received at the same time by an assumed PDC. All three synchronous generators are considered with 2-axis fourth order model and have the same characteristics as presented previously in Table 5-3. The simulation scenario is a symmetrical three phase fault at $t = 0.5\ sec$ on bus 8 which is cleared after $0.1\ sec$. The results of dynamic state estimation for each generator in this stable case study are presented in Figure 6-13 to Figure 6-15. It should be noted that Equation (6.3) is the discrete state space model considered for each synchronous generator. In other words, 12 state variables and 3 measurements are estimated in each iteration. Although models of the exciters and governors are not validated in Chapter 5 of this thesis, all of the generators of this case study are controlled by an exciter and a governor. As it is assumed that the PMUs are installed on the main buses of the generators, it is not theoretically necessary to validate models of the exciter and governor for dynamic state estimation; however, it can be a separate field of study for further investigation in this area.
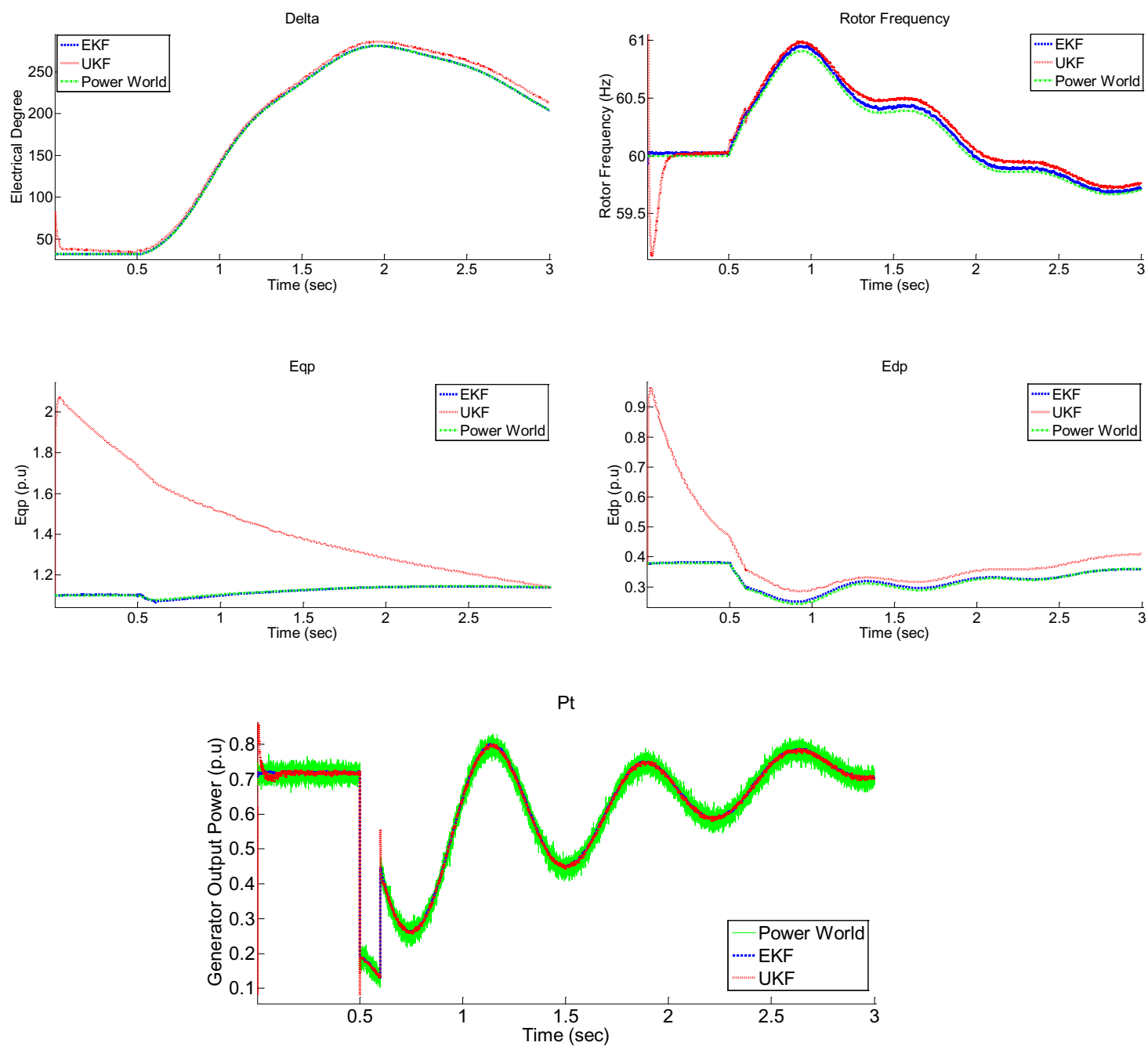
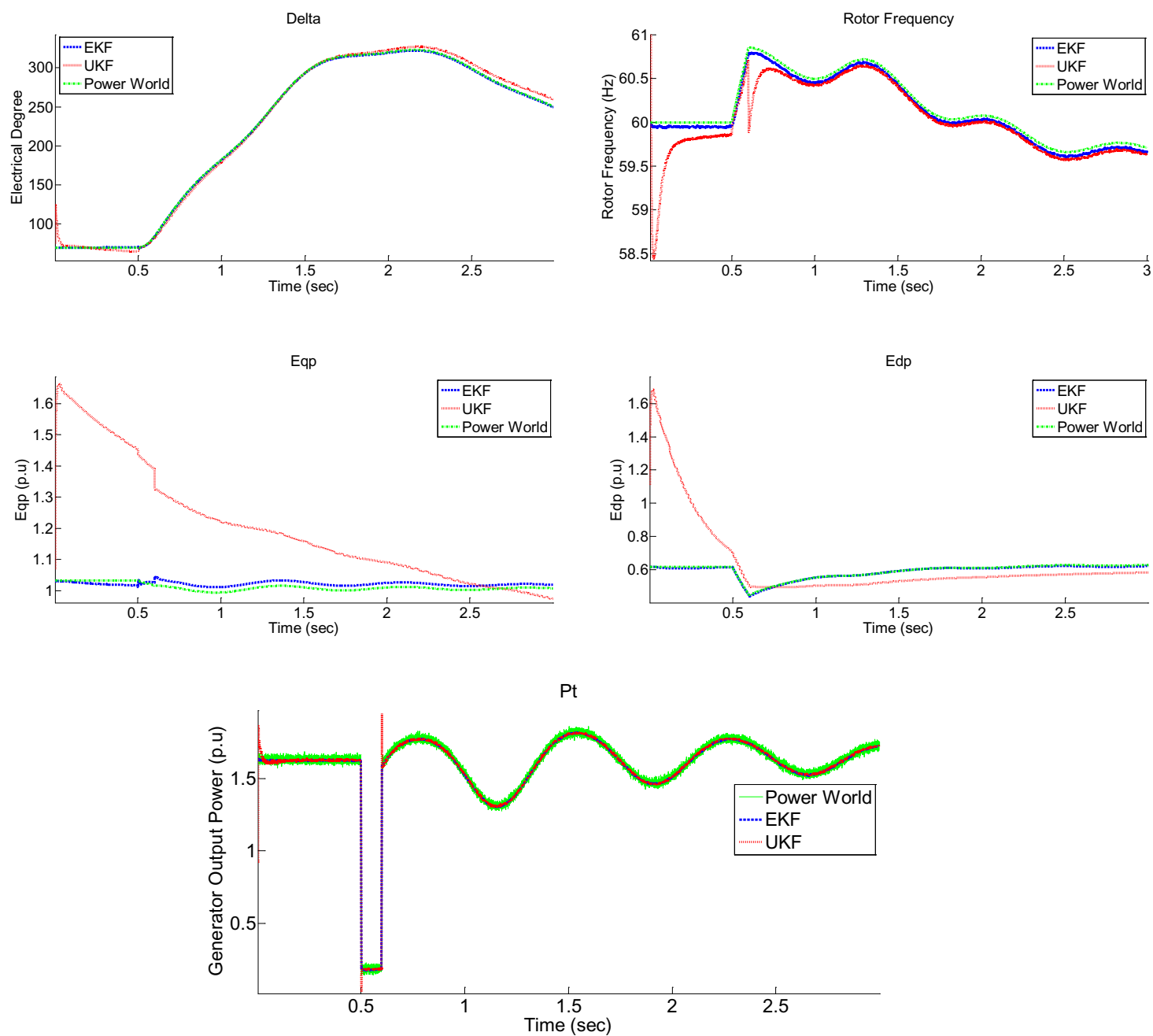**Figure 6-13: States and output estimation of Generator 1 using EKF and UKF**

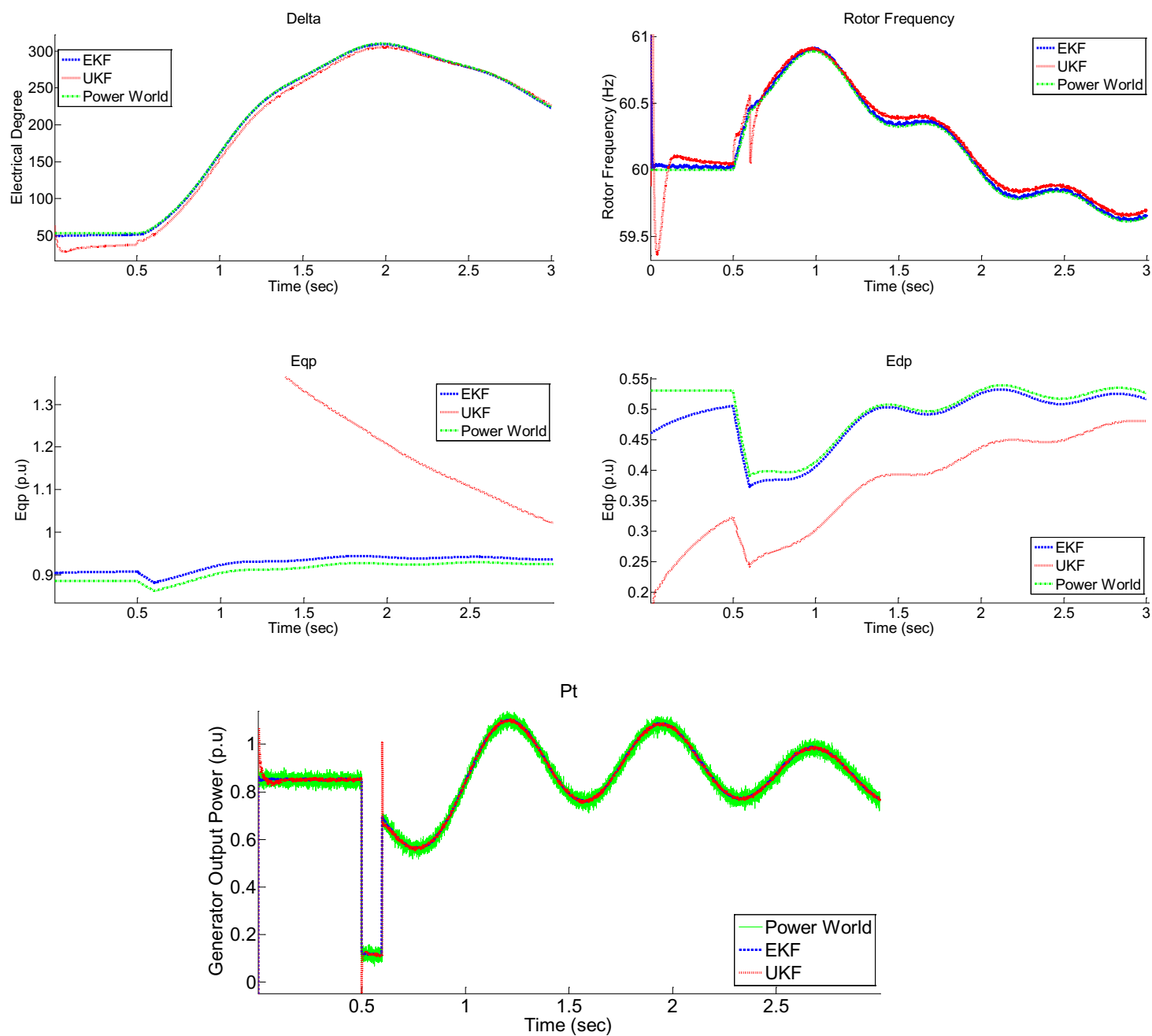**Figure 6-14: States and output estimation of Generator 2 using EKF and UKF**

Figure 6-15: States and output estimation of Generator 3 using EKF and UKF

Simulation results, presented in Figure 6.13 to Figure 6.15, reveal the ability of both EKF and UKF based observers for tracking and noise rejection of output power signals of the generators during transient and steady state response. However, in terms of accuracy of the estimation, EKF based estimator is more accurate than UKF. In addition, EKF is able to track states of the system with PMU data rate of 100 samples/sec, while UKF diverges with low data rate.

6-5. Applications of Dynamic State Estimation in Power Systems

The procedure of designing an estimator for a synchronous machine which can be used for dynamic state estimation in a power system is explained in the previous sections of this chapter in detail. In this section, a possible application of dynamic state estimation in power system is discussed. Figure 6.16 shows the complete idea of a Kalman Filter based estimator designed in this study for a synchronous machine.
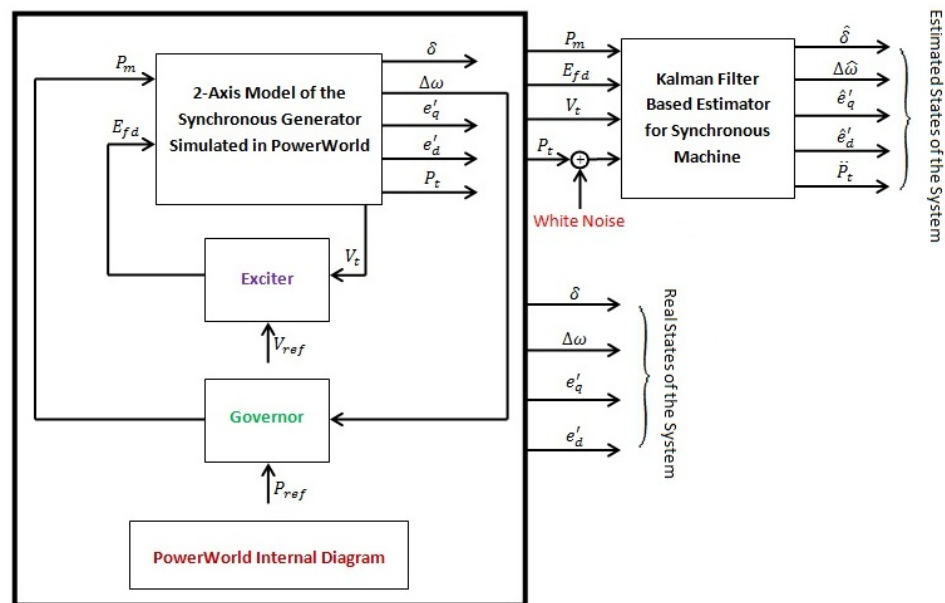

Figure 6-16: Complete diagram of a KF based estimator for a synchronous machine

Figure 6-16 shows that the basic model simulated in PowerWorld simulator is being controlled by two separate control feedback loops for the exciter and governor. Some of the outputs of the simulator (P_m, E_{fd}, V_t, and P_t) are used as inputs for the optimal estimator block, and the others (δ, $\Delta\omega$, e_q', e_d') are obtained to be compared with the estimated states. It is clear from this figure that the observer is designed to accurately estimate the main states of the synchronous machine (δ, $\Delta\omega$, e_q', e_d'), and eliminate the effect of noise on the measurement signal, which in this case is externally added to this signal (P_t) before injecting to the observer block. This is done to make the case study much more similar to a practical case. The estimated power is also used to evaluate the ability of the estimator block for eliminating noise of input signals.

A practical application of dynamic state estimation for a power system is to put the estimator block in the feedback loop of the governor of the machine. This can be considered as a sensorless control of the machine where the input signal of the governor ($\Delta\omega$) is not provided by a physical sensor and is actually the estimated speed provided by the KF based estimator. The complete diagram of this application is presented in Figure 6-17. The main advantage of this control approach is its sensorless property which eliminates the speed sensor and the related physical wiring. In addition, it is capable of input signal noise rejection which enhances the total reliability of the decision made by the control block. Also, the other estimated states of the synchronous machine ($\hat{\delta}$, $\hat{e}_q'$, $\hat{e}_d'$) can be effectively used in more complicated control schemes.
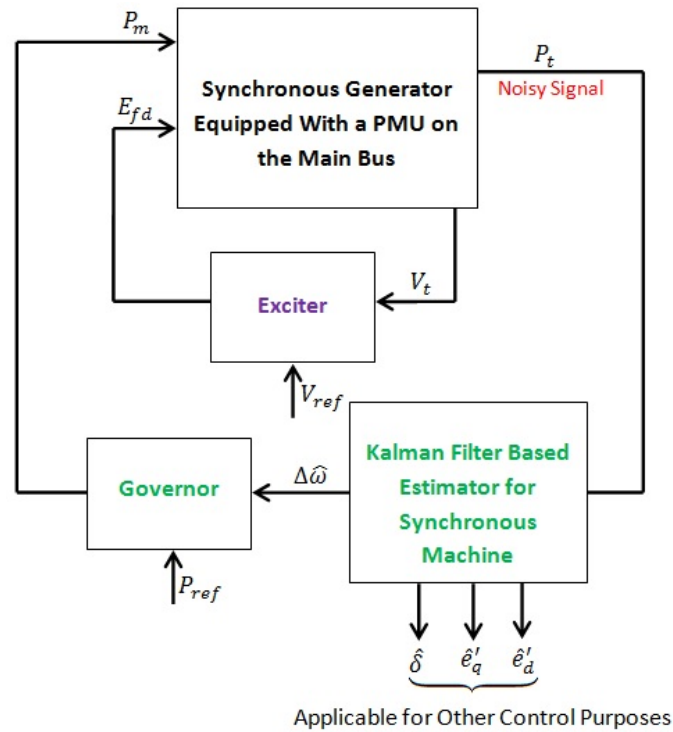
Figure 6-17: Block diagram of the sensorless control of a synchronous machine using Kalman Filter estimator

6-6. Dynamic State estimation: Main challenges for a Large Power System

The main current challenges of dynamic state estimation in large scale power systems are the inadequate number of the installed PMUs and the quite low data rate. Although the number of installed PMUs in large interconnected power systems is gradually increasing, it is not still adequate to implement dynamic state estimation. In addition, the data rate of the PMUs is still low which decreases the accuracy of the estimation to some extent. A complete advanced dynamic control system for a large scale power grid needs a movement from conventional SCADA to PMU based system, which needs huge investment in power systems, communication infrastructure, and more advanced PMU

technology. However, it might be possible to implement a complete local dynamic control system based on PMU measurement in a small area of a large power system. The block diagram for this purpose is presented in Figure 6-17. The fourth or higher order of the synchronous generator which is used for dynamic state estimation needs powerful processors for online application which makes the implementation more expensive. Nevertheless, there are numerous other models for synchronous machine with higher degree of accuracy which may have better performance than the model used in this study. The accurate models of the exciter and governor are also needed for state feedback control of the synchronous machine; therefore, these models should be derived and validated by real data, which might be a challenging task. In Chapter 7, some future works for dynamic state estimation in a large power system are proposed and the corresponding block diagrams are presented.

6-5. Summary

In this chapter, after a brief introduction about the dynamic state estimation in power systems, the state space model of the Single-Machine-Infinite-Bus (SMIB) is derived, and the discretized model of the system is presented. After deriving the Jacobian matrix, EKF and UKF are applied for dynamic state estimation in a SMIB for stable and unstable modes, and the simulation results are presented. The dynamic state estimation in a larger power system, represented by the IEEE 3-Generator-9-Bus Test System, and the simulation results of fault analysis are presented. Simulation results reveal the capability

of the proposed estimators for dynamic state estimation and measurement noise rejection in power systems using PMU high rate data. Although UKF is theoretically able to propagate the mean and covariance of the states through a nonlinear model up to the third order, the simulation results of EKF are more accurate in low rate PMU data stream (less than 200 frame/sec), which makes it more practical for the present large scale interconnected power systems. A possible application of the dynamic state estimation in power system is discussed, and a block diagram is presented for this purpose. Finally, some major current challenges of dynamic state estimation in large power grids are addressed.

CHAPTER 7

7. Conclusion and Future Works

7-1. Conclusions

Dynamic system modeling and state estimation is necessary for optimal control of complicated systems. Beside the noise rejection capability, an estimator uses the state space model of a system to provide information about the states of the system which are in some cases immeasurable. In this research, the mathematical background of the state space modeling and the principles of optimal state estimation using nonlinear Kalman Filters (Extended and Unscented) are explained in detail. Then, different state space models and nonlinear Kalman Filter based state and parameter estimators are designed and applied for estimation process in an induction motor. The simulation results of this

section show the capability of the extended model and estimation approaches in complicated operational conditions of the machine. The principles of synchrophasors, phasor measurement unit and internal blocks, and the advantages of Wide Area Monitoring, Protection, and Control are then explained to provide a background for the later chapters of the thesis which are dedicated to dynamic state estimation in power systems. The mathematical description of a synchronous generator is then presented, and classical and 2-axis model of the machine are derived and validated. The Equal Area Criterion is explained and simulated to provide an overview for transient stability in power systems. The classical model of the machine is also used to model a large multi-machine power system (IEEE 3-Generator-9-Bus Test System). The algorithm of sequential integration of the differential equations of the system is explained in detail. The results of the model integration are compared with data provided by PowerWorld Simulator to evaluate the accuracy of the model and the numerical integration method. The validated model is then used for dynamic sate estimation in a Single-Machine-Infinite-Bus (SMIB) and the large power system (IEEE 3-Generator-9-Bus Test System) in both stable and unstable modes to effectively evaluate the capability of the Kalman Filter based estimators for this purpose. A practical application of the dynamic state estimation in a power system is also proposed in this study which can be used for further investigation in this field of study.

7-2. Contributions of the Thesis

The main contribution of this research is the design and simulation of the fourth order UKF and EKF based estimator for the IEEE 3-Generator-9-Bus Test System model and comparing the simulation results of the estimators. In addition, a step-by-step state space modeling and validation procedure is presented to provide a complete modeling package for synchronous machines. The simulation results reveal the accuracy of the developed state space model and capability of the proposed estimation approaches for dynamic state estimation which can be used for transient stability analysis and control purposes in power systems. The simulation scenarios are also designed to cover both the simplest model of a power system (Single-Machine-Infinite-Bus) and a large power system (IEEE 3-Generator-9-Bus Test System) in either stable or unstable operational conditions.

Also, a comprehensive simulation is provided for the dynamic state and parameter estimation in an induction machine, and the results of EKF and UKF based estimators are compared through several simulation scenarios. The simulation scenarios designed in this study cover almost all real operational conditions of an induction motor in different applications. The basic state space model of the induction motor is gradually extended to the other states and parameters of the machine, and the drawbacks of each model are shown by different simulation scenarios. This effort is done to reasonably justify the need for more accurate modeling of the induction motor.

7-3. Future Works

Dynamic state estimation has recently been among the popular fields of research in power system studies. Different estimation approaches are applied to various models of the synchronous machine to evaluate the feasibility of the dynamic estimation in power systems. Nevertheless, little literature is available on the application of this idea. One open research area in this regard can be the study of sensorless control of a synchronous generator using Kalman Filter based estimators. Another challenging subject can be the closed loop state feedback control of a large power system, as for the example 3-Gnerator-9-Bus system. A complete block diagram for this topic is proposed in Figure 7-1. The first step for this work is to develop and validate appropriate models for exciter and governor of the machine. Then, the estimator can be inserted into the feedback path of the closed loop system and the reliability and accuracy of this control scheme can be compared with conventional control systems. The state feedback control proposed in this figure is based on a simple control block for the exciter and governor. More complicated control systems can be designed for the synchronous machine using the other states of the machine provided by the estimator.

In addition, most of the papers in dynamic state estimation in power systems, including the investigation in this thesis, have used simulation tools to generate real data which is then used in the evaluation of the proposed models and control algorithms. Therefore, the lack of practical works in this area is noticeable. Design and validation of power system models with real data provided by PMU and applying a state feedback control to a real synchronous machine is another interesting field of research.

Another interesting research in this field is the online state and parameter estimation for a synchronous machine. An EKF based estimator extended to the parameters of the synchronous machine can be designed for this purpose. The updated parameters can be used in the feedback loop to enhance the control performance. A block diagram is proposed for this purpose which is presented in Figure 7-2.
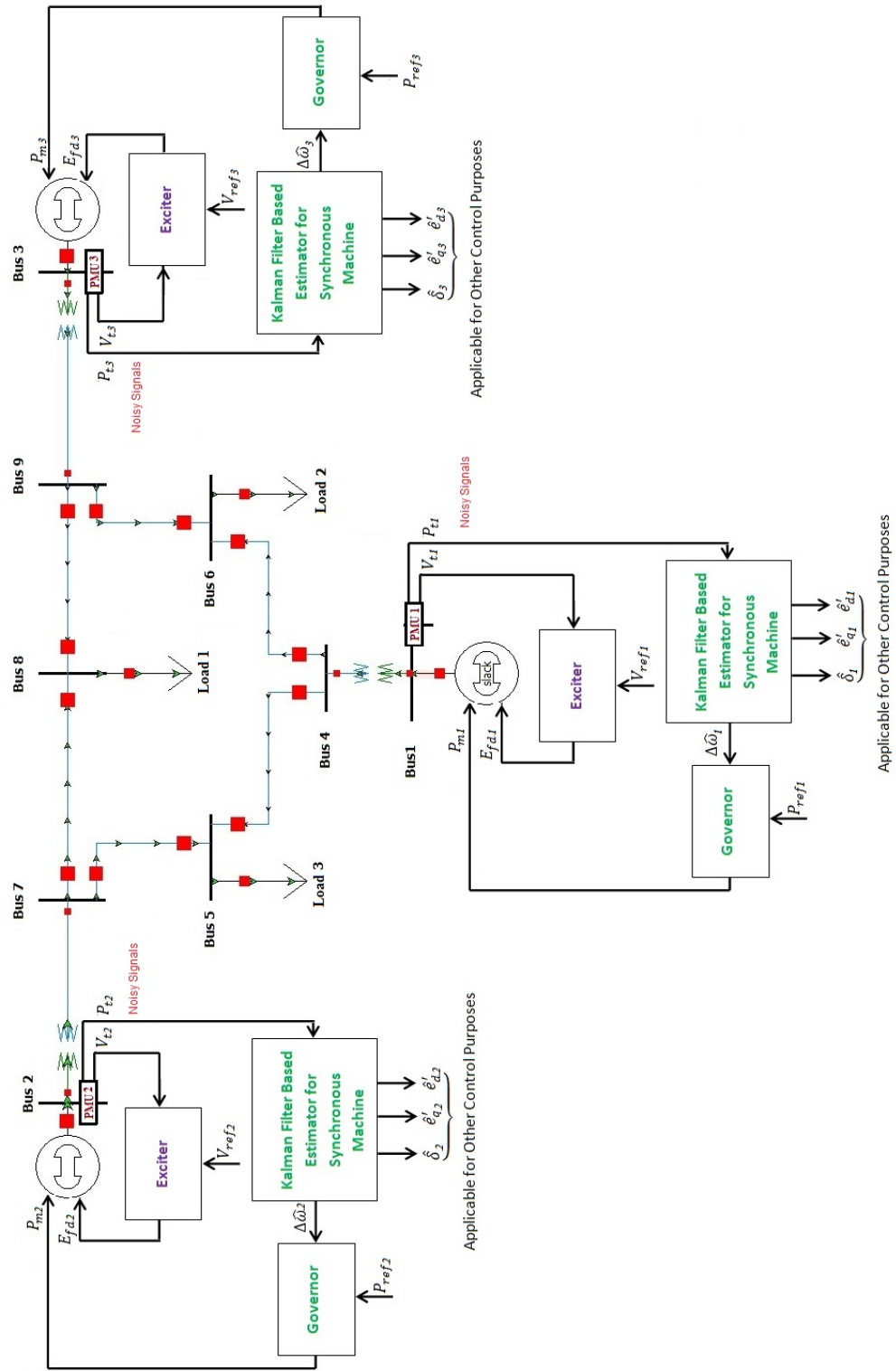
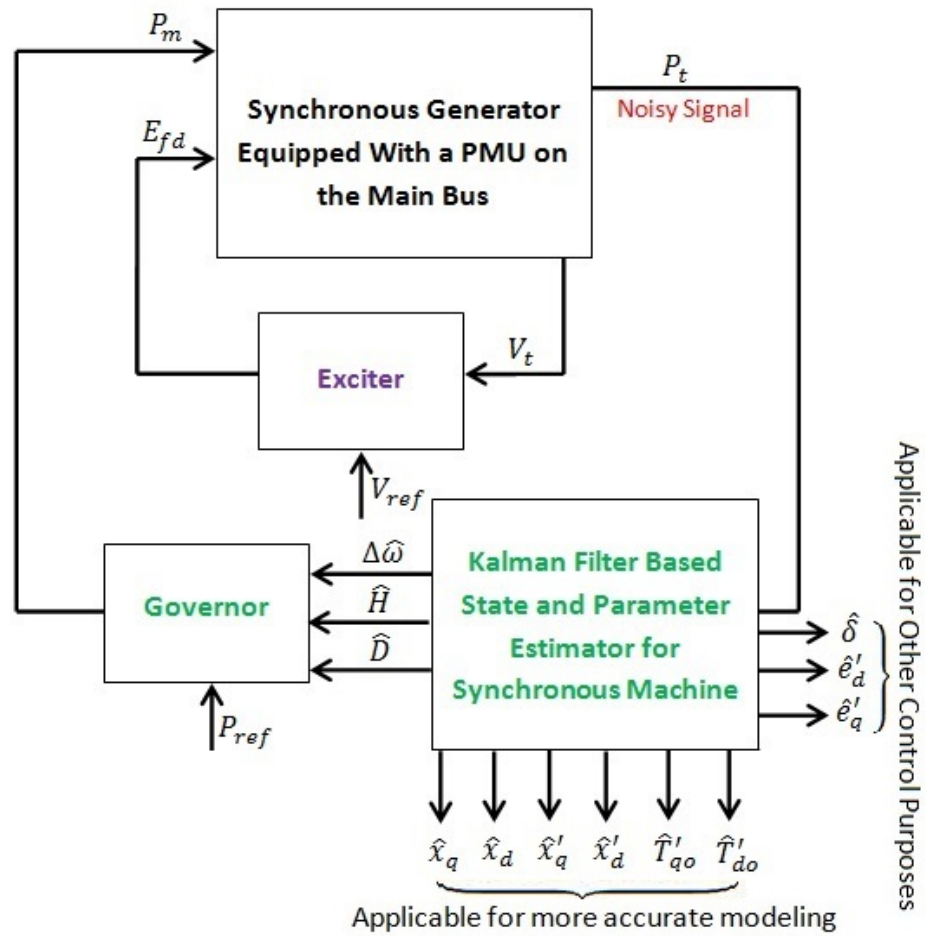**Figure 7-1: Closed loop state feedback control scheme for the IEEE 3-Generator-9-Bus Test System using Kalman Filter**

Figure 7-2: Closed loop state feedback control scheme for a synchronous machine using EKF state and parameter estimator

References

[1] Z. Huang. Peng, K. Schneider, and J. Nieplocha, "Feasibility studies of applying Kalman Filter Techniques to Power System Dynamic State Estimation," *Power Engineering Conference*, IPEC, Singapore, pp. 376-382, Dec. 2007.

[2] E. Ghahremani, and I. Kamwa, "Dynamic state estimation in power system by applying the extended Kalman filter with unknown inputs to phasor measurements," *IEEE Transactions on Power Systems*, Vol. 26, No. 4, pp. 2556-2566, Nov. 2011.

[3] W. Gao, and S. Wang, "On-line dynamic state estimation of power systems," *North American Power Symposium (NAPS)*, USA, pp. 1-6, Sep. 2010.

[4] S. Wang, W. Gao, and A. P. S. Meliopoulos, "An Alternative Method for Power System Dynamic State Estimation Based on Unscented Transform," *IEEE Transactions on Power Systems*, Vol. 27, No. 2, pp. 942-950, May 2012.

[5] P. Tripathy, S. C. Srivastava, S. N. Singh, "A Divide-by-Difference-Filter Based Algorithm for Estimation of Generator Rotor Angle Utilizing Synchrophasor Measurements," *IEEE Transactions on Instrumentation and Measurement*, Vol. 59, No. 6, pp. 1562-1570, June 2010.

[6] N. Zhou, D. Meng, and S. Lu, "Estimation of the Dynamic States of Synchronous Machines Using an Extended Particle Filter," *IEEE Transactions on Power Systems*, Vol. 28, No. 4, pp. 4152-4161, Nov. 2013.

[7] A. G. Phadke, and J. S. Thorp, *Synchronized Phasor Measurements and Their applications*, New York, Springer, 2008.

[8] V. Terzija, G. Valverde, D. Cai, P. Regulski, V. Madani, J. Fitch, S. Skok, M. M. Begovic, A. Phadke, "Wide-area monitoring, protection, and control of future electric power networks," *Proceedings of the IEEE* , Vol. 99, No. 1, pp. 80-93, Jan. 2011.

[9] D. Simon, *Optimal State estimation; Kalman, H∞, and Nonlinear Approaches*, New Jersey, John Wiley & Sons, 2006.

[10] G. Welch, and G. Bishop, "An introduction to Kalman filter," TR 95-041, Department of Computer Science, University of North Carolina, Chapel Hill, USA, 2006.

[11] L.McGee, and S. Schmidt, "Discovery of the Kalman filter as a practical tool for aerospace and industry," *NASA Technical Memo 86847*, Nov. 1985.

[12] S. Julier, J. Uhlmann, and H. Durrant-Whyte, "A new approach for filtering nonlinear transformation of means and covariances in filters and estimators," *IEEE Transactions on Automatic Control*, Vol. 45, No. 3, pp. 477-482, March 2000.

[13] L. H. Peng, and Z. Q. Fan, "Research on a modified EKF for speed estimation in induction motor drives," *Proceeding of IEEE International Conference on Integration Technology*, Shenzhen, China, pp. 432-436, March 2007.

[14] A. V. Leite, R. E. Araujo, and D. Freitas, "Full and reduced order extended Kalman filter for speed estimation in induction motor drives: a comparative study," *Annual IEEE Power Electronics Specialists Conference*, Aachen, Germany, Vol. 3, pp. 2293-2299, June 2004.

[15] S. C. Velázquez, R. A. Palomares, and A. N. Segura, "Speed estimation for an induction motor using the extended Kalman filter," *Proceedings of the 14th IEEE*

International Conference on Electronics, Communications and Computers, pp. 63-68, Feb. 2004.

[16] K. L. Shi, T. F. Cha, Y. K. Wong, and S. L. Ho, "Speed estimation of an induction motor drive using an optimized extended Kalman filter," *IEEE Transaction on Industrial Electronics*, Vol. 49, No. 1, pp. 124-133, Feb. 2002.

[17] K. B. Mohanty, and A. Patra, "Flux and speed estimation in decoupled induction motor drive using Kalman filter," *Proceeding of 29th National System Conference (NSC)*, IIT Mumbai, India, pp. 1-9, Dec. 2005.

[18] M. Barut, S. Bogosyan, and M. Gokasan, "Speed-sensorless estimation for induction motors using extended Kalman filters," *IEEE Transaction on Industrial Electronics*, Vol. 54, No. 1, pp. 272-280, Feb. 2007.

[19] D. J. Atkinson, P. P. Acarnley, and J. W. Finch, "Observers for induction motor state and parameter estimation," *IEEE Transaction on Industry Application*, Vol. 27, No. 6, pp. 1119-1127, November/December 1991.

[20] M. Barut, S. Bogosyan, and M. Gokasan, "Speed sensorless direct torque control of IMs with rotor resistance estimation," *Energy Conversion and Management Elsevier*, Vol. 46. No. 3, pp. 335-349, Feb. 2005.

[21] M. Barut, S. Bogosyan, and M. Gokasan, "Experimental evaluation of braided EKF for sensorless control of induction motors," *IEEE Transaction on Industrial Electronics*, Vol. 55, No. 2, pp. 620-632, Feb. 2008.

[22] M. Barut, S. Bogosyan, and M. Gokasan, "Switching EKF technique for rotor and stator resistance estimation in speed sensorless control of IMs," Energy *Conversion and Management Elsevier*, Vol. 48. No. 12, pp. 3120-3134, Dec. 2007.

[23] M. Barut, S. Bogosyan, and M. Gokasan, "Braided extended Kalman filters for sensorless estimation in induction motors at high-low/zero speed," *IET Control Theory and Appicationsl,* Vol. 1, No. 4, pp. 987-998, July 2007.

[24] S. Jafarzadeh, C. Lascu, and S. Fadali, "State estimation of induction motor drives using the unscented Kalman filter," *IEEE Transaction on Industrial Electronics,* Vol. 59, No. 11, pp. 4207-4216, Nov. 2012.

[25] Matlab, ver. 7.14.0.739 (R2012a), MathWorks, Natick, USA.

[26] S. Chakrabarti, E. Kyriakides, T. Bi, D. Cai, and V. Terzija, "Measurements get together," *IEEE Power & Energy Magazine*, Vol. 7, No. 1, pp. 41-49, January/February 2009.

[27] K. E. Martin, and J. R. Carroll, "Phasing in the technology," *IEEE Power & Energy Magazine*, Vol. 6, No. 5, pp. 24-33, September/October 2008.

[28] E. Ghahremani, and I. Kamwa, "Online state estimation of a synchronous generator using unscented Kalman filter from phasor measurements units," *IEEE Transactions on Energy Conversion*, Vol. 26, No. 4, pp. 1099-1108, Dec. 2011.

[29] PowerWorld Simulator, ver. 17.0, PowerWorld Corporation, Champaign, IL, USA.

[30] J. D. Glover, M. S. Sarma, and T. J. Overbye, *Power System Analysis and Design*, Stamford, Thomson-Engineering, 2011.

[31] M. Pavella, and P. G. Murthy, *Transient Stability of Power Systems*, West Sussex, John Wiley & Sons, 1994.

[32] H. Saadat, *Power System Analysis*, USA, PSA Publishing, 2010.

Papers during the M.Eng Program

1. H. Tebianian, B. Jeyasurya, "Dynamic State Estimation in Power Systems Using Kalman Filters," *IEEE Electrical Power and Energy Conference, EPEC*, Halifax, Canada, Aug. 2013. (Selected among the best papers of the conference)

2. H. Tebianian, B. Jeyasurya, "State Estimation in Induction Motors," *IEEE Newfoundland Electrical and Computer Engineering Conference, NECEC*, St. John's, Canada, Nov. 2013.